Development and optimisation of a process for cellulose nanoparticle production from waste paper sludge with enzymatic hydrolysis as an integral part

by

Lia Mari Bester

Thesis presented in partial fulfilment
of the requirements for the degree

of

MASTERS OF ENGINEERING

(CHEMICAL ENGINEERING)

in the Faculty of Engineering
at Stellenbosch University

Supervisor

Dr AFA Chimphango

Co-supervisor

Prof JF Görgens

December 2018

Declaration

By submitting this thesis electronically, I declare that the entirety of the work contained therein is my own, original work, that I am the sole author thereof (save to the extent explicitly otherwise stated), that reproduction and publication thereof by Stellenbosch University will not infringe any third party rights and that I have not previously in its entirety or in part submitted it for obtaining any qualification.

Date: December 2018

Plagiarism Declaration

1. Plagiarism is the use of ideas, material and other intellectual property of another's work and to present is as my own.

2. I agree that plagiarism is a punishable offence because it constitutes theft.

3. I also understand that direct translations are plagiarism.

4. Accordingly all quotations and contributions from any source whatsoever (including the internet) have been cited fully. I understand that the reproduction of text without quotation marks (even when the source is cited) is plagiarism.

5. I declare that the work contained in this assignment, except where otherwise stated, is my original work and that I have not previously (in its entirety or in part) submitted it for grading in this module/assignment or another module/assignment.

Student number: 16502965

Initials and surname: LM Bester

Signature:

Date: 07-09-2018

Abstract

The identification of low-cost and renewable resources is critical to meet environmental concerns associated with fossil-based materials. Waste pulp and paper fibres is a renewable, low-cost, cellulose-rich resource with potential for the production of cellulose nanoparticles. Cellulose nanoparticles are light materials that have desired properties such as biodegradability, non-toxicity, electrical conductivity and high tensile strength. Current production methods involve enzymatic, mechanical pressure and/or chemical treatments.

This project developed and optimised a process of enzymatic hydrolysis of waste paper sludge for cellulose nanoparticle production. Based on content of inorganics, two types of paper sludge (PS) from South-African paper and pulp mills, namely printed recycle PS and virgin pulping PS were selected as feedstocks. Commercial enzymes were screened for lab scale enzymatic hydrolysis of PS to cellulose nanoparticles. A cellulase cocktail, Cellic® CTec2, and a monocomponent endoglucanase, FiberCare® R, were preferred commercial enzymes for nanoparticle formation and minimisation of by-product formation for both PS feedstocks. Multi-response statistical optimisation of enzymatic hydrolysis of both feedstocks were conducted, investigating solids loading, hydrolysis times and different ratios of the Cellic® CTec2 and FiberCare® R.

Optimised enzymatic hydrolysis conditions based on the mean cellulose particle size and the glucose concentration models indicated that FiberCare® R dosage, Cellic® CTec2 dosage, hydrolysis time and solids loading of 75 ECU/gdPS, 10 FPU/gdPS, 9 hrs and 3% (w/w), respectively were optimum for virgin pulp PS. These optimised conditions resulted in mean cellulose particle size and glucose concentrations of 232 nm and 5.44 g/L, respectively. Selected conditions for printed recycle PS required higher FiberCare® R and Cellic® CTec2 dosages of 100 ECU/gdPS and 20 FPU/gdPS, respectively, at longer hydrolysis times of 12 hrs and a higher solids loading of 6% (w/w). At these selected conditions a mean cellulose particle size and glucose concentrations of 226 nm and 6.38 g/L, respectively were achieved for printed recycle PS. Spherical cellulose nanoparticles (SCN) were produced by these mentioned conditions of both enzymatically-hydrolysed PS feedstocks.

Microfiltration of hydrolysed supernatant through a 0.45 μm membrane increased the cellulose nanoparticle quality with decreased mean particle sizes and improved particle size distributions for both PS feedstock. Addition of a high-shear homogenization step subsequent to enzymatic hydrolysis marginally decreased the mean size of microsized particles, with no effect on samples with particles smaller than 1000 nm. Dialysis of the hydrolysed suspensions with a membrane with cut-off molecular weight of 12400 Da improved the purity of produced cellulose nanoparticles. Washing and centrifugation of isolated cellulose nanoparticles from residual hydrolysed solids further increased purity and quality. After purification, final cellulose nanoparticle yields of 7.5% for virgin pulp PS and 6.9% for printed recycle PS were achieved.

By controlled stand-alone enzymatic hydrolysis conditions, a selected cellulose nanoparticle type, including cellulose nanocrystals (CNC) and SCN could be produced which is beneficial over the stand-alone acid hydrolysis process, producing only a mixture of CNC and CNF. Furthermore, a proposed mechanism for the formation of spherical cellulose nanoparticles from cellulase hydrolysis of higher cellulose crystallinity feedstock was formulated for specifically short-period hydrolysis with a higher endoglucanase to exoglucanase ratio.

Uittreksel

Die identifisering van laekoste en hernieubare hulpbronne is van kritieke belang om te voldoen aan die groeiende omgewingsbekommernisse wat verband hou met fossielgebaseerde materiale. Afvalpulp en papiervesels is 'n hernubare, laekoste, sellulose-ryke hulpbron met potensiaal vir die vervaardiging van sellulose-nanopartikels. Sellulose nanopartikels is ligte materiale wat verlangde eienskappe soos biologiese afbreekbaarheid, nie-giftigheid, elektriese geleidingsvermoë en hoë treksterkte het. Huidige produksiemetodes behels ensimatiese, meganiese–druk en/of chemiese behandelings.

Hierdie projek ontwikkel en optimaliseer 'n proses van ensimatiese hidrolise vir sellulose-nanopartikels wat vervaardig word uit papierafval. Gebaseer op die persentasie van anorganiese materiaal, was twee soorte papierslyk (PS) van Suid-Afrikaanse papier- en pulp meule, naamlik gedrukte hersirkuleerde PS en reinpulp PS gekies as roumateriaal. 'n Siftingsproses op grond van die gebruik van kommersiële ensieme vir laboratoriumskaal-ensimatiese hidrolise van PS na sellulose-nanopartikels was uitgevoer. Sellulase ensiem, Cellic® CTec2, en monokomponent endoglukanase, FiberCare® R, was betergeskikte, beskikbare, kommersiële ensieme gebaseer op nanopartikels en minimale byprodukvorming vir beide PS-roumateriale. Multi-respons statistiese optimalisering van ensiematiese hidrolise op beide roumateriale was uitgevoer, waartydens soliedemateriaalladings, hidrolise tye en verskillende verhoudings van die Cellic® CTec2 en FiberCare® R ondersoek was.

Geoptimaliseerde ensiematiese hidrolise-toestande gebaseer op modelle vir gemiddelde sellulose-partikelgrootte en die glukosekonsentrasie het aangedui dat 'n monokomponent-endoglukanase dosis, sellulase ensiem dosis, hidrolise tyd en soliedemateriaalladings van 75 ECU/gdPS, 10 FPU/gdPS, 9 uur en 3% (w/w) onderskeidelik optimum was vir reinpulp PS, wat tot gevolg gehad het 'n onderskeidelike gemiddelde sellulose partikelgrootte en glukosekonsentrasie van 232 nm en 5.44 g/L. Die gekose toestande vir gedrukte hersirkuleerde PS benodig hoër dosisse vir monokomponent-endoglukanase en sellulase ensieme van 100 ECU/gdPS en 20 FPU/gdPS, onderskeidelik met langer hidrolise tye van 12 uur en 'n hoër soliedemateriaallading van 6% (w/w). By hierdie gekose toestande was 'n onderskeidelike gemiddelde partikelgrootte en glukosekonsentrasie van 226 nm en 6.38 g/L vir gedrukte hersirkuleerde PS behaal. Sferiese sellulose nanopartikels (SSN) was geproduseer deur bogenoemde toestande van beide ensiem-gehidroliseerde PS-roumateriale.

Mikrofiltrasie van gehidroliseerde supernatant deur 'n 0.45 μm membraan het die gehalte van sellulose nanopartikels verhoog met verminderde gemiddelde partikelgroottes en verbeterde partikelgrootteverdelings vir beide PS-roumateriale. Toevoeging van 'n hoë-skuif homogenisasie stap verminder die gemiddelde grootte van mikro-grootte partikels, maar het geen effek op die monsters met partikels kleiner as 1000 nm nie. Dialise van die hidroliseerde suspensies met 'n membraan met 'n afsny molekulêre gewig van 12400 Da, het die suiwerheid van geproduseerde sellulose-nanopartikels verbeter.

Was en sentrifugasie van geïsoleerde sellulose-nanopartikels uit residuele hidroliseerde vastestowwe het verder die suiwerheid en kwaliteit verhoog. Na suiwering was'n uiteindelike sellulose nanopartikels opbrengs van 7.5% vir reinpulp PS en 6.9% vir gedrukte hersirkuleerde PS behaal.

Deur gekontroleerde alleenstaande ensimatiese hidrolise toestande, kan 'n geselekteerde sellulose nanopartikeltipe, insluitende sellulose nanokristalle (SNK) en SSN vervaardig word wat voordelig is oor die alleenstaande suurhidrolise-proses, wat slegs 'n mengsel van SNK en SNF produseer. Verder is 'n voorgestelde meganisme vir die vorming van sferiese sellulose-nanopartikels uit sellulase-hidrolise van hoër sellulose-kristallisiteits-materiale geformuleer vir spesifiek korttermyn-hidrolise met 'n hoër endoglukanase tot eksoglukanase-verhouding.

Acknowledgements

I would like to thank the following people, for their assistance and contribution to this study:

- Dr Annie Chimphango and Prof Johann Görgens, for this opportunity and your guidance throughout the project
- Dr Lalitha Gottumukkala for your valuable input and guidance
- Mr. Henry Solomon for your assistance and prayers
- Ms Sonja Boshoff, for all your help and top-tips
- Dr Eugene van Rensburg, für Ihre Eingabe und Unterstützung bei der Statistik
- Mrs Levine Simmers, Mr Jaco van Rooyen and Mrs Hanlie Botha for all the assistance with analyses
- Mr Anton Cordier, Mr Jos Weerdenburg, Mr Alvin Petersen and Mr Oliver Jooste for the technical assistance and laughter at the Chemical Engineering Department
- Mrs Adine Visser and Mrs Pauline Skillington at Mpact Ltd
- Dr L Tyhoda, Mr Mark February and Mr Jan Swart from the Department of Forest and Wood Science
- Mr Kyle Raatz, Mr Marthinus van Niekerk, Dr Divann Robertson and Mrs Marehette Liprini from the Department of Polymer Science
- Dr Paul Reader at Kansai Plascon
- Dr Paul Verhoeven at the Department of Inorganic Chemistry
- Dr Michael Ioelovich from Designer Energy Ltd, Israel
- Mr Sebastian Brown from CSIR
- Dr Elrika Harmzen-Pretorius and Mrs Madelaine Frazenburg from CAF Microscopy Unit
- Novozymes, Denmark for kindly supplying FiberCare® R
- Fellow laboratory dwellers Ohene Donkor, Lorinda du Toit, Lukas Swart, Julia Annoh-Quarshie, Martin Hamann, Tunet Koekemoer and Marli de Kock
- Elsabè en Andrè Bester, my mom and dad as well as my little brother and sister, Joshua and Mikal, for your motivation, love and support
- My friends and family away from home
- My dearest Guddu, Jurgen Kriel, for all your ligen, motivation and patience – a million thank you's will never be enough
- God – all the glory to You

List of Abbreviations

Abbreviation	Description
AIL	Acid-insoluble Lignin
AIR	Acid-insoluble Residue
ASL	Acid-soluble Lignin
CIr	Crystallinity Index
CCD	Central Composite Design
CNC	Cellulose Nanocrystals
CNF	Cellulose Nanofibrils
CNW	Cellulose Nanowhiskers
DLS	Dynamic Light Scattering
DP	Degree of Polymerization
EG	Monocomponent Endoglucanase
EM	Electron Microscopy
FTIR	Fourier Transform Infrared Spectroscopy
H_2SO_4	Sulphuric Acid
HCl	Hydrochloric Acid
HPLC	High Performance Liquid Chromatography
hrs	hours
W	Weight
MCC	Microcrystalline Cellulose
MFC	Microfibrillated Cellulose
MW	Molecular Weight
N/A	Not Applicable
NaOH	Sodium hydroxide
NREL	National Renewable Energy Laboratory Analysis Procedures
O_2	Oxygen
ODW	Oven Dry Weight
PAMSA	Paper Manufacturers Association of South Africa
PdI	Polydispersity Index
PS	Paper sludge
RO	Reverse Osmosis
PR	Printed recycle Paper Sludge
SEM	Scanning Electron Microscopy
STEM	Scanning Transmission Electron Microscopy
tpa	Ton per annum
VP	Virgin Pulp Paper Sludge
X_i	Independent Variable
XRD	X-Ray Diffraction
Y_i	Dependent Variable

Table of Contents

List of Figures

List of Tables

Chapter 1.   Introduction

1.1. Background

Cellulose is the most abundant carbohydrate in nature and a renewable source of carbon for biorefinery applications (Siqueira, et al., 2010). It is one of the main components present in waste paper sludge (PS) generated by the primary clarifiers in the waste water treatment sections of pulp and paper mills. The South African pulp and paper industry generates at least 0.5 million tons (dry weight) of waste PS per annum (Dwiarti, et al., 2012), with this waste stream containing 45 to 80 % moisture, with 40 to 80 % of the dry mass consisting of relatively fine fibres (Hsu & Hu, 2002).

Due to the high moisture content, which increases the bulk of the waste material, the cost of disposal is extensive. South-African PS disposal costs range between R350 and R705 per metric ton (Kimberly-Clark Springs, 2017; Robus, 2013). Furthermore, environmental regulations are becoming increasingly stringent (Mahmood & Elliott, 2006). Consequently, pulp and paper mills are determined to find green alternatives by conducting research on new applications of PS to minimise its disposal (Monte, et al., 2009). Different mills produce waste pulp and paper sludge with distinct composition, and therefore the energy and chemical demand may vary for bioprocessing of the different PS types. Based on similarity of the feedstock utilized in the mills, these sludge types are categorised by Boshoff et al. (2016) and are termed printed recycle, corrugated recycle, non-recycle and virgin pulping.

Recent techno-economic studies on South-African PS indicated economic viability of the biorefinery processes of enzymatic hydrolysis and fermentation production of bio-ethanol (Robus, et al., 2016). Enzymatic hydrolysis of low cost cellulosic residues like PS to cellulose nanoparticle substrates reduces the waste disposal costs and concurrently meets the growing demand for renewable material production, and could be integrated into bioprocess for PS conversion. Cellulose nanoparticles are renewable biopolymers with novel applications. These cellulose nanomaterials are biodegradable and provide a more environmentally friendly alternative to plastics and other non-degradable materials.

Enzymatic bioprocessing methods are of interest as an alternative to the traditional stand-alone or combined chemical, biological and mechanical processing steps. This is due to the potential for reduced energy and chemical usage, as well as high selectivity of these biocatalysts (Moon, et al., 2011). Furthermore, chemical methods require corrosive, environmentally-unfriendly chemicals which also may cause undesired surface modifications leading to poor aqueous dispersion (Anderson, et al., 2014).

In recent ethanol production studies, commercial cellulase blends have been used to enzymatically hydrolyse PS to glucose, without the need for chemical or mechanical pre-treatment (Robus, 2013; Boshoff, et al., 2016). With the aid of customised enzymes or blends of different enzymes into cocktails, the ethanol production process may be combined with cellulose nanoparticle production, where the non-

nanocellulose residue from the cellulose nanoparticle process can be used in the ethanol production process. The potential further exists to recover the cellulose nanoparticle product by a single stage of centrifugation and filtration or precipitation (Kazimierczak, et al., 2016; Marino, et al., 2015; Satyamurthy & Vigneshwaran, 2013). The major disadvantages to commercialization of enzymatic hydrolysis processing are the high cost of enzymes (up to R3.28/L (Robus, et al., 2016)) and the slow hydrolysis rates (Walker & Wilson, 1991).

Research efforts on the manipulation of cellulase systems have found that desired cellulase action for the production of cellulose nanoparticles can be achieved by developing application specific enzyme cocktails (Fattahi Meyabadi & Dadashian, 2012; Filson, et al., 2009). Cellulose from various sources have the same molecular structure, consisting of linear polymers of unhydroglucose units linked by β-glycoside bonds, yet may have different crystalline structures. As the two major cellulase subgroups, endoglucanase and exoglucanase, target the hydrolysis of β-glucosidic and terminal glycosidic bonds, respectively, effective degradation of even highly crystalline sources can be achieved (Aliyu & Hepher, 2000). Furthermore, as many of the commercial cellulases are devoid of a third cellulase subgroup, glucosidase, which hydrolyse cellobiose into glucose, they are suitable for the production of cellulose nanoparticles (Boshoff, 2015). With use of enzyme processes, there is potential to target specific types of nanostructured cellulose particles with qualities defined by their morphology; specifically the mean particle size, such as cellulose nanocrystals (CNC), spherical cellulose nanoparticles (SCN) and cellulose nanofibrils (CNF) (Moon, et al., 2011; Ioelovich, 2014). This is advantageous over conventional mechanical or chemical methods which are often limited to either a single nanostructure, or a mixture of nanostructures.

The focus of the research is firstly to identify effective enzymes suitable for producing a majority of cellulose nanoparticles with minimal glucose production. Secondly, the focus is to identify optimal process conditions for controlled enzymatic hydrolysis of PS to cellulose nanoparticles. Most research conducted on PS conversion to nanomaterials had multiple processing steps, such as enzymatic hydrolysis with sonication (Song, et al., 2014; Filson, et al., 2009), mechanical pre-treatment in combination with enzymatic hydrolysis (Anderson, et al., 2014) or enzymatic hydrolysis as a pre-treatment to high-pressure homogenisation (Pääkkö, et al., 2007; Jonoobi, et al., 2012; Ankerfors, et al., 2009; Lindström, et al., 2007). There is a lack of information on the production of cellulose nanoparticles from waste PS with firstly, a stand-alone enzymatic hydrolysis process and secondly, a short-period (< 24 hrs) enzymatic hydrolysis process.

Ranges for the process parameters of the enzymatic hydrolysis process were identified from literature (Boshoff, et al., 2016; Robus, 2013; Song, et al., 2014) around which screening of commercial enzymes were conducted. Laboratory scale enzymatic hydrolysis experiments were designed statistically, to optimise enzyme dosage, hydrolysis time and solids loading for cellulose nanoparticle production.

Different post-hydrolysis downstream processes, including microfiltration, high-shear homogenization, dialysis and washing were investigated to assess whether the cellulose nanoparticles from enzymatic hydrolysis can be obtained with a comparable quality and purity to that of established cellulose nanoparticle processes such as acid hydrolysis. A possible mechanism for the preferred short-time cellulase hydrolysis was also investigated.

1.2.   Thesis layout

The following is an overview of the structure of this thesis.

Chapter 1: Presents the introduction and the research aims of this study.

Chapter 2: Discusses the background and literature findings around cellulose nanoparticle production.

Chapter 3: Presents a full overview of the experimental, analytical and statistical procedures used in the study.

Chapter 4: Discusses the optimisation, characterization and the extraction of cellulose nanoparticles.

Chapter 5: Discusses the general conclusions and the future recommendations.

Chapter 2. Literature review

2.1. Waste paper sludge

2.1.1. Waste paper sludge as biomass feedstock

Plant-based biomass can be categorised into five categories: energy crops, virgin wood, agricultural residues, food wastes, and also industrial wastes or co-products (Prasetyo & Park, 2013). The solid residue recovered from the primary clarifiers in waste-water treatment of pulp and paper milling, here referred to as paper sludge (PS), is one material categorised as industrial waste, and more specifically biomass feedstock due to its plant source and high cellulose content. Primary sludge rich in cellulose, is recovered from the primary clarification stage, carried out by sedimentation or flotation. Secondary sludge usually results from a biological treatment in which micro-organisms convert the waste to carbon dioxide and water. The resulting solids are removed through a second clarification step, remixed with the primary sludge, dewatered and disposed (Scott & Smith, 1995). The disposed PS contains rejected cellulose fibres which makes it possible for depolymerisation into regenerated biomaterials (Kádár, et al., 2004), including nanomaterials.

2.1.2. Composition of paper sludge

PS from paper and pulp milling waste streams contains lignocellulosic biomass material, papermaking fillers (inorganic materials such as calcium carbonate ($CaCO_3$), titanium oxide (TiO_2), etc.), inert solids rejected during the chemical recovery process, and ash (Ochoa de Alda, 2008). Unprocessed lignocellulosic biomass typically contains approximately 35 – 50% cellulose, 20 – 35% hemicellulose, 10 – 25% lignin (Crespo, et al., 2012), with the minor constituents including extractives and inorganic materials (Prasetyo & Park, 2013). Cellulose is a glucose polymer, linked by β-(1→4)-glycosidic bonds. Hemicellulose is a heteropolymer composed of both 5- and 6-carbon ring sugars. Lignin is an aromatic heteropolymer which contain multiple hydroxyl and methoxyl groups per building unit (Vassilev, et al., 2013; Salehudin, et al., 2012).

Due to different feedstock for pulping and different processes, as well as differences in the pulping or paper-making processes, mills produce varying amounts of primary sludge, with the sludge being distinctly different in composition (Fan & Lynd, 2007). A study by Ochoa de Alda (2008) indicated that sludge can be characterised in two main types, namely high-ash sludge (> 30% w/w dry weight) and low-ash sludge (< 30% w/w dry weight). Figure 2.1 shows the chemical composition (g component/g sludge) of PS samples collected from South African paper and pulp mills as summarised by Boshoff et al. (2016). The study shows that the ash component in the PS can vary from 0.09 to 0.62 g/g substrate (Boshoff, et al., 2016).
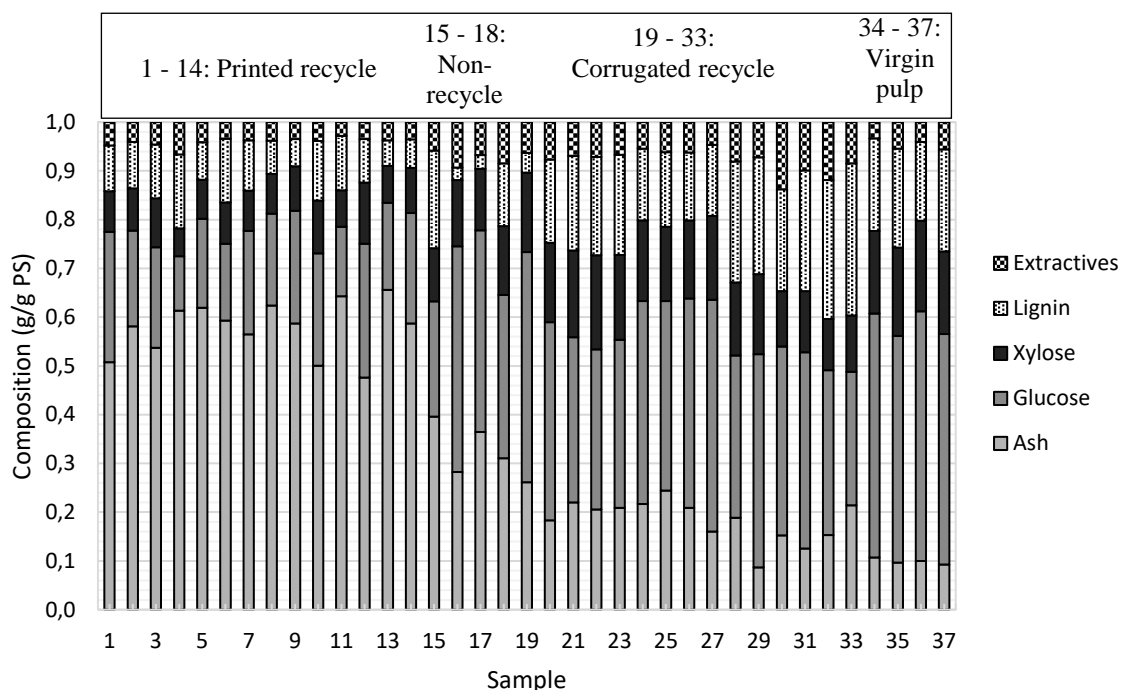
Figure 2.1: Chemical composition (g component/g sludge) of PS samples collected from South African paper and pulp mills as redrawn from Boshoff et al. (2016)

2.1.3. Effect of pulping processes on digestibility/pre-treatment of paper sludge

Cellulose fibres from wood-based products are isolated for paper and pulp production via pulping and re-pulping processes. Lignin, the organic polymer that forms structural support of plant fibres, and hemicellulose, the fibril-linking homopolymers are partially removed with mechanical or chemical pulping. In *mechanical pulping* the wood is processed into fibre-form by grinding or refining with water addition (Vena, 2005). During *chemical pulping* the cellulose fibres are isolated by cooking the wood/wood products in chemical solutions at high temperatures, dissolving the lignin and carbohydrates (Bujanovic, et al., 2010). PS produced via chemical pulping achieves higher solubilisation of hemicellulose and lignin in comparison to PS produced from mechanical or thermomechanical pulping (Migneault, et al., 2011).

When compared to mechanical pulping, the fibres of chemical pulping are more accessible to cellulose-hydrolysing enzymes during bioprocessing, due to decreased hindrance from the lignin as lignin dissolved in chemical pulping is washed out. This will result in increased digestibility for PS from chemical pulping processes in comparison to mechanical pulping operations (Zhu, et al., 2012).

In South Africa (SA), Kimberly-Clark and Sappi are two of the major paper and pulp companies. The Kimberly-Clark mill in Springs, Gauteng utilises recycled low-grade paper waste to produce tissue products via the mechanical pulping process. The waste paper is pulped, cleaned, deinked, bleached and often blended with small portions of virgin pulp before use on the paper machines. Recycled paper is

known to have changes in the basic fibre characteristics, such as strength, surface free area, swelling and length, which have been known to cause inferior fibre properties in comparison to virgin fibres (Wistara & Young, 1999). Furthermore, due to the recycled raw material used, ash and contaminants accumulate and results in high-ash content in the waste streams (Macdonald, 2004). As the ash and contaminants act as inhibitor to cellulase enzymes, PS with high ash-content will require ash removal pre-treatment to hydrolysis processing (Boshoff, et al., 2016).

The Sappi Ngodwana mill in Mpumalanga utilizes softwood to produce fully bleached pulp, and hardwood timber to produce unbleached pulp. Newsprint, linerboard, unbleached and bleached market pulp are the final chemical (Kraft) process products produced at the Ngodwana mill (Macdonald, 2004). PS from this pulping process has much lower inorganic content and therefore de-ashing pre-treatment of the low ash-content PS is not a concern (Robus, et al., 2016).

2.1.4. Processes for PS utilization

Landfilling, which is the most common PS disposal method in current practice (Monte, et al., 2009) is becoming increasingly difficult to implement due to greenhouse gas emissions, water-loss through high moisture materials, shrinking landfilling space, increasing regulatory pressure, stringent legislation and increased taxes (Mahmood & Elliott, 2006; Robus, et al., 2016). A number of non-conventional disposal alternatives for the management of PS are presented below.

Anaerobic digestion: Organic matter in PS can be used through co-digestion for conversion (in an oxygen-free system) to biogas (carbon dioxide and methane) and organic fertilizers from sludge digestion. Due to high energy recovery and limited environmental impact, the process is often viewed as the most cost-effective PS utilization process (Monte, et al., 2009; Lin, et al., 2012).

Bioethanol production: Through processes of hydrolysis and fermentation, PS can be used for bioethanol production (Boshoff, et al., 2016; Robus, et al., 2016). Increasing research has been conducted in ethanol production from PS in search of low cost second generation raw material and to avoid competition with human needs occurring when food crops are utilized (Prasetyo, et al., 2011).

Cement and brick industry: For brick production, 5-15% PS addition as raw material improves both the product as well as the process. During brick production, the fibre content of PS increases the porosity of the matrix, which enables the manufacture of lighter bricks. At the same time the PS addition saves fuel in the oven which reduces the cooking time (Monte, et al., 2009).

Composting and land application: Composting and soil amendments are of the lowest cost disposal routes, yet frequently only accounts for less than 5% of the total paper and pulp residues generated (Mahmood & Elliott, 2006). Composts are made from organic waste mixed with various amounts of paper wastes and recovered paper from industry (Migneault, et al., 2011).

Thermal processing: Various high-temperature, high-pressure processes such as pyrolysis (organic waste heated in an oxygen-free system), incineration or combustion and steam reforming have been extensively researched (Fytili & Zabaniotou, 2008; Mahmood & Elliott, 2006; Ridout, et al., 2016). These processes have an array of advantages, yet introduces problems such as inefficiency due to high moisture content in feedstock (Ridout, et al., 2016), air pollution and high costs (Monte, et al., 2009).

Due to the variety and fluctuation of chemical composition of different types of PS, based on the pulping process and feedstock, a range of PS utilization processes, similar to the existing non-conventional disposing processes, need to be availed. One such potential process is the production of cellulose nanoparticles (Moon, et al., 2011). These cellulose nanoparticle products have been estimated at a total of 33 million metric tons for potential applications on the global market including industries like paper, cosmetics, automotive, pharmaceutical, textile, etc. (Cowie, et al., 2014).

2.2. Cellulose nanoparticles

2.2.1. Cellulose

Cellulose is widely considered as the most abundant organic compound derived from plants. Natural cellulose chains have a degree of polymerization (DP) in the range of 10 000 to 30 000, which translates to chain lengths of 5000 to 15 000 nm (Lavoine, et al., 2012; Ioelovich, 2008).
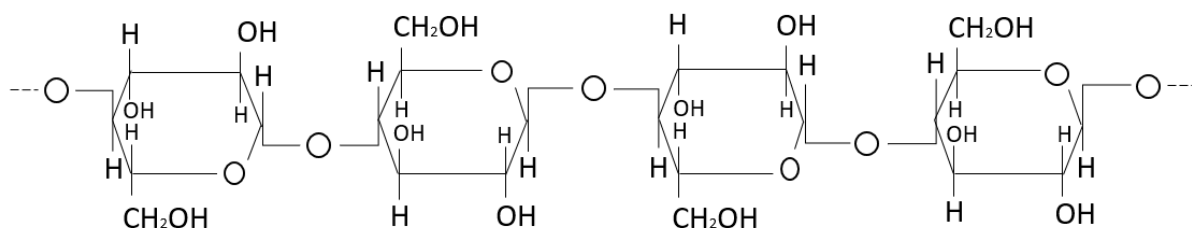
Figure 2.2: Cellulose chain composed of glucose subunits (redrawn from Robus, 2013)

Cellulose is a linear homopolysaccharide which is viewed to be amphiphilic (Medronho, et al., 2015). These polysaccharides are biosynthesized of repeated dimers of cellobiose constituting of two β-1.4-linked β-D-glucopyranose subunits (Figure 2.2) (Hendriks & Zeeman, 2009). Each glucose molecule bears three hydroxyl groups which has the ability to form strong intermolecular hydrogen bonds (Figure 2.3).

The multi-scaled microfibrillated structure of cellulose is broken down into solid microcrystalline structures with varying proportions of crystalline regions (higher order crystallinity), amorphous regions (lower order crystallinity) and paracrystalline regions (intermediate state between crystalline and amorphous cellulose regions) (Poletto, et al., 2013; International Standards Organization, 2017). These crystalline regions have high wettability and swells in aqueous solutions (Lindman, et al., 2017). Crystallinity indices of cellulose in various biomass and organic feedstock are measured through X-ray diffraction, nuclear magnetic resonance, acid hydrolysis and infrared spectroscopy (Hall, et al., 2010).

8

The results from the various analysis methods are seldom comparable. Kostylev & Wilson, (2012) reported over 30% variability for the same substrate analysed through different methods. The variation is mainly due to the specific arbitrary definition of cellulose crystallinity of each analysis (U.S. Congress, 1989). Nevertheless, crystallinity index is still a widely used and useful parameter for comparing cellulose of different feedstock to each other (Kostylev & Wilson, 2012).
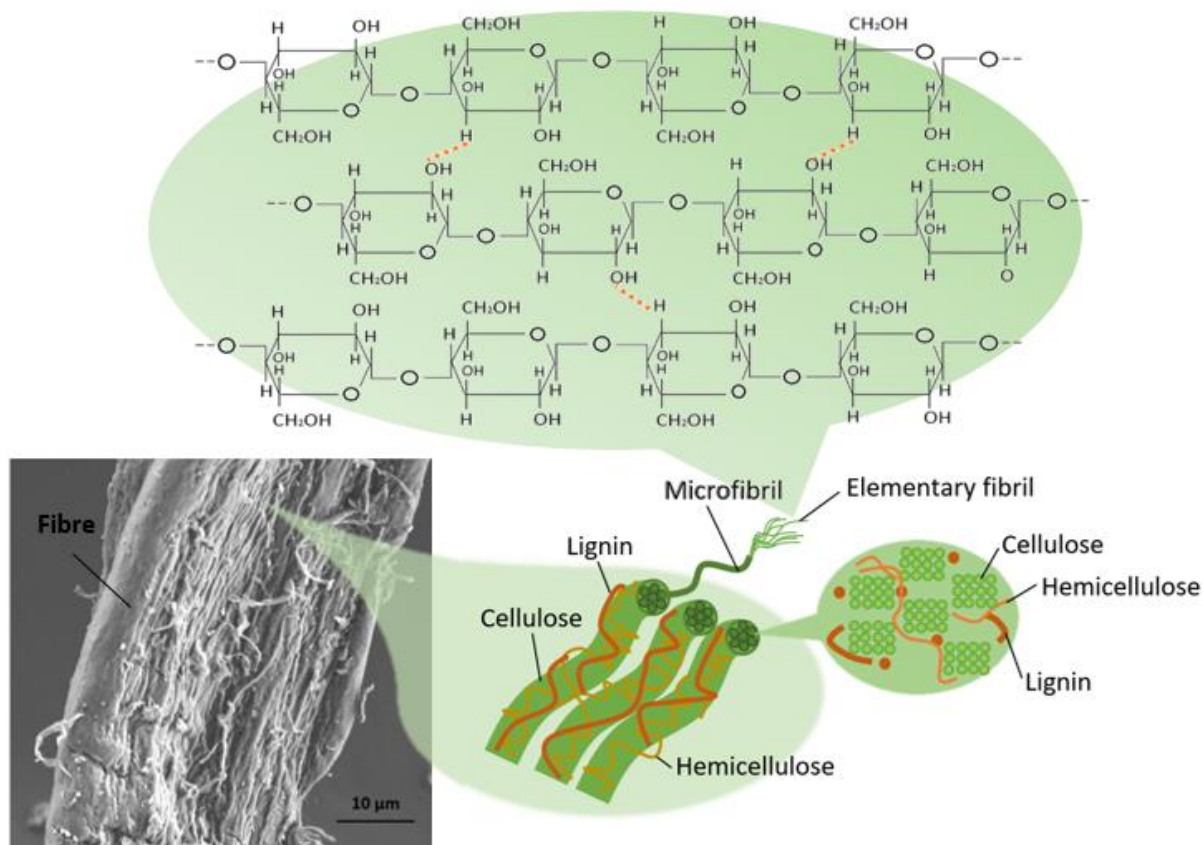
Figure 2.3: SEM image of biomass fibre with hierarchical structure of intermolecular hydrogen linkages of cellulose (indicated by orange dotted lines) partly redrawn from (Chirayil, et al., 2014)

It is evident from abovementioned that the chemical and physical properties of cellulose as well as the reactivity is greatly influenced by the arrangement of the molecules with respect to each other as well as the fibre axis. Thermal, chemical and enzymatic reactants penetrate the amorphous regions with greatest ease, followed by the lower ordered regions and only consecutively, the surfaces of the swollen crystalline regions are penetrated (Ciolacu, et al., 2010). These characteristics can be exploited to produce various nanostructured cellulose particles, largely referred to as cellulose nanoparticles or nanocellulose (Moon, et al., 2011; Ioelovich, 2008).

2.2.2. Types and properties of cellulose nanoparticles

2.2.2.1.   Types of cellulose nanoparticles

Cellulose nanoparticles comprise the different types of nanostructured cellulose particles such as SCN, CNC and CNF. These are currently of great industrial interest due to unique properties such as low

density, abrasivity and strength, biocompatibility, biodegradability as well as its ability towards structural and chemical modification (Moon, et al., 2011; Ioelovich, 2014).

From literature, it is apparent that until recently, cellulose nanoparticle terminology has not been standardized, resulting in a lack of generally accepted definition of the unique properties of individual products for the full range of possible types of cellulose nanoparticles (Pääkkö, et al., 2007; Brinchi, et al., 2013). Various critical reviews on cellulose particle classification have been done (Dufresne, 2013; Moon, et al., 2011; Klemm, et al., 2011; Siqueira, et al., 2010). As of August 2017, the International Standards Organisation (ISO) have provided preliminary standards on the most common types of cellulose nanostructures (International Standards Organization, 2017). Table 2.1 summarises some of these micro- and nano-sized cellulose structures with the defined physical properties that will be used as standard for specific product quality in terms of dimensions throughout this study.

Table 2.1: Terminology and defined dimensions of different micro- and nano-sized cellulose structures (International Standards Organization, 2017)

Cellulose Structure	Abbreviation	Diameter (nm)	Length (nm)	Aspect Ratio (L/d)
PS Fibres		> 10 000	> 100 000	> 10
Microcrystalline Cellulose	MCC	> 1000	> 1000	~ 1
Spherical Cellulose Nanoparticles	SCN	40 - 600	N/A	N/A
Cellulose Nanofibrils	CNF	3 – 100	100 – 100 000	10 – 2500
Cellulose Nanocrystals/Nanowhiskers	CNC/CNW	3 – 50	100 – 4000	5 – 50

On a macro scale, cellulose nanoparticles are solid or gel-like substances. On a micro level, it is a material consisting of nano-sized cellulose particles with at least one dimension between roughly 1.0 and 100 nm (Mörseburg & Chinga-Carrasco, 2009; Cowie, et al., 2014; Song, et al., 2014). Figure 2.4 illustrates microscopy images of different cellulose nanoparticles.
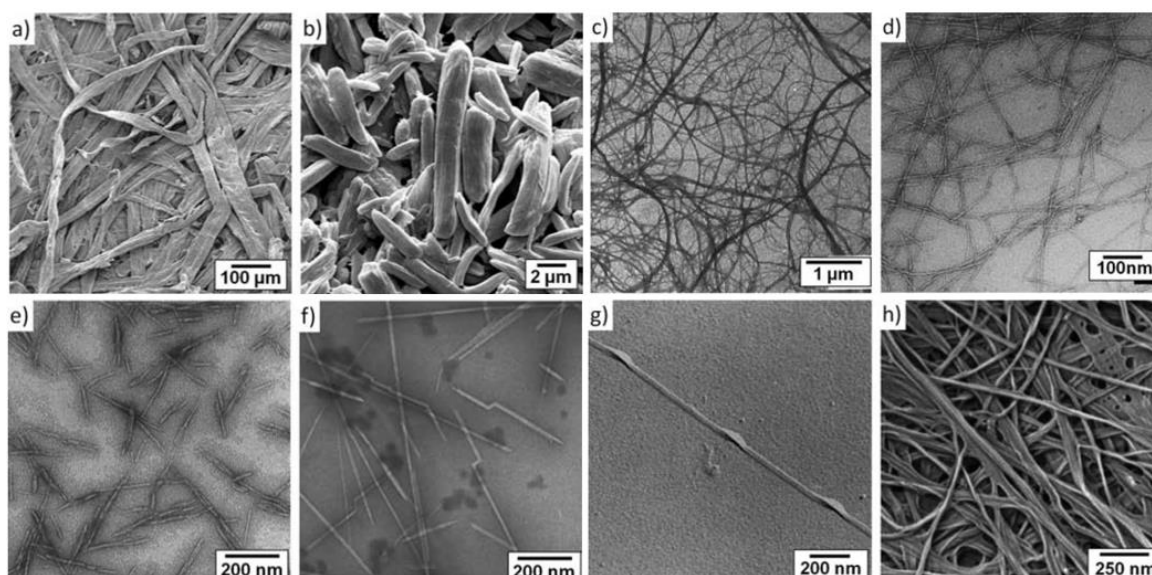
Figure 2.4: a) Wood Fibre, b) Microcrystalline Cellulose, c) Microfibrillated Cellulose, d) Cellulose Nanofibres, e) Cellulose Nanocrystals f) Cellulose Nanocrystal g) Microfibrillated Cellulose from algae h) Microfibrillated Cellulose from bacteria. Images reproduced from Moon et al. 2011 with permission from the Royal Society of Chemistry.

2.2.2.2.   Cellulose nanoparticle quality and purity

CNF, also known as microfibrillated cellulose (MFC), has a web-like shape with widths and lengths in nano and micro-scale, respectively (Mtibe, et al., 2015; International Standards Organization, 2017). The quality for CNF is defined by ISO standards (2017) and will be used throughout this work as '*cellulose nanofiber composed of at least one elementary fibril, containing crystalline, paracrystalline and amorphous regions, with aspect ratio usually greater than 10, which may contain longitudinal splits, entanglement between particles, or network-like structures*'. CNF is manufactured through various types of mechanical treatments with/without chemical pre-treatments and can be employed in industries such as paper processing, pharmaceutical and cosmetic industries, composites and adhesives (Shatkin, et al., 2014; Nguyen, et al., 2013).

CNC, also termed cellulose nanowhiskers (CNW) are rod-like in shape with both their diameters and lengths in nano-scale (Mtibe & Muniyasamy, 2016). CNC from tunicate are larger (length < 4 µm) than CNC from plants/trees (length < 500 nm) (Moon, et al., 2016). According to ISO standards (2017), the quality of CNC is defined and will be used throughout this work as '*nanocrystal predominantly composed of cellulose with at least one elementary fibril, containing predominantly crystalline of paracrystalline regions, with aspect ratio of usually less than 50 but greater than 5, not exhibiting longitudinal splits, inter-particle entanglement, or network-like structures*'. CNC exhibit exceptional product characteristics, such as high aspect ratio, low density and high specific strength. It can be used in packaging films, sensors, textiles, and personal care products (Anderson, et al., 2014). Nanocrystals are generally produced from acid hydrolysis in combination with mechanical or sonication treatment (Moon, et al., 2011).

A relatively new subcategory of CNC is SCN. SCN have been obtained by enzymatic -, microbial - or acid hydrolysis, usually accompanied with mechanical treatment (Ioelovich, 2014). SCN from alkaline pre-treatment and acid hydrolysis have been reported to having diameters of 60 – 570 nm (Ioelovich, 2014; Ioelovich, 2013; Li, et al., 2001; Zhang, et al., 2007), and from microbial hydrolysis with similar diameters of 40 – 490 nm (Satyamurthy & Vigneshwaran, 2013). From enzymatic and vibrational treatment with a variety of pre-treatments including NaOH pre-treatment or sonication, diameters of 6 – 250 nm were found, as in Figure 2.5 (Chen, et al., 2012). SCN is defined by the same quality as that of CNC, except for the fact that SCN has only one dimension as it is a spherically shaped, and will therefore be compared to the quality of sources such as Satyamurthy & Vigneshwaran, (2013) and Chen, et al., (2012). As the rod-like shape of CNC can injure cells and tissue of human and animal organisms, it is therefore less suitable for medicine and cosmetics (Ioelovich, 2013). SCN can address this limitation due to their spherical shape and therefore, applications include immobilization of biological active substances and drugs, and thickening of cosmetic and pharmaceutical products (Zhang, et al., 2007).
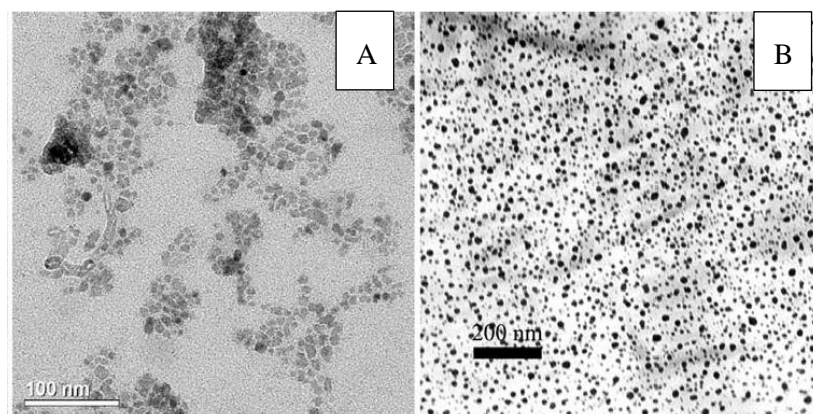
Figure 2.5: TEM images of SCN prepared by enzymatic hydrolysis and vibrational treatment with A) NaOH pre-treatment and B) ultrasonic pre-treatment, reproduced with permission from Chen et al. (2012)

Many combinations of pre-treatment, treatment and post-treatments exists for the production of cellulose nanoparticles for the same feedstock (Desmaisons, et al., 2017). Consequently, a wide range of grade qualities is possible and available; product application being a determining factor. Mostly, literature comparison of the production of cellulose nanoparticles in a specific type only relies on a single criterion comparison such as nanoparticle dimensions (Oksman, et al., 2014; Rosa, et al., 2010), disregarding the higher-scale part and other properties of the sample (Besbes, et al., 2011). A few studies have also focused on nanoparticle suspension comparisons by multi-criteria approaches (Moser, et al., 2015; Qing, et al., 2013). However, proposed methods to date result in a qualitative classification, and even if multi-criteria tests are performed, no manufacturing method exists and the suspensions are ultimately compared test by test (Desmaisons, et al., 2017).

Furthermore, ISO-standards specify that cellulose nanoparticles such as CNF from plant-based materials contains predominantly cellulose, but usually also contain small amounts of hemicellulose,

12

lignin and can have functional groups on the cellulose surface as a result of the manufacturing process (International Standards Organization, 2017). Small amounts of hemicellulose in the purified cellulose nanofibres had been found to play a positive role in facilitating of nanofibrillation as well as aiding in preventing the cellulose particle agglomeration (Chen, et al., 2011). In the light of no established single quality or purity index (Desmaisons, et al., 2017), it is accepted that samples with the higher amount of cellulose material, in a narrow nanometre size range (Li & Ragauskas, 2011), will have higher cellulose nanoparticle quality (Garcia, et al., 2016).

2.2.3. Cellulose nanoparticle isolation from lignocellulosic materials

Several cellulose sources have been used to obtain cellulose nanostructures with variant morphologies and crystallinities. Pre-treatment is required to delaminate the fibre cell walls, break apart the lignin structure (Figure 2.6) and make the crystalline structure of cellulose accessible to acids and enzymes to efficiently hydrolyse the cellulose (Kumar, et al., 2009).
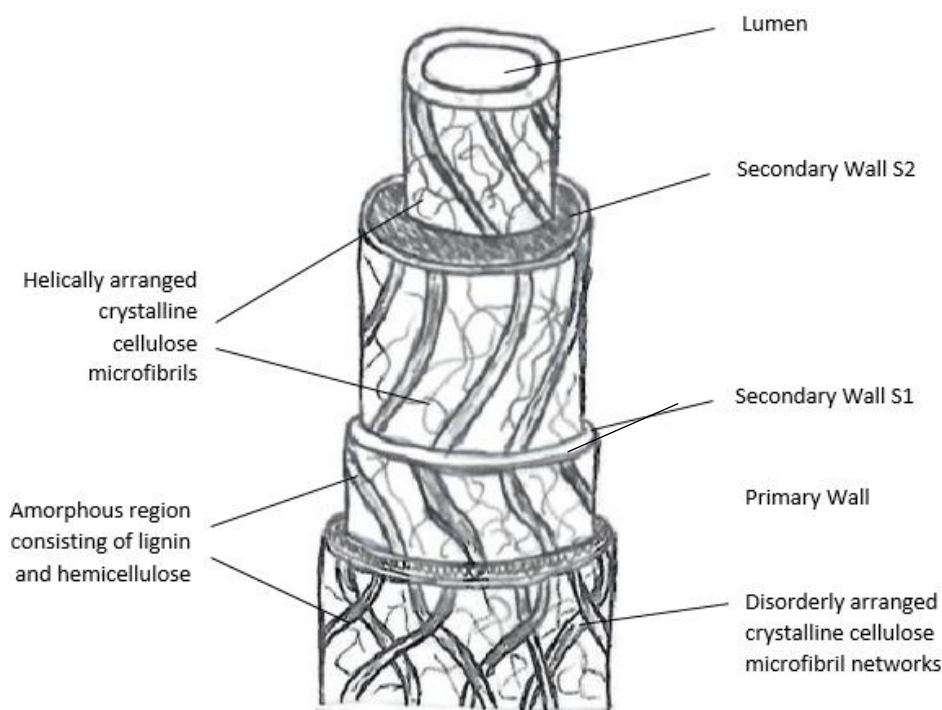
Figure 2.6: Structural representation of a natural fibre cell, redrawn from Kalia et al. (2011)

2.2.3.1. Pre-treatments of feedstock for enzymatic hydrolysis for cellulose nanoparticle production

Due to the interest in maximizing the effectiveness of enzymatic hydrolysis, various pre-treatments have been investigated. Such pre-treatments aim to increase the enzymatic digestibility of the cellulose in the pre-treated feedstock and reduce the cost of the hydrolysis treatment. One pre-treatment process to enzymatic hydrolysis is steam explosion (Deepa, et al., 2015). During steam explosion pre-treatment, saturated steam accesses the inner structures of fibres and with instantaneous release of pressure

(explosion of steam), lignin and hemicellulose bonds are cleaved (Pielhop, et al., 2016), increasing the cellulose accessibility. Another common pre-treatment is alkali treatment, where NaOH or ammonia pre-treatments swells the fibres, in the process removing portions of the lignin and hemicellulose and simultaneously decreasing the crystallinity of the cellulose (Chen, et al., 2012). Figure 2.7 illustrates the effect of pre-treatment of lignocellulosic material.
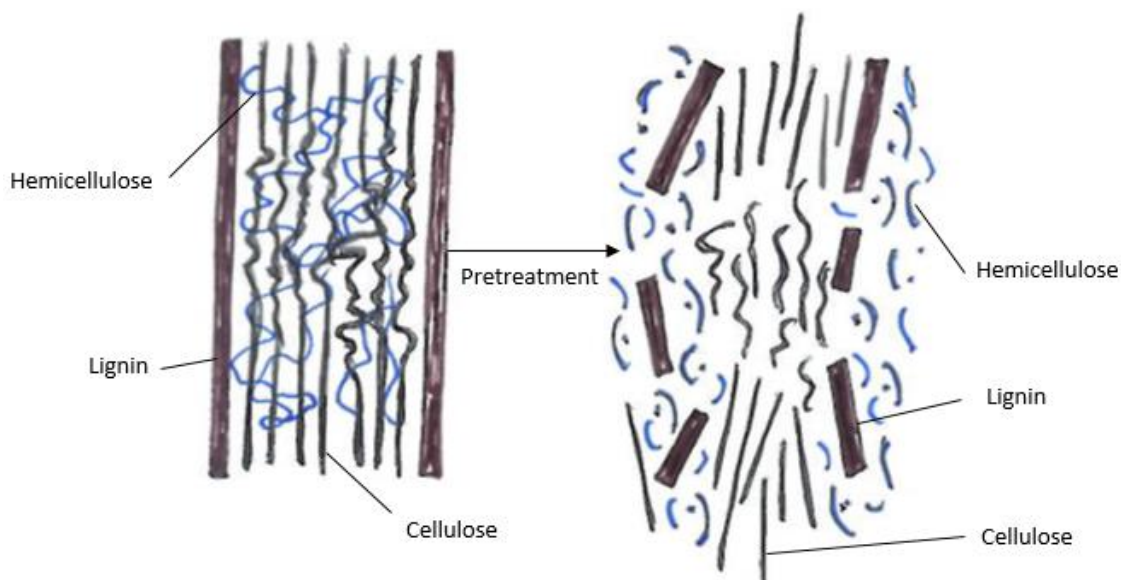
Figure 2.7: Effect of pre-treatment of lignocellulosic material, redrawn from Kumar et al. (2009)

PS from paper and pulp mills have been subjected to extensive mechanical and chemical processing that removes lignin and hemicellulose (Prasetyo, et al., 2011). The PS is moderately defibrillated, has a smaller fibre size and therefore has enhanced amenability for enzymatic hydrolysis (Peng & Chen, 2011). It is therefore possible that PS can be processed into nano-sizes without pre-treatment (Jonoobi, et al., 2012; Wang, et al., 2010).

2.2.3.2.   Cellulose nanoparticle production

Table 2.2 summarises processes for the production of the different types of cellulose nanoparticles, indicating the starting material as well as the yields achieved. The studies on cellulose nanoparticles in Table 2.2 were classified according to ISO standards, save for two significant studies who did not specify a type; instead just referred to the product as *nanoparticles*, as well as available research on SCN. Yield estimations are seldom reported, as the yield from plant based raw materials can be very low, which negatively affect production economics (Anderson, et al., 2014; Moon, et al., 2011). In general, higher yields were reported with a combination of processes, especially including acid hydrolysis and/or sonication.

Table 2.2: Different production processes of types of cellulose nanoparticles reported with specific particle terminology used in literature, including cellulose source and cellulose nanoparticle yield.

Name/Acronym	Feedstock (particle size)	Process	Yield	Reference
NFC (also referred to as MFC)	Softwood pulp (1 mm)	Acid hydrolysis & mechanical milling Enzymatic hydrolysis & mechanical milling	N/A	(Henriksson, et al., 2007)
	Sulphite pulp	Mechanical refining & enzymatic hydrolysis	N/A	(Ankerfors, et al., 2009)
	Bleached sulphite pulp	High-pressure homogenization, enzymatic hydrolysis & microfluidization	N/A	(Pääkkö, et al., 2007)
	Bamboo fibres (20 - 50 µm)	Acid hydrolysis, dialysis & sonication	N/A	(Nguyen, et al., 2013)
	Citrus waste	Enzymatic hydrolysis, dialysis & sonication	N/A	(Marino, et al., 2015)
	Bamboo pulp	Sonication & high-shear homogenization	N/A	(Zhao, et al., 2014)
	Banana, jute & pineapple leaf	Two steam explosion steps & acid hydrolysis	N/A	(Abraham, et al., 2011)
	Wood powder of Japanese cedar	High-speed blender & grinder	N/A	(Uetani & Yano, 2011)
Nanoparticles	Waste cotton fibres (< 2 mm)	Enzymatic hydrolysis & sonication	< 20% (w/w)	(Fattahi Meyabadi & Dadashian, 2012)
	Cotton	Enzymatic hydrolysis (repeated cycles) & mechanical treatment	N/A	(Paralikar & Bhatawdekar, 1984)
CNC (also sometimes referred to as CNW)	Cotton Whatman filter paper	Acid hydrolysis & sonication	1% (w/w)	(Paralikar, et al., 2008)
	Pure cotton	Acid hydrolysis, sonication & TEMPO-mediated carboxilation	< 1% (w/w)	(Mangalam, et al., 2009)
	Bacterial cellulose	Acid hydrolysis	N/A	(Grunert & Winter, 2002)
	Cotton wool	Acid hydrolysis, dialysis & sonication	N/A	(Morandi, et al., 2009)
	MCC (10 – 15 µm)	Acid hydrolysis & sonication	30% (w/w)	(Bondeson, et al., 2006)
	Recycled pulp and MCC	Sonication & acid hydrolysis	MCC – 5 - 10% (w/w) Recycled pulp – 2% (w/w)	(Filson & Dawson-Andoh, 2009)
	Recycled pulp (ca. 100 - 200 µm)	1. Enzymatic hydrolysis & sonication 2. Microwaved enzymatic hydrolysis & sonication	1. 29% (w/w) 2. 38.2% (w/w)	(Filson, et al., 2009)
	Maize stalk residues	Acid hydrolysis, dialysis & sonication	N/A	(Mtibe, et al., 2015)
	Maize stalk residues	Mechanical blending & mechanical grinding	N/A	(Mtibe, et al., 2015)
	Ramie	Acid hydrolysis, dialysis & high-shear homogenization	N/A	(Habibi, et al., 2008)
	MCC	Acid hydrolysis, dialysis & sonication	N/A	(Petersson, et al., 2007)

	MCC	Acid hydrolysis & sonication	N/A	(Rojas, et al., 2009)
	Grass Fibre	Acid hydrolysis & sonication	N/A	(Pandey, et al., 2009)
	MCC	DMAc:LiCl & sonication	17% (w/w)	(Oksman, et al., 2006)
	MCC (45 – 53 µm)	Microbial hydrolysis	22% (w/w)	(Satyamurthy, et al., 2011)
	Cotton linter	Acid hydrolysis, sonication & dialysis	N/A	(Braun, et al., 2008)
SCN	MCC	High-concentration H_2SO_4 hydrolysis & high-pressure homogenization	30-40%	(Ioelovich, 2012)
	MCC from cotton fibers (45 – 53 µm)	Microbial hydrolysis	12.3%	(Satyamurthy & Vigneshwaran, 2013)
	Buckeye cellulose (100% pure; 237 – 465 µm)	Acid hydrolysis & ultrasonication	62-74%	(Zhang, et al., 2007)
	Natural cotton fibre	Acid hydrolysis & ultrasonication	N/A	(Li, et al., 2001)

The most common cellulose nanoparticle production methods are discussed as follows:

Mechanical treatments: The first reported MFC was developed by Herrick et al. (1983) and Turbak et al. (1983) via grinding of diluted pulp suspensions in a high pressure mill. Today, various types of mechanical processes have been applied single-step or in combination, including ultrafine grinding or refining (Mtibe, et al., 2015; Nechyporchuk, 2015), microfluidization (Zhu, et al., 2011; Zimmerman, 2007), ultrasonication (Tonoli, et al., 2012; Chen, et al., 2011), high-pressure homogenization (Börjesson & Westman, 2015; Milford, et al., 2001), high-shear homogenization (Zhao, et al., 2014; Kazimierczak, et al., 2016) and cryo-crushing in liquid nitrogen (Alemdar & Sain, 2008; Wang & Sain, 2007). Due to different intensities and shearing mechanisms, the morphologies of the cellulose nanoparticles vary significantly.

Microfluidization and other high-pressure homogenizers are very effective in removing external layers of the plant cell wall, due to shear forces, causing the fibres to experience axial tensile failure. These processes provide considerably higher shear than other mechanical operations (Qing, et al., 2013). During high-shear homogenization, cellulose nanoparticles are isolated with high-speed rotation, leading to shearing forces individualizing fibres (Zhao, et al., 2014; Kazimierczak, et al., 2016).

Mechanical processes are advantageous due to the variety of different possible treatments that can produce well-fibrillated cellulose nanoparticles (Bilodeau & Paradis, 2013). However, mechanical processes create very high demand for energy. In various cases, temperature control is required with mechanical treatments, which increases the environmental impact (Lavoine, et al., 2012).

Chemical treatment: A controlled chemical method such as strong acid hydrolysis or oxidant (ammonium persulfate) treatment allows dissolution of amorphous regions of cellulose as well as the longitudinal cutting of microfibrils (Leung, et al., 2011; Dufresne, 2013). Sulphuric acid (H_2SO_4) (typically 64% (w/w)) is mostly used as it produces negatively surface charged sulphate esters, leading to increased colloidal stabilities, but hydrochloric, phosphoric, maleic acid and combinations thereof have also been used (Rebouillat & Pla, 2013; Wang, et al., 2007). During acid hydrolysis of cellulosic materials specifically pre-swelled with NaOH or dimethyl sulfoxide (DMSO), the dissolution of cellulose with simultaneous acid hydrolysis occurs, and after dilution of the solution, flocs of low-molecular weight amorphous cellulose precipitate. Thereafter, these flocs are comminuted using ultrasound or high-power mechanical equipment until spherical nanoparticles are obtained (Ioelovich, 2014; Li, et al., 2001). Through this dissolution mechanism and combined treatments, much higher cellulose nanoparticle yields were achieved (up to 62 - 74%; Table 2.2) in comparison to yields reported with any other treatments.

Acid hydrolysis is a well-known process for the production of cellulose nanoparticles with increased crystallinities, stability and yields (Bondeson, et al., 2006). However, the use of strong acids produces undesired by-products (furfural and 2-hydroxymethylfurfural (HMF)), complicates washing and increases the need for purification; rendering its environmental impact more complex (Leung, et al., 2011). Therefore, the industrial use of acid hydrolysis for producing cellulose nanoparticles on a large scale may be disadvantageous (Rebouillat & Pla, 2013).

Enzymatic Hydrolysis: Cellulase, the secreted enzymes that specifically target cellulose, is an enzyme complex involving synergistic action of three types of cellulase: endo-glucanase (EC 3.2.1.4), exo-glucanase (EC 3.2.1.91) and β-glucosidase (EC 3.2.1.21). Many detailed synergistic cellulase mechanisms have been proposed in literature, likely due to multiple cooperative interactions of cellulase (Kostylev & Wilson, 2012). Generally, three simultaneous and repeated processes can describe one prevalent hydrolysis mechanism, where cellulases act *in vitro* on insoluble cellulosic substrates, as also illustrated in Figure 2.8 (Balat, et al., 2008; Börjesson & Westman, 2015; Fattahi Meyabadi, et al., 2014):

i) Enzymes are adsorbed onto cellulose surface to form enzyme-substrate complexes.

ii) Soluble intermediates are released from the surface of the cellulose molecules. Endoglucanase acts on the amorphous and paracrystalline sites of the cellulose, and randomly hydrolyse accessible intramolecular β(1→4)-glucosidic linkages in the cellulose fibres, swelling the fibrils and generating oligosaccharides of several lengths with new chain ends (primary hydrolysis). Breaking of interfibrillated (intermolecular) hydrogen bonds result in the formation of fibrils with micrometre sized lengths (non-crystalline regions still remain intact) and nanometre sized widths.

iii) Exoglucanase hydrolyses the reducing ends, non-reducing ends and soluble intermediates to release low molecular weight intermediates (Kostylev & Wilson, 2012) and finally, secondary hydrolysis of cellodextrins and cellobiose by β-glucosidase to form glucose takes place (Liu, et al., 2009).
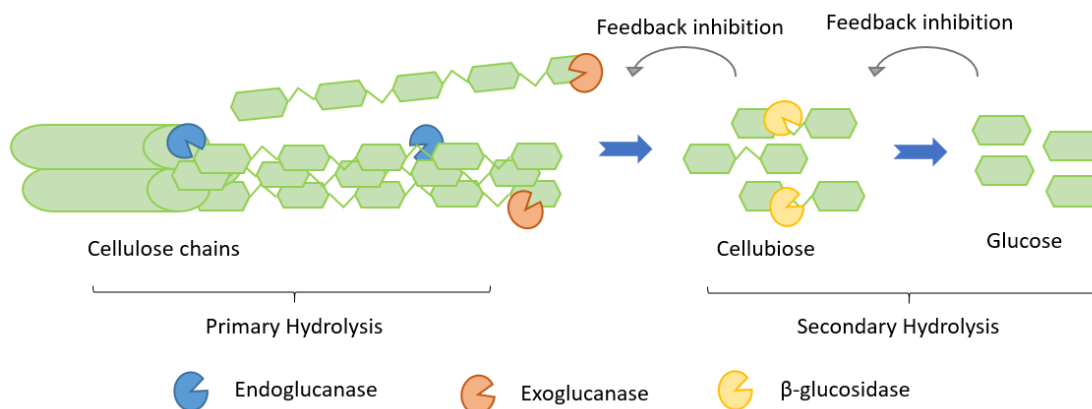
Figure 2.8: Enzymatic hydrolysis with specific action of endoglucanase, exoglucanase and beta-glucosidase, also indicating cellobiose and glucose acting as inhibitors of enzyme activity, redrawn from Gottumukkala & Görgens, 2016

2.2.3.3. Enzyme cocktails for cellulose nanoparticle production

It can be argued for cellulose nanoparticle production, that a cellulase cocktail containing only endoglucanases would be ideal for enzymatic hydrolysis. This would prevent the cellulose loss in form of soluble oligomers and glucose that can pose as inhibitors (so-called feedback inhibition) and affect the product purity. However, it has been found that in the absence of exoglucanases, the effectiveness of cellulose hydrolysis was limited by the lack of synergy (Liu, et al., 2009). Moreover, the use of monocomponent endoglucanase has mainly been used to facilitate the production of MFC (or nanofibrillated cellulose) through mechanical treatments (Ankerfors, 2015; Ankerfors, et al., 2009; Henriksson, et al., 2007).

Optimum ratios of the individual enzymes activities in cellulase preparations are dependent on the desired products as well as the properties of the substrate (Kostylev & Wilson, 2012). PS has lower cellulose crystallinity than that of untreated or natural substrates (Kumar, et al., 2008; Kostylev & Wilson, 2012). For PS hydrolysis, a cellulase cocktail therefore requires a high endoglucanase-to-exoglucanase (endo-to-exo) ratio. This is for removal of the larger quantities of easy-to-react amorphous regions of cellulose fibres to as high an extent as possible, in order to take advantage of the recalcitrant crystalline domains in cellulose fibres to produce non-entangled cellulose nanoparticles.

Endoglucanases termed classical endoglucanases, have a cleft configuration allowing it to randomly cleave amorphous or paracrystalline cellulose, which releases polymer chains of various lengths (Cohen, et al., 2005). Some endoglucanases have the ability to processively cleave internally of the cellulose chains (continually interact with a single chain), releasing soluble oligomers (Kostylev & Wilson, 2012). These cellulase are called processive endoglucanases and are produced amongst others by *Thermomonospora fusca (T. fusca)* and *Saccharophagus degradans* (*S. degradans*) (Watson, et al., 2009).

18

The degrading capability of the exoglucanase is dependent on the concentration of available chain ends (Josefsson, et al., 2008). The two main exoglucanases, Cel7A (CHBI) and Cel6A (CBHII), hydrolyze cellulose chains with a tunnel configuration from the reducing and the non-reducing ends, respectively (Silveira, et al., 2012; Teeri, et al., 1995). Progressive hydrolysis of exoglucanases will expose crystalline or amorphous chains underneath, for further hydrolysis at a smaller fibril diameter (Josefsson, et al., 2008). It is also known that exoglucanases produced by *T.reesei* and *T. fusca* make up approximately 70 - 80% of the total cellulase produced (Herpoël-Gimbert, et al., 2008) and it has been claimed that exoglucanases carry out the most of the digestion work (Kostylev & Wilson, 2012). Therefore, to partially hydrolyse cellulose for short insoluble chain formation and prevent degradation to soluble oligomers, as well as simultaneously incorporating the synergistic effect, the necessity for a high (classical) endoglucanase to exoglucanase ratio is once again emphasized. Furthermore, as complete digestion to glucose is undesired, the ideal cellulase cocktail would not contain β-glucosidase.

Additionally, it is generally preferred to have improved hydrolysis efficiencies, i.e. faster hydrolysis rates and higher enzyme activities. The hydrolysis efficiency of cellulase depends on the adsorption capacity of the cellulases to the substrate. Cellulase enzymes containing catalytic core domains (CD) and cellulose-binding domains (CBD), enhance this absorption capacity to substrates. All *Trichoderma reesei* (*T. reesei*) cellulases, except Cel12A, consist of both a CBM as well as a CD (Karlsson, et al., 2002).

This concludes to a preferred cellulase cocktail for PS hydrolysis to non-entangled cellulose nanoparticles having the characteristics of:

1. Classical endoglucanase activity
2. Absence of β-glucosidase activity
3. A high endoglucanase to exoglucanase activity ratio
4. Enzymes containing catalytic core domains and cellulose-binding domains

Commercial cellulase cocktails, mainly optimised for the production of ethanol, have been used to study the production of cellulose nanoparticles (Song, et al., 2014). Additional to the endoglucanase, exoglucanase and low activity of β-glucosidase in these cocktails, these commercial cellulase cocktails often contain some levels of hemicellulases (Novozymes Bioenergy, 2012; Kádár, et al., 2004).

Commercial application of enzyme hydrolysis of cellulose materials has been discouraged by the high cost of enzymes, decreased reaction rates and very low yields (Kang, et al., 2011). Nevertheless, the utility cost of enzymatic hydrolysis is much lower compared to acid hydrolysis because it is carried out at milder reaction conditions, requires decreased energy inputs, has less side reactions and minimal reactor resistance to corrosion (Marques, et al., 2008). Notably, Novozymes (Denmark) has been able to achieve significant reductions in enzyme costs over the years, from $5.1 per litre in 1999 to $0.2 per litre in 2005 (Destexhe, 2007), and furthermore, the 50 % reduction announced in 2009 (Duran, et al., 2011).

In comparison with acid hydrolysis, enzymatic hydrolysis does not show favourable results in terms of product yield and dispersions (Fattahi Meyabadi & Dadashian, 2012). Furthermore, CNC produced with enzymes have unmodified hydroxyl surface groups similar to CNC produced by hydrochloric acid hydrolysis, leading to unstable suspensions (Mtibe & Muniyasamy, 2016; Anderson, et al., 2014). Other shortcomings include viscosity limitations for high-solids processes, as is desired for economic reasons in industrial scale productions, which result in insufficient uniform mixing and incomplete mass transfer of the enzymes (Ioelovic & Morag, 2012). Yet, the process of enzymatic hydrolysis can be viewed as environmentally friendly as it reduces water consumption as well as toxic, corrosive waste by eliminating the use of hazardous chemicals (Anderson, et al., 2014).

2.2.4. Influence of enzymatic hydrolysis process parameters on cellulose nanoparticle quality and yield

This subdivision describes the operating parameters that influence the production and quality of cellulose nanoparticles with specifically enzymatic hydrolysis as production process.

2.2.4.1. Temperature, pH and agitation

Cellulases are active in the pH range of 4.5 to 7 though the optimum for most cellulases in enzymatic hydrolysis is 4.8 (Walker & Wilson, 1991; Kazimierczak, et al., 2016). Optimum conditions for the cellulase cocktail, Cellic® CTec2, is at an agitation speed of 150 rpm, a pH range of pH 4 – pH 6 and a temperature range of 45 to 55°C (Novozymes Bioenergy, 2012). The monocomponent endoglucanase, FibreCare® R (previously called Novozym 476), has stable activity in a pH range of 5 to 9 (Novozymes, 2016) and has been used at temperatures up to 50°C (Desmaisons, et al., 2017). Therefore, the ideal pH range for enzymatic hydrolysis with these enzymes is 4.5 to 6, and the ideal temperature for enzymatic hydrolysis would be 45 to 50 °C. The addition of sodium citrate or acetate buffers provide the required pH-controlled environments during enzymatic hydrolysis experiments (Lakshmidevi & Muthukumar, 2010).

2.2.4.2. Enzyme Dosage

Boshoff et al. (2016) used Optiflow RC 2.0 (activity of 130 FPU/mL) with optimum enzyme dosages of 11 FPU/g sludge for corrugated recycle PS and 25 FPU/g sludge for virgin pulp PS during bioethanol production. Song et al. (2014) conducted enzymatic hydrolysis with Cellic® CTec2 at even higher dosages of 30 FPU/g dry pulp (activity of 148 FPU/mL) in combination with sonication to successfully co-produce CNF with bioethanol. These results indicated that different feedstock types have different optimum enzyme dosages and therefore wide enough dosage ranges should be investigated. As enzymes are one of the costliest running expenses in any biomass conversion process (Kang, et al., 2011), it is critical to minimize the amount of enzyme used, but still achieve acceptable cellulose nanoparticle yields.

For dosing of monocomponent endoglucanases such as Novozym 476 (Novozym A/S) a preferred enzyme dosages of 0.6 to 100 ECU/g fibres was specified in a patent using enzymatic hydrolysis pre-treatment to mechanical treatment for the production of cellulose nanoparticles from lignocellulosic biomass (Ankerfors, et al., 2007).

2.2.4.3.   Residence time and solids loading

It is desired that enzymatic hydrolysis is conducted at increased biomass solid loading and increased hydrolysis rates for techno-economic purposes (Boshoff, et al., 2016). In this way, it is possible to achieve high concentrations of products which can bring substantial economic savings. However, the viscosity of the system increases substantially at increased solids loading, which results in insufficient mixing and restricted action of the enzymes creating hot spots (Ioelovic & Morag, 2012). Only very low solids loadings (0.5 – 1.5% w/w) have been reported for the enzymatic production of cellulose nanoparticles (Fattahi Meyabadi & Dadashian, 2012; Anderson, et al., 2014). Therefore it is required to test cellulose nanoparticles production at higher solids loadings (3 – 9% w/w).

Due to enzyme deactivation and industrial economic considerations, it is recommended that shorter hydrolysis periods (time of 24 hrs) are used (Song, et al., 2014). Furthermore, the use of commercial cellulase cocktails for longer hydrolysis periods (24 hrs or more), will hydrolyze large portions of cellulose into soluble monomers (glucose and oligomers), and only low amount of submicron cellulosic polymers remain (Ioelovich, 2014). During a study of enzymatic hydrolysis of cellulosic suspensions with commercial cellulase cocktails (Novozyme enzymes), at 5 to 10% (w/w) solids loadings, glucose concentrations increased exponentially within the first 24 hrs (Roberts, et al., 2011). Even for use of a monocomponent endoglucanase in enzymatic hydrolysis to produce cellulose nanoparticles, shorter time than 48 hr hydrolysis is recommended (Fattahi Meyabadi & Dadashian, 2012).

Short hydrolysis processes (1 to 5 hrs) with low enzyme dosages will limit the glucose formation and simultaneously loosen and weaken the structure of cellulose fibres, but will also limit the release of fibrils and nanoparticles. Therefore, for nano-fibrillation of the weakened cellulose fibres, subsequent mechanical treatment is required (Kazimierczak, et al., 2016; Ankerfors, 2015). For studies on cellulose nanoparticle production by enzymatic hydrolysis (with monocomponent endoglucanase) in combination with mechanical treatment, short incubation periods of 0.5 – 8 hrs were used (Pääkkö, et al., 2007; Henriksson, et al., 2007). In order to stop the hydrolysis reaction, enzymes are denatured immediately after hydrolysis with use of a waterbath at 80°C for 15 – 30 min, or in an autoclave at 121°C for 20 min (Kazimierczak, et al., 2016; Ankerfors, et al., 2009).

2.2.4.4.   Substrate and cellulase inhibitors

In a study of cellulose conversion to sugars, it was reported that xylan and lignin strongly inhibit cellulase (Kumar & Wyman, 2014; Visser, et al., 2015), while glucose and oligomers cause feedback

inhibition (Roberts, et al., 2011). Ash content in PS cause further obstruction to enzymatic action (Boshoff, et al., 2016). Therefore, even though PS fibres have already been disengaged from the plant wall matrix, it is desired that non-cellulosic plant materials and ash content is as low as possible for enzymatic hydrolysis. Many agricultural by-products have been used as feedstock to isolate cellulose nanoparticles, such as wheat straw, soy hulls and rice hulls (Yu, et al., 2009). Industrial bio-residue such as pulp sludge (Jonoobi, et al., 2012) and recycled pulp (Filson, et al., 2009) has also been used as feedstock, indicating the potential of substrates with ash components to still be practical feedstocks for cellulose nanoparticle production.

2.2.4.5. Substrate crystallinity

The degree of crystallinity of cellulose is one of the main predictors of the rate of enzymatic hydrolysis (Hall, et al., 2010). An amorphous sample is hydrolysed faster in comparison to a crystalline sample (Park, et al., 2010). Furthermore, it has been found that highly crystalline materials reduce the degree of synergism between subgroups of cellulase enzymes (Kostylev & Wilson, 2012). As waste materials such as PS has been extensively processed, the cellulose crystallinity indices tend to be lower than that of natural lignocellulosic materials (Kumar, et al., 2008; Jonoobi, et al., 2015) or more pure cellulose sources, such as cotton and filter paper (Kostylev & Wilson, 2012). For cellulose nanoparticle production, a balance should be obtained between a high crystallinity which would require higher enzyme dosages and longer hydrolysis times, and a low crystallinity which would result in higher yields of the undesired by-products such as glucose and soluble oligomers.

2.2.4.6. Sterilization

Sterilization is required to prevent undesired bacterial contamination during enzymatic hydrolysis. A reasonable assumption with use of commercial cellulase cocktails can be that it has no microbial load. To prevent bacterial growth, Pääkkö et al. (2007) added 0.4 µL/mL of microbicide, 5-chloro-2-methyl-4-isothiazolin-3-one, to the PS slurry during enzymatic hydrolysis. Autoclaving of dry PS or buffering solutions at 121°C for 15 min in order to kill any contaminants is an alternative to antibiotics addition (Boshoff, 2016a).

2.2.4.7. Purification processes

After hydrolysis, a mixture of hydrolysed celluloses of varying sizes, biomass residue and impurities including enzymatic material and sugars are present in the buffered solution. To isolate the cellulose nanoparticles from this mixture, different purification processes include washing with reverse osmosis (RO)/distilled water and centrifugation, and dialysis.

Washing and centrifugation in multiple cycles separates the cellulose nanoparticles from the residual solids based on the particle interactions with the supernatant solution. Dilution with water, allows for a

neutral pH, favouring cellulosic material-water interactions, which causes the turbid suspension of cellulose nanoparticles. Turbidity is an indication of the presence and high-concentration release of the cellulose nanoparticles (Filson, et al., 2009). A patent on the preparation of cellulose nanofibrils claims that after the alkaline treatment, delignification, enzymatic hydrolysis and homogenization of stalks of annual plants, Büchner funnel filtration and centrifugation at 4000 rpm for 20 min is sufficient to generate the nanoparticle-containing supernatant (Kazimierczak, et al., 2016).

During a study on the enzymatically-mediated sonication of recycled pulp, enzyme-hydrolysed suspensions were centrifuged at 12,000 rpm for 10 min using a superspeed centrifuge. The supernatant was decanted and the cellulose particles from the residual solids obtained by washing repeatedly with deionized water to remove enzyme from the solute until the supernatant turned turbid (Filson & Dawson-Andoh, 2009). From the above studies it is evident that cellulosic nanomaterials can be present in the supernatant, but also in the residual solids, and hence washing of both fractions should be considered.

Dialysis works on the principles of diffusion of solutes in a liquid across a semi-permeable membrane, against RO water for 4 to 7 days, or until neutrality is reached (Beck-Candanedo, et al., 2005). Marino et al. (2015) performed enzymatic hydrolysis on citrus waste for the production of nanocellulose where no denaturing, washing or centrifugation steps were included. Instead, the hydrolysates were filtered before dilution of the bio-residue to around 1% (w/v), and the dilute filtrate was dialyzed against water in a cellulose membrane, and subsequently sonicated. Dialysis membranes with molecular weight cut-off of 8 000-14 000 Dalton are recommended for cellulose nanoparticle purification processes, in order to limit product loss (Wang, et al., 2007). In comparison to dialysis which requires expensive membranes, washing could provide a less costly and much faster cellulose nanoparticle isolating process (Wondraczek, et al., 2013). However, a disadvantage of washing could be product loss, especially at low cellulose nanoparticle concentrations.

The supernatant can be separated from the residual solids with filtration through filter paper in order to isolate nano-sized cellulose particles. Furthermore, ultrafiltration membrane (0.1 μm pore size) to 0.45 μm filter paper membranes have been used in cellulose nanoparticle production studies (Zhu, et al., 2011; Satyamurthy & Vigneshwaran, 2013).

2.2.4.8. Drying processes

One of the largest manufacturing challenges is to obtain dry cellulose nanoparticles while maintaining their nano-scale dimensions, preventing fibre agglomeration. Once dried, it is difficult to re-disperse and preserve many of the properties unique to cellulose nanoparticles. After being dried, cellulose nanoparticles irreversibly assemble into a plastic-like substance. Therefore, a low intensity (low heat) drying process is desired, to prevent particle agglomeration and allow for redispersion (Fairman, 2014).
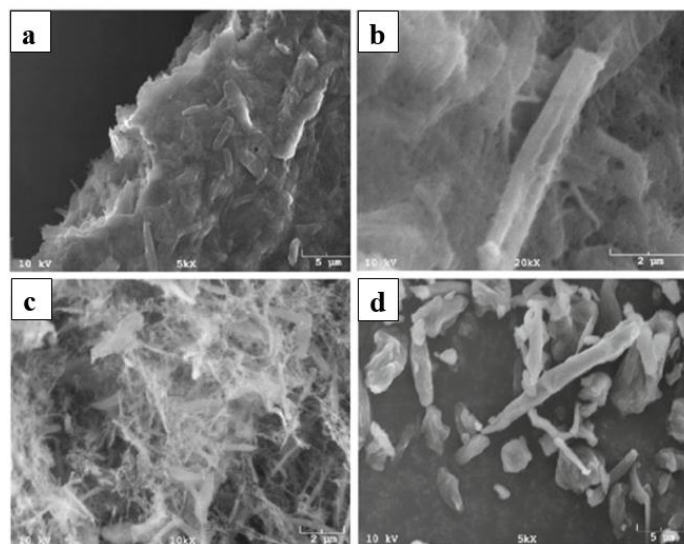
Figure 2.9: Scanning Electron Microscopy images of CNF dried a) oven drying (scale bar 5 µm) b) freeze-drying (scale bar 2 µm) c) supercritical drying (scale bar 2 µm) and d) spray drying (scale bar 5 µm), (images with permission from Peng et al. (2011))

A study by Peng et al. (2011) examined oven drying, supercritical drying, freeze drying (lyophilisation), and spray-drying of CNF, with images portrayed in Figure 2.9. Oven drying is conducted by exposing treated suspensions in a conventional oven with circulating air. To avoid thermal degradation of the fibres, temperature should not exceed 45 °C. A more subtle drying technique is freeze drying that removes water or organic solvents by sublimation after freezing (Salajková, 2013). Spray drying is achieved through multi-fluid atomization as it is mixed with hot air. The suspension film gets disrupted and tiny droplets reduce in size from diameters with several to tens of micrometres (Thybo & Hovgaard, 2008). These droplets then evaporate and subsequent cyclone separation is used to produce a dried powder product from moist air (Peng, et al., 2012). Of the four techniques, spray drying and freeze drying were recommended for their ability to best preserve the cellulose nanoparticle properties.

2.3. Advantages and disadvantages of PS as feedstock to enzymatic hydrolysis for cellulose nanoparticle production

2.3.1.1. Advantages

Limited pre-treatment requirement before enzymatic hydrolysis: Several different pre-treatments have been used for pre-treatment of biomass feedstocks such as woodpulp and other plant material for the production of cellulose nanoparticles. Such pre-treatments include alkali treatments (Marsden & Gray, 1986), delignification (Kumar, et al., 2009), microbial and enzymatic pre-treatments and more (Lai, 2010; Blanchette, 1991; Kumar, et al., 2009).

PS from paper and pulp mills has been subjected to extensive mechanical and chemical processing that removes lignin and hemicellulose (Prasetyo, et al., 2011; Peng & Chen, 2011). Furthermore, the sludge is moderately defibrillated, has a smaller fibre size and therefore has enhanced amenability for

24

enzymatic hydrolysis and can be processed into nano-sizes without pre-treatment, which makes it an ideal feedstock for cellulose nanoparticle production and provides economic benefits to the process (Jonoobi, et al., 2012; Wang, et al., 2010). However, the treatment during papermaking essentially aims to make paper and not to pre-treat cellulosic materials for biological conversion processes (Prasetyo, et al., 2011). Therefore selective pre-treatment should be carefully considered, especially PS from certain mechanical pulping processes which may contain high lignin content.

High feedstock availability: South Africa's paper industry discards around 0.5 million tpa of PS (Dwiarti, et al., 2012). Estimates from the World Wide Fund for Nature predict total paper consumption in South Africa to be approximately 500 million tpa by 2020, indicating that waste generation will increase (Africa Green Media, 2013). This annual stream of waste PS is traditionally land-filled, but is rich in cellulose and hence qualifies as second-generation feedstock for energy and material production.

Industrial waste reduction: By utilizing PS as a feedstock will decrease industrial waste that paper and pulp companies dispose by landfill. This will reduce transport, disposal and other costs related to exceeding of strict waste disposal regulations. Landfill space uptake will be decreased with additional benefits of reduction in water pollution and greenhouse gas (Crespo, et al., 2012).

2.3.1.2.   Disadvantages

High water holding capacity: The water holding capacity (WHC) is a water to substrate ratio (Chen, 2014). High WHC is considered a problem because more water is retained than the mass of dry substrate, which causes limited free water during the process to result in increased viscosities that leads to improper agitation (Fan & Lynd, 2007). The problem continues as it affects disposal. Fisher International reported on world-wide paper and pulp mills dispose of sludge by landfilling (22%), landspreading (24%), and agricultural applications (23%) while the rest are incinerated or sent to other mills. High moisture content sludge results in significant loss of water, which drives legislations further to prohibit landfilling (FisherSolve, 2017).

High inorganic contents: High ash fractions has a limiting effect on the cellulose loading capacity as it lowers the cellulose portion of the feedstock and can also influence compositional analysis (Kang, et al., 2011). During enzymatic hydrolysis, the enzymes irreversibly bind to the ash, as ash-enzyme interaction has a higher affinity than cellulose-enzyme interaction (Chen, 2014), resulting in poor yields (Boshoff, 2015). Therefore washing pre-treatment of high-ash content PS for ash removal is a key focus for enzymatic hydrolysis.

2.4.   Paper and pulp industry in South Africa

Since 1970, the annual growth rate of the South African paper and pulp manufacturing industry has outdone the international average, which has a significant contribution to the nation's economy (FP&M

SETA, 2014). The paper and pulp sector effectively includes the renewable resource sector (plantation forestry), the primary processing sector (pulp milling) as well as the secondary beneficiation sector (paper and pulp products). Paper Manufacturers Association of South Africa (PAMSA) is an industry representative organisation for the major paper and pulp companies operating in South Africa. These include Sappi, Mondi, Kimberly-Clark, Nampak and Mpact (PAMSA, 2012).

In order for the pulp and paper industry to keep up profits it needs to continually invest in material, chemicals and energy saving initiatives. Market penetration of cellulose nanoparticle production in regions such as South Africa is low as compared to North America and Europe due to lack of product awareness and technological matters. The global cellulose nanoparticle market had an estimated value of US$54.9 million in 2014 and is projected to reach US$700 million in 2023 (Transparency Market Research Analysis, 2015). It can therefore be beneficial for the paper and pulp industry to investigate the possibility of firstly, utilizing the large waste streams for cellulose nanoparticle production, secondly, utilization of these cellulose nanoparticles for improved paper and paper products (Besbes, et al., 2011) and simultaneously create job opportunities and minimise the amount of waste generated.

2.5.   Research gaps in literature

Although research has been conducted on the production of cellulose nanoparticles from various feedstocks, little research has been conducted with PS as feedstock (Abraham, et al., 2011; Brinchi, et al., 2013; Filson, et al., 2009). Furthermore, the potential for PS as feedstock for enzymatic hydrolysis, which requires no pre-treatment has been studied for ethanol production (Boshoff, et al., 2016; Robus, et al., 2016), but not for cellulose nanoparticle production.

Literature shows that enzymatic hydrolysis for nanocellulose production is frequently used only as a pre-treatment to mechanical treatment (Pääkkö, et al., 2007; Jonoobi, et al., 2012; Ankerfors, et al., 2009; Lindström, et al., 2007; Kazimierczak, et al., 2016; Henriksson, et al., 2007), or as a combination process with sonication (Song, et al., 2014; Filson, et al., 2009; Fattahi Meyabadi & Dadashian, 2012), or mechanical treatment in combination with enzymatic hydrolysis (Anderson, et al., 2014). Furthermore, the use of commercial cellulase cocktails in different ratios to a monocomponent endoglucanase for cellulose nanoparticle production has not been investigated before. Additionally, short-period enzymatic hydrolysis for the production of cellulose nanoparticles have been recommended by various literature sources (Fattahi Meyabadi & Dadashian, 2012; Fattahi Meyabadi, et al., 2014). This was because partial hydrolysis should result in the production of cellulose nanoparticle-sized particles. Yet, this short-period enzymatic hydrolysis has not been explored up to date. Therefore, investigation of enzymatic hydrolysis processes as a sole treatment need to be conducted. These processes must be able to produce cellulose nanoparticles at reasonable enzyme dosages, hydrolysis times and solids loading, while still resulting in acceptable cellulose nanoparticle median sizes and yields. Factors affecting these hydrolysis processes, and their influence on cellulose nanoparticle PSD and yields, also require further investigation. The

particles produced were comprehensively characterised for proper classification (International Standards Organization, 2017). The commercial cellulose nanoparticle production method of acid hydrolysis were also investigated from the same PS feedstock, as a control process.

2.6. Aims and Objectives

PS from several South African paper and pulp mills has previously been characterised for the production of ethanol through enzymatic hydrolysis processes (Boshoff, 2015; Robus, 2013). The experimental aim of this project is the development and optimisation of a process for cellulose nanoparticles production from waste PS with enzymatic hydrolysis as the integral part.

The objectives followed to achieve this aim:

i.   Investigation of increase in digestibility of organic content of PS feedstock as preparation for enzymatic hydrolysis

ii. Screening of significant process conditions including hydrolysis time, solids loading and enzyme dosages, and selection of preferred commercial cellulase cocktails and/or monocomponent endoglucanase for controlled hydrolysis of PS to cellulose nanoparticles

iii. Statistical design of experiments to develop models for controlled enzymatic hydrolysis of PS to minimise the mean particle size of the cellulose nanoparticles and minimise glucose formation in the products, with input parameters defined from the screening process

iv. Comparison of enzymatic hydrolysis with the conventional acid hydrolysis process, to investigate the characteristics of cellulose nanoparticles produced from PS feedstocks.

v.   Assessment of the effect of microfiltration and high-shear homogenisation as post-enzymatic hydrolysis treatment processes on quality aspects, including the particle size distribution and morphology of the cellulose nanoparticles

vi. Assessment of enzymatically hydrolysed cellulose nanoparticle product washing and - dialysis as recovery processes on purity and yield of cellulose nanoparticles

Chapter 3.   Materials and Methods

3.1.   Experimental approach

The experimental approach, as presented in Figure 3.1, depicts the structure of research approach that was followed for this study. The selection of two PS feedstock (printed recycle PS versus virgin pulp PS) was done based on previous studies by Boshoff et al. (2016). Printed recycle PS has the least amount of fibres due to the high ash component, a PS was selected from this category to demonstrate whether cellulose nanoparticles can be produced, providing assurance that recycled sludge types will work for cellulose nanoparticle production. Therefore, a printed recycled PS, representing the PS from Kimberly Clark Springs was selected as the high-ash content feedstock. For comparison, a virgin pulp PS, containing higher fibre content, a representative of PS from Sappi Ngodwana was selected as the low-ash content feedstock. The printed recycle PS was de-ashed to test for increased organic content and the virgin pulp PS was steam exploded to assess fibre digestibility.

Screening of enzymes for cellulose nanoparticle production was conducted to analyse and compare commercial cellulases, Viscamyl^{TM} Flo and Cellic® CTec2, as well as monocomponent endoglucanases from a commercial enzyme, FiberCare® R, for highest cellulase activity. Enzyme screening for PS hydrolysis was conducted at lower and higher solid loadings (3 and 9% w/w) and different intervals for short-time hydrolysis (0 to 32 hrs). From the two commercial cellulase cocktails, Cellic® CTec2 was selected. The Cellic® CTec2 selection was due to the formation of smaller mean particle sizes of cellulose nanoparticles and minimal by-product (glucose) formation when compared to Viscamyl^{TM} Flo. FiberCare® R provided particle sizes in the same range as Cellic® CTec2, yet with lower by-product formation.

Statistical optimisation on enzymatic hydrolysis of both PS feedstock with different ratios of the Cellic® CTec2 and FiberCare® R was conducted according to a Central Composite Design (CCD) prepared using a Statistica software program. The design was based on smaller mean cellulose particle size (< 500 nm) and lower glucose concentrations (as responses. Validation of the design was done by conducting hydrolysis runs at the predicted optimum conditions for cellulose nanoparticle production.

A set of enzymatic hydrolysis conditions for both PS feedstock were designated for characterisation of post-hydrolysis processes of microfiltration versus high-shear homogenization. This set of conditions was based on 1) enzyme dosage ratios and 2) glucose concentration ranges; and included the optimised conditions for virgin pulp PS and selected conditions for printed recycle PS. For the same set of conditions, post-hydrolysis downstream recovery experiments, including dialysis and washing were conducted with the focus on cellulose nanoparticle quality, purity and yield. Based on experimental findings, a proposed short-period enzymatic hydrolysis mechanism was discussed, specifically for higher

endoglucanase to exoglucanase ratios. Lastly, validation of mass balances were constructed for each feedstock.
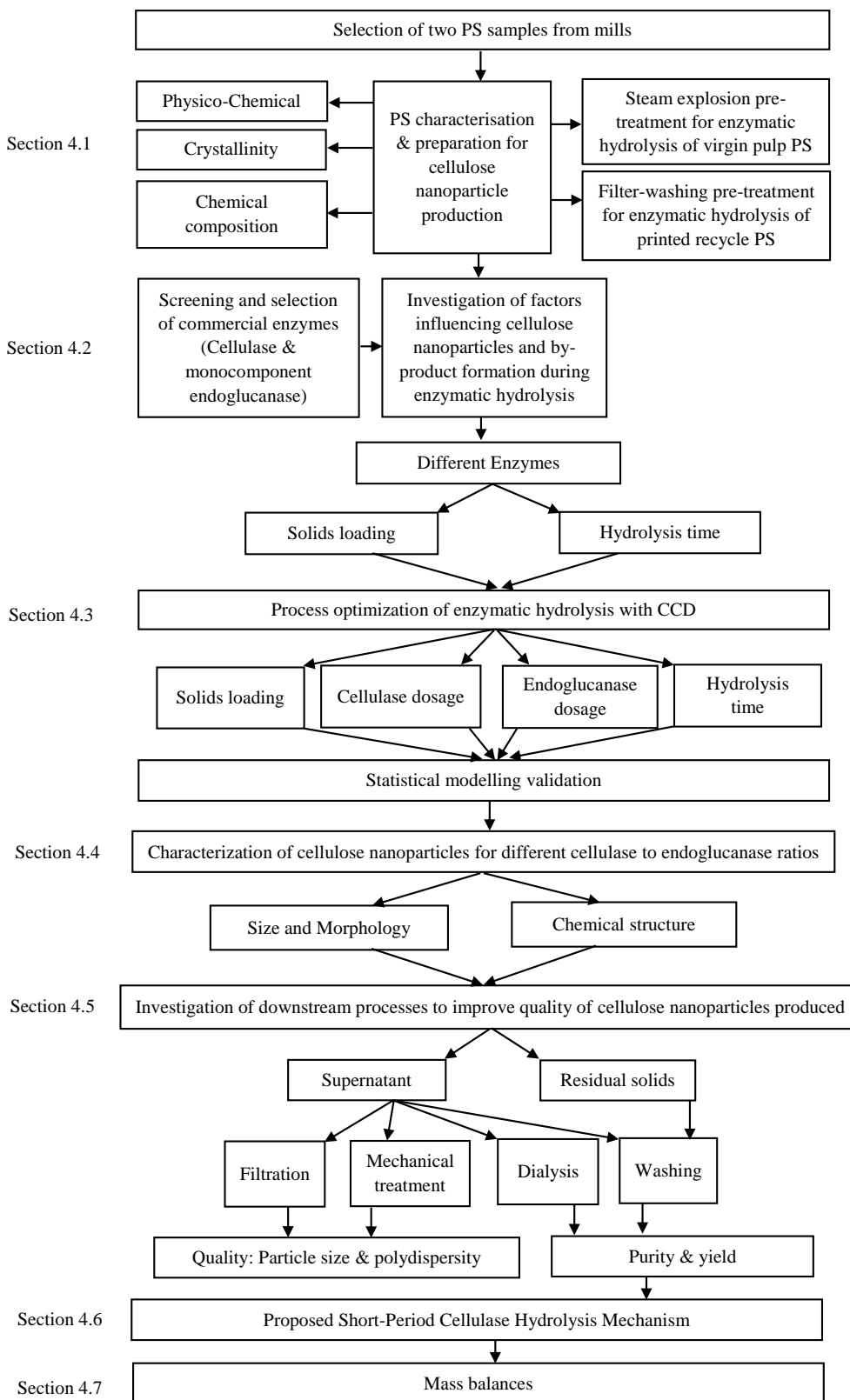
Figure 3.1: Research approach for production of cellulose nanoparticles from waste PS with enzymatic hydrolysis as integral part

3.2. Materials

3.2.1. Paper sludge feedstock

Two PS samples were collected from South African paper and pulp mills, namely a high-ash content PS (± 60% w/w ash content) categorised as printing recycle PS from Kimberly-Clark South Africa (Pty) Ltd (Springs, Gauteng) versus a low-ash content PS (± 10% w/w ash content) categorised as virgin pulp PS from Sappi South Africa Ltd (Ngodwana, Mpumalanga). The PS samples used for enzymatic hydrolysis were air dried in a greenhouse with consecutive convection oven drying at 40 °C until constant weight. Dried samples were quarter-coned according to the standards procedures of National Renewable Energy Laboratory (NREL), milled to particle sizes of less than 6 mm and stored in closed plastic storage bags at room temperature (Hames, et al., 2008).

3.2.2. Enzyme cocktails

Cellic® CTec 2 (Novozymes, Denmark), Viscamyl^{TM} Flo (DuPont Industrial Biosciences, USA) and monocomponent endoglucanase, FiberCare® R (a generous gift from Novozymes, Denmark), supported for cellulose nanoparticle production (Zhu, et al., 2011), were used for the screening experiments. Cellic® CTec2 is an industrial cellulosic enzyme derived from *Trichoderma reesei* consisting of a blend of aggressive cellulases (two main exoglucanases, five different endoglucanases and β-glucosidase) and approximately 10% (w/w) hemicellulases (Novozymes Bioenergy, 2012). Viscamyl^{TM} Flo is a viscosity reducing maltogenic cellulase enzyme blend, which contains some hemicellulases (Enzyme Solutions Pty. Ltd., 2016; Ko, et al., 2015). FiberCare® R is produced from the micro-organism *Humicola insolens*, and unlike many other monocomponent endoglucanases, contains a cellulose-binding domain (CBD), which therefore has greater absorption capacity to substrates (Ibarra, et al., 2010). The cellulose and endoglucanase activities were determined using microplate-based filter paper (FPU) method and carboxymethyl-cellulose (CMC) method, respectively, as developed by Ghose, (1987).

3.2.3. Control samples for cellulose nanoparticles

Commercial CNF and CNC samples produced via mechanical treatment and acid hydrolysis, respectively, obtained from the Process Development Centre (Maine University, US) were used as control samples. CNC particles had declared lengths of 150 – 200 nm and diameters of 5- 20 nm, whereas CNF particles had declared lengths up to several hundred μm and diameters of 50 nm (University of Maine, 2016).

3.3. Methods

Printed recycled PS was washed (for de-ashing purposes) and virgin pulp PS was steam exploded as pre-treatment processes to enzymatic hydrolysis. Both PS feedstock were subjected to enzymatic hydrolysis followed by centrifugation and vacuum-filtration. After vacuum-filtration, the sample was

split into two parts; 1) the filtrate, referred to as supernatant, and 2) the filtered cake (referred to as the residual solids). The supernatant was subject to different downstream processes including centrifugation-washing, dialysis, micro-filtration and homogenization in order to investigate the effect of each process on the quality of the cellulose nanoparticle product. The residual solids part was subject to centrifugation-washing. Figure 3.2 shows the flow diagram of cellulose nanoparticle production with enzymatic hydrolysis as the integral part, including the considered downstream quality-improvement processes.
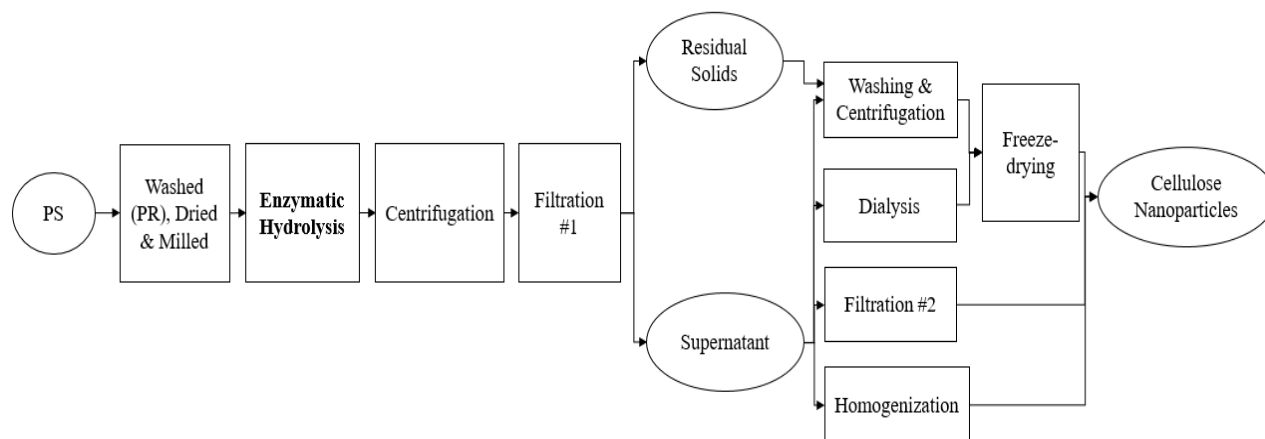
Figure 3.2: Process flow diagram of cellulose nanoparticle production with enzymatic hydrolysis of paper sludge (PS) as integral part with downstream processes considered to test for quality, purity and yield

3.3.1. Pre-treatment of paper sludge from different milling operations

3.3.1.1.   Ash removal of high-ash paper sludge

Ash removal from the high ash-content PS is required to make it a feasible feedstock for bioprocess conversion. This pre-treatment is referred to as PS de-ashing or PS filter-washing.

A de-ashing protocol from Tappi (1995) described an aqueous PS slurry made up (20 g/L) and disintegrated for 37500 revolutions, thereafter washed over a 200 µm filter screen until the supernatant was clear. Disintegration is required to mix the dried PS into a slurry, and dissolving the inorganic materials (ash) for separation over a filter sieve. This protocol was adapted for optimal small-scale PS de-ashing. Ash content was determined by furnace combustion at $575 \pm 25°C$ (Sluiter, et al., 2005a).

Larger quantities of printed recycle PS at a consistency of 20 g/L were disintegrated with a British Pulp Evaluation Apparatus, Mavis Engineering, London (located at Wood Science Department of Stellenbosch University) for 3750 revolutions and filter-washed with distilled water over a 190 µm sieve until the clay-like slurry appears to have a wet tissue nature, and the supernatant became clear. Washed sludge was dried overnight at 40°C in a convection oven.

3.3.1.2.   Steam explosion of low-ash paper sludge

A mass of 500 g of the virgin pulp PS (with longer fibres and higher water holding capacity than printed recycle PS) was soaked overnight in distilled water, spin-dried in a spin-dryer (AEG, Germany) and loaded into a steam explosion unit (Steam Gun STG 19-40, Austria) with a 19 L vessel reactor. The PS types were steam treated with conditions as set out in Table 3.1. A built-in automated panel display (IAP, Germany) was used to control the steam treatment. After treatment, the whole slurry from the pre-treatment was pressed manually using an air-press/hydraulic jack to obtain a separate pressed solid product. The slurry was spin-dried, weighed and dried at 40°C for three days for use in enzymatic hydrolysis. The solids were characterised using the NREL standard laboratory analytical procedures for biomass analysis (Sluiter, et al., 2011).

Table 3.1: Experimental conditions for steam explosion of low-ash paper sludge

Run	T	t	Soaked
	°C	min	
1	200	10	Yes
2	200	5	No
3	200	10	No
4	210	5	No
5	210	10	No

Steam exploded PS was subjected to enzymatic hydrolysis with use of Cellic® CTec2 (dosed at 25 FPU/gdPS) for a hydrolysis time of 24 hrs in an incubator at 150 rpm and 50 °C. An antibiotic, Ampicillin (Sigma-Aldrich, South-Africa), was further added at the concentration of 100 mg/L to prevent any bacterial growth throughout hydrolysis.

3.3.2. Cellulose nanoparticles production by enzymatic hydrolysis of paper sludge

3.3.2.1.   Enzyme activity assays

Filter paper strips (Whatman No. 1) were used as substrate for determination of the cellulase activities according to the filter paper assay (FPA) method of Ghose (1987). 1 mL of 0.05 M Na-Citrate solution (pH 4.8) were added to a 25 mL test tube. 0.5 mL of enzyme was diluted with citrate buffer. Six dilutions were made of each enzyme investigated. A water bath was heated to 50°C and the filter paper strips of 0.5 g were added to each test tube. All the tubes were incubated for 60 minutes at 50°C. A volume of 3 mL DNS were added to each test tube and boiled for 5 min. The reaction mixture was diluted with water in ratio of 1:4. The colour developed was measured against a spectro zero sample at a wavelength of 540 nm.

Endoglucanase activity was measured by the CMC assay as developed by Ghose (1987). A volume of 0.5 mL enzyme, diluted in 0.05 M Na-Citrate solution at a pH of 4.8 was added to a test tube (25 ml).

A water bath was heated to 50°C. A volume of 0.5 mL 2% CMC solution was added to each test tube and well mixed. All the test tubes were incubated at 50°C for 30 min. A volume of 0.3 mL DNS was added, well mixed and transferred to rack on table. The test-tubes were boiled for 5 min. The reaction mixture was diluted with deionised water in ratio of 1:4. The colour developed was measured against a spectro zero sample at a wavelength of 540 nm.

For both assays, the reagent blank was used to calibrate the spectrometer to zero absorbance. The spectro zero sample was prepared by the same stepwise procedure as above but without enzyme and substrate addition. Also, the substrate blank was prepared by the same procedure but without substrate addition, and the enzyme blank was prepared without enzyme addition. The glucose standards were prepared in the same way as the reagent blank but with glucose at different concentrations. The activities for cellulase and endoglucanase were calculated and expressed as FPU/mL and ECU/mL respectively, according to Ghose (1987) standard methods. To calculate the activity in FPU and ECU, the construction of a linear glucose standard curve was plotted against A_{540}.

3.3.2.2. Enzymatic hydrolysis of paper sludge

Stock solution of sodium citrate buffer was made-up to a concentration of 1 M with 60 g NaOH (Radchem Laboratory Suppliers), 210 g citric acid monohydrate (Merck, South Africa) and RO water to a pH of 4.3. The working concentration of the buffer was made by diluting with RO water to a concentration of 0.05 M and pH 4.8. Enzymatic hydrolysis was carried out for different hydrolysis times (> 32 hrs) in 250 mL (100 mL reaction volume) Erlenmeyer flasks at 50°C and 150 rpm (MRC Orbital shaker TS600, United Scientific, South Africa). Before addition of enzymes to the Erlenmeyer flasks, the flasks with dry solids, and the citrate buffer were autoclaved at 121°C for 15 min as sterilization step. An antibiotic, Ampicillin, was further added to each flask (100 mg/L) to prevent any bacterial growth throughout hydrolysis. The pH of the slurry was in the range of pH 4.8 – pH 6 and was not adjusted.

After hydrolysis, the enzymes were denatured by placing the Erlenmeyer reactor flasks in a water bath at 80°C for 30 min. The hydrolysed sample was decanted into 50 mL Greiner tubes for centrifugation (Lasec Hermle, electric benchtop centrifuge, max 8000 rpm) at 4000 rpm for 30 min and the supernatant containing cellulose nanoparticles was vacuum filtered with a Büchner funnel through a 1.6 μm glass-membrane filter (47 mm cellulose acetate (CA) membranes; Lasec, South Africa).

3.3.3. Cellulose nanoparticles isolation by acid hydrolysis of paper sludge as control process

A PS suspension (5% w/w, in deionised water) in a 200 mL glass beaker (working volume of 60 mL) was left to stand overnight. Acid hydrolysis was conducted by dripping 60 mL H_2SO_4 into the PS-suspension with a pipette over a period of 60 min (at a rate of 1 mL/min), to achieve a total working volume of 120 mL at 2.5% (w/w) consistency. During the acid-addition period (exothermic reaction), the

glass reactor was cooled in an ice-bath where the melting ice was continually drained and replaced with more ice. The glass reactor was removed from the ice-bath and placed in a water bath on a heating plate. This acid-PS suspension was temperature controlled in the water bath on a heating plate at 50 °C for 90 min. An overhead stirrer at 900 - 1000 rpm mixed the slurry continuously throughout the total hydrolysis (150 min).

After air-cooling to room temperature, the acid-PS suspension was washed. With each washing step, a 50 mL centrifuge tube was filled with acid-PS suspension and deionized water in a ratio of 1:5, and vortexed. The tubes were centrifuged (Labotec, Universal 320R electric benchtop centrifuge, max 8000 rpm) at 5000 rpm for 5 min, and the clear suspension was discarded. Deionised water was added in the same ratio, vortexed and centrifuged again. The procedure was repeated a third time until the supernatant became turbid, indicating cellulose nanoparticles dispersion in the supernatant. The turbid supernatant was sampled. The washing steps were repeated another 3 times, or until the supernatant became clear and the pH reached pH 7, indicating that all cellulose nanoparticles were removed from the sample. The cellulose nanoparticles suspension was thereafter dialysed in distilled water with 12.4 kDa dialysis tubing in a jar with magnetic stirring at 100 rpm (at room temperature). The distilled water was changed every 3 hrs for 5 days. The pH was adjusted to pH 6.5 – pH 7 with 0.001 M NaOH addition, and the suspension was dialysed for another 2 days to remove the remaining salts. The dialysed sample was freeze-dried.

3.3.4. Downstream purity-improvement processes

3.3.4.1. Microfiltration

To improve the particle size distribution, exclusion of the large particles by microfiltration was considered. The glass-membrane filtered supernatant (which removed the large particles) was further vacuum filtered through a 0.45 µm filter membrane (47 mm CA membranes; Lasec, South Africa) to isolate a suspension with cellulose nanoparticles smaller than 500 nm in length.

3.3.4.2. Homogenization of selected enzyme hydrolysed samples

For investigation of improvement of particle size distribution, post-hydrolysis mechanical treatment was conducted. Centrifuged and glass-membrane filtered supernatant samples were homogenized with a high-speed homogenizer (handheld PRO250, Pro-Scientific, USA). These samples in 15 mL tubes (working volume of 8 mL) were cooled in an ice-bath and homogenised at 14 000 rpm. To minimise aerosol and foam-formation, the homogenisation was conducted in three 10 min cycles (to a total of 30 min), with latent periods of 2 – 3 min between cycles.

3.3.4.3. Dialysis

For purification of the hydrolysed, centrifuged and glass-membrane filtered suspensions, dialysis was conducted. For selected samples, 15 mL supernatant was dialysed against RO water with dialysis

tubing (molecular weight cut-off of 12.4 kDa, 43 mm flat diameter) for 4 - 5 days until the pH reached neutrality. The tubing was double-folded and sealed with plastic clips at each end to ensure no leakage of sample. The samples were placed on a magnetic stirring plate at 100 rpm throughout the dialysis period. The RO water was changed every three hrs on the first day and every 12 hrs thereafter for the remaining days. Dialysed suspensions were freeze-dried for analysis.

3.3.4.4.   Washing of hydrolysate and residual solids samples

The supernatant as well as the residual solids of selected samples were separately subjected to washing in order to purify and isolate the cellulose nanoparticles produced. For the supernatant, 25 mL RO water was added to ±15 mL supernatant sample and centrifuged for 15-20 min at 8000 rpm per cycle. The aim was to capture the cellulose nanoparticles and discard of the top layer of liquid. This was repeated twice, to collect the cellulose nanoparticle-containing bottom layer (± 10 - 15 mL) of the liquid.

For the residual solids, the aim was to suspend the entrapped cellulose nanoparticles to the supernatant by centrifugation and collect all the supernatant. 25 mL RO water was added to the residual solids and vortexed for 1 - 2 min. Three centrifugation cycles were conducted for 15 min at 4500 rpm per cycle, after which the supernatant was sampled individually after each run. Washed suspensions were freeze-dried for subsequent analysis.

3.4.   Analytical methods

Cellulose nanoparticles can possess different dimensions and morphologies, even in the same nanoparticle category, i.e. CNC or CNF. They are composed of various structural components: nanofibres (nanoscale), fibrillated fibres (micrometre scale), and fibres (millimetre scale) resulting from incomplete hydrolysis during enzymatic hydrolysis (Bondeson, et al., 2006). In order to characterize and compare the cellulose nanoparticle product to standard or commercially produced products, the morphology, shape, purity, crystallinity, polydispersity and the agglomeration were considered.

SEM give direct multi-dimensional information about nanofibril morphology and structural properties (Desmaisons, et al., 2017). The downfall of these techniques is that they focus only on nanoscale regions and consequently miss information. On the other hand, DLS has the advantage of accounting for the mean size of all the particles in the sample, yet the disadvantage is that it does not account for particle agglomeration. Microscopy in combination with the DLS results would be able to provide advanced insight to the morphology of the cellulose nanoparticles. An exact size to the decimal point is not realistic for nanoparticle size description; instead, ranges are of more importance.

3.4.1. Compositional analysis

Triplicate PS samples of each feedstock were randomly selected from each quarter-coned batch for chemical composition analysis using NREL methods (Sluiter, et al., 2011). Moisture content of the PS samples were determined gravimetrically by oven drying at $103 \pm 2°C$. The ash content analysis of each PS was conducted by furnace combustion at $575 \pm 25°C$ for four hrs (Sluiter, et al., 2005a). Chemical composition of the PS (structural carbohydrates, acid-soluble lignin, acid-insoluble lignin and extractives) was determined using the summative mass closure procedures for pre-treated slurries provided by NREL (Sluiter, et al., 2008; Sluiter & Sluiter, 2011). Sugar content of the PS was determined by high performance liquid chromatography (HPLC) fitted with an Aminex HPx-87 column and AutoSampler (Thermo Scientific Products, Bio-Rad, South Africa). The column was operated at a temperature of $65°C$ with 5 mM H_2SO_4 as the mobile phase (at 0.6 mL/min). The acid-soluble lignin composition in the PS was determined by spectrophotometry at 205 - 320 nm (Sluiter, et al., 2011).

3.4.2. Water holding capacity

The WHC was determined with an adapted method from Boshoff (2015) for both the PS feedstock milled to less than 6 mm sizes. The milled PS samples were oven dried to constant weight at $103 \pm 2°C$. 30 mL of RO water and 3 g of PS was added to 50 mL Greiner tubes and the slurries stood overnight at room temperature. The slurry sample tubes were centrifuged at 4000 rpm for 15 min and the excess water carefully decanted, without external force applied. The pellet was weighed before and after drying at $103 \pm 2°C$ until constant weight, and cooled in a desiccator for 30 min. The WHC was determined with Equation 1.

Equation 1:
$$WHC \left[\frac{ml\ dH_2O}{g\ substrate} \right] = \frac{wet\ PS\ (g) - oven\ dried\ PS\ (g)}{oven\ dried\ PS\ (g)}$$

3.4.3. Particle size measurement and polydispersity index analysis

The particle size distribution and the polydispersity index (PdI) of the cellulose nanoparticles particles in dilute suspension (<0.01% (w/w), diluted with Millipore water) were analysed using a Zetasizer® Nano-ZS90 size analyser (Malvern Instruments). The instrument employs a design which allows for multi-angle particle size analysis by dynamic light scattering (DLS) (Malvern Instruments Ltd, 2004), accurately measuring *mean* particle sizes between 0.3 nm and 5 µm. Please note that the mean particle size indicates a single-value average size over the particle size distribution, and NOT an absolute value which often refers to the maximum size. Triplicate measurements were carried out each after 120 seconds of temperature equilibration time and using He–Ne laser at a wavelength of 633 nm and at a scattering angle of 90° at a temperature of 25°C. The intensity-weighted mean hydrodynamic diameter was calculated from intensity autocorrelation data peaks with a programmed cumulant method using software provided with the instrument, where intensity peaks representing the majority of the particles were used to determine mean particle length. A control sample of CNC was analysed in triplicates,

resulting in a mean particle size of 168 ± 7 nm, which is in the range of the declared 150 – 200 nm, indicating that the dimension of length is reported through DLS.

The PdI is a dimensionless measure of the broadness of size distribution computed from the cumulant analysis. This PdI value range from 0 to 1.0. A PdI value < 0.08 indicates a closely monodispersed sample, while a larger PdI value of > 0.7 designates a very broad distribution of particle sizes (International Standards Organization, 2008).

3.4.4. Scanning electron microscopy (SEM)

SEM available at the Central Analytical Facilities (Chamber of Mines Building, Stellenbosch University) was used to examine and capture images of untreated, enzyme hydrolysed, acid hydrolysed and control CNC/CNF samples. The Zeiss MERLIN Field Emission Gun with a tungsten crystal was used to capture images under ultrahigh vacuum conditions at an accelerating voltage of 5 kV or higher for a focused nano-field of up to 1 nm. Specimens for SEM were prepared by four preparation protocols, for optimisation of the microscopy. The first protocol consisted of drying (overnight in a desiccator) drops of the dilute aqueous suspensions of freeze-dried particles on aluminium mounts. For the second protocol, sample without any resuspension was mounted on aluminium stubs. For the third and fourth protocol, suspended freeze-dried particles were mounted with/without double-sided carbon tape covered with a drying agent, bis(trimethylsilyl)amine (HMDS) and dried overnight. All SEM specimens were sputter-coated with gold particles to provide adequate conductivity.

Particle diameters and length were measured using Image J (National Institute of Health) and SEM_Img_Studio (National Instruments LVRunTime Engine, version 7.1) imaging software. The software comprises of digital image processing tools and includes adequate tools that facilitate quantitative size measurements. An average of 100 measurements were performed for 3 - 5 images per sample, with a representative processed image in Appendix B.

3.4.5. Scanning Transmission Electron Microscopy (STEM)

The Zeiss MERLIN Scanning Transmission Electron Detector Field Emission Gun (STEM-FEG) at Central Analytical Facilities (Chamber of Mines Building of Stellenbosch University) was used for imaging of hydrolysed and freeze-dried samples. A drop of diluted suspension was dried on a carbon-coated copper grid in a desiccator. To enhance the imaging contrast, the grid was placed in a 2% (w/w) uranyl acetate solution for 3 min. Samples on the grid were dried in a fumehood over night at room temperature before examination.

3.4.6. X-ray diffraction (XRD)

The non-constructive analysis of X-ray diffraction were used for cellulose crystallinity measurements. X-ray diffraction patterns of the PS were obtained using a Bruker D2 Phaser X-ray diffractometer with Cu tube ($\lambda = 1.5418$ Å) and 30 kV (10 mA) X-ray radiation. The diffractive intensities were recorded from 5° to 40° 2θ angles. Various methods of estimating relative cellulose crystallinity exists, of which the Segal peak height method is the most popular (Park, et al., 2010). The crystalline index of cellulose, C_{Ir}, was determined by use of the Segal empirical peak height method from Equation 2 (Nam, et al., 2016):

Equation 2
$$C_{Ir(\%)} = \frac{I_{200} - I_{am}}{I_{200}} \, x \, 100$$

I_{200} is the peak intensity corresponding to crystalline cellulose, and I_{am} is the peak intensity of the amorphous fraction, at 2θ of around 22 – 27° and 18°, respectively.

3.4.7. High-performance liquid chromatography

Monomeric sugar (glucose, arabinose, xylose and cellobiose) concentrations were analysed through HPLC instrumentation fitted with an Aminex HPx-87 column, a cation-H Micro Guard Cartridge and RI-101 detector (Thermo Scientific, Bio-Rad, South Africa). The column was operated at a constant temperature of 65°C and 5 mM H_2SO_4 as a mobile phase with a flowrate of 0.6 mL/min.

3.4.8. Energy dispersive X-ray spectroscopy

Elemental identification and semi-quantification was conducted at Central Analytical Facilities (Chamber of Mines Building, Stellenbosch University) with Energy dispersive X-ray spectroscopy (SEM-EDX) (Zeiss MERLIN) for selected washed and freeze-dried samples. Freeze-dried samples were dispersed in Millipore water (< 0.1% w/w) and a droplet was allowed to dry on a polished aluminium (Al) stub in a desiccator overnight. Samples were gold (Au) coated for increased conductivity. Chemical mapping and selected target point analysis were conducted for duplicate samples under ultrahigh vacuum conditions and an accelerating voltage of 20 kV at an electron beam width distance of 9.5 mm, with Au and Al identification removed from analysis. With SEM-EDX, hydrogen (H) could not be analysed.

3.4.9. Fourier Transform Infrared Spectroscopy (FTIR)

FTIR spectra of the cellulose nanoparticles produced, the standard samples and the control samples were measured using the attenuated total reflectance (ATR) mode on a Thermo Nicolet Nexus 670 spectrometer (with Smart Golden Gate Accessory). A total of 32 cumulative scans were recorded, with a resolution of 4 cm^{-1}, in the frequency range of 4000 - 600 cm^{-1}. For each condition, duplicate measurements were made.

3.5. Experimental design

3.5.1. Screening

Screening of the enzymatic hydrolysis of PS feedstock with the three different commercial enzymes (Cellic® CTec2, Viscamyl™ Flo and FiberCare® R), was conducted at a high (9% w/w) and a low (3% w/w) level of solids loading to test the cellulose nanoparticles production at low and high solids loadings. Thereafter, screening of the three enzymes was conducted with different hydrolysis time periods (up to 32 hrs) where 1.5 mL volume samples were taken at regular time intervals.

3.5.2. Enzymatic Hydrolysis Optimisation

Statistica, (TIBCO Software Inc., version 13.2), was used to design a CCD with four variables each at three levels. The experimental data from the CCD design was used to set up models and optimise the process factors affecting (1) the mean particle size (nm) and (2) glucose concentration (g/L) of the hydrolysed PS feedstock. The four variables are: (1) solids loading, (2) hydrolysis time, (3) ratio of monocomponent endoglucanase enzyme concentration to mass of PS and (4) ratio of commercial cellulase cocktail to mass of PS were explored. To reduce the number of treatments in the CCD design, a fractional factorial experimental design with six repeat runs of the centre points was used. A total of thirty runs for both feedstock was generated by this experimental design.

3.6. Calculations

3.6.1. Yield: Gravimetric analysis of scale-up experiments with freeze-drying

The theoretical yield of cellulose for ideal hydrolysis without complete hydrolysis to glucose and other oligomer by-products, is calculated by Equation 3, taking into account the unhydro correction factor.

Equation 3
$$Y_{theoretical} (\%) = glucan\ fraction * \frac{162 \frac{g\ cellulose}{mol}}{180 \frac{g\ glucose}{mol}} \times 100$$

A set of enzymatically hydrolysed samples with scaled-up working volume of 250 mL were collected and purified with the downstream processes specified in Section 3.3.4. Approximately an eighth of the hydrolysed sample was freeze-dried, weighed and calculated to the full volume of the sample. It was assumed that the eighth of the sample was representative of the entire sample and that a homogeneous distribution of particles existed. This up-scaled method was to accommodate the gravimetric calculation of the very low yields (Y_1) of cellulose nanoparticles that were found for enzymatic hydrolysis of PS feedstocks, as presented in Equation 4.

Equation 4:
$$Y_1 (\%) = \frac{Weight\ of\ dried\ nanocellulose\ (g)}{Weight\ of\ initial\ PS\ solids\ loading\ (g)} \times 100$$

For purification of hydrolysed and glass-membrane filtered *supernatant* (filtrate), 20 - 25 mL of the supernatant was diluted with RO water to a total volume of 40 mL. The diluted supernatant sample was centrifuged for 15-20 min at 8000 rpm with the aim to settle the cellulose nanoparticles and drain the impurities. The top layer was drained, and the process was repeated twice.

3.6.2. Statistical analysis

All statistical calculations of replicated measurements (means and standard deviations) were conducted in the software program, Excel (Microsoft Office, 2016).

Response Surface Methodology (RSM) is a statistical function of Statistica comprising of a collection of statistical and mathematical procedures that can be used to model the response of a system affected by numerous variables to predict the interaction between the four independent variables, commercial cellulase cocktail dosage, monocomponent endoglucanase dosage, solids loading and hydrolysis time, and the response variables; mean particle size and glucose concentration.

By use of desirability surface and contour plots developed with the experimental data on Statistica software, the effects of the independent variables on the overall multi-response desirability were interpreted. The desirability function entails assigning a desirability value to each dependant variable with 0 being very undesirable to 1 being very desirable. Statistical significance was reported with $p < 0.05$ (for a 95% level) and was determined with analysis of variance (ANOVA) using Statistica software. The percentage error of the model predictions in comparison to the experimentally determined values were calculated from Equation 5.

Equation 5: $$Error\ (\%) = \frac{(theoretical\ value) - (experimental\ value)}{(theoretical\ value} \times 100$$

Chapter 4.   Results and Discussion

4.1. Paper sludge characterisation and preparation for enzymatic hydrolysis

4.1.1. Paper sludge chemical composition

The chemical composition of the two selected PS feedstock are compared in Table 4.1 as determined by NREL analytical methods (Hames, et al., 2008). The virgin pulp PS has a high average glucose fraction of 0.61 g/g substrate, together with a low ash fraction of 0.08 g/g substrate, resulting in the higher theoretical cellulose nanoparticles yield of 55.6% (w/w from initial glucan content as determined with Equation 3). In comparison, the printed recycle PS has a low theoretical cellulose nanoparticles yield of 15.5% (w/w), due to an ash fraction of 0.625 g/g substrate. The high ash content was due to recycled waste paper utilized as feedstock at the mill (U.S. Congress, 1989). This showed that a de-ashing pre-treatment step was required for the printed recycle PS which was not essential for the virgin pulp PS. The ash and glucan fractions for printed recycle and virgin pulp PS correlated very well with the fractions obtained by Boshoff et al. (2016). In the study, compositional analysis reported 0.53 – 0.62 g ash/g substrate and 0.11 - 0.18 g glucan/g substrate for printed recycle PS from Kimberly-Clark, while virgin pulp PS from Sappi Ngodwana contained 0.08 – 0.10 g ash/g substrate and 0.43 - 0.50 g glucan/g substrate (Boshoff, et al., 2016).

Table 4.1: Chemical composition of PS feedstock (on dry basis) selected for cellulose nanoparticle production. Averages were determined from single measurements of triplicate samples. All standard deviations for the compositions of were determined as < 0.64% (w/w).

Sludge	Ash	Extractives	Lignin	Glucan	Xylan	∑Components
	% (w/w)	% (w/w)	% (w/w)	% (w/w)	% (w/w)	% (w/w)
Printed recycle	62.46	4.61	8.97	17.09	4.23	97.36
Virgin pulp	8.26	7.09	15.33	61.20	14.06	105.7

4.1.2. Effect of filter-washing on removal of ash from paper sludge

The aim of PS filter-washing was to reduce the ash content in the printed recycled PS (Table 4.1). This was firstly, to increase the cellulose content per solids loading of feedstock for hydrolysis. Secondly, seeing as ash has been found to have an inhibitor effect on cellulase activities (Kang, et al., 2011), the filter-washing was to increase fibre susceptibility to enzymes for hydrolysis to produce cellulose nanoparticles.

Washing with a 190 µm sieve mesh filter (the closest available to 200 µm sieve mesh filter) resulted in 55.6% (w/w) ash reduction to achieve an averaged ash fraction of 0.277 g/g substrate (Table 4.2). Similar results were found by Robus (2013) where washing of high ash-content PS decreased the ash fraction with 56.3 – 65.5% (w/w). The decrease in ash content resulted in more than two-fold increase in

the glucan fraction on a mass basis (Table 4.2), from which could be concluded that filter-washing removed sufficient amounts of ash for the washed PS to be classified as the low-ash sludge type ($< 30\%$ w/w dry basis) (Ochoa de Alda, 2008). The xylan content followed the same trend with an approximately two-fold increase, however the lignin and extractives content did not increase by two-fold. It is possible that the lignin and extractives, which had been subjected to pre-treatment during pulping at the mills, had partially been washed away in the $CaCO_3$-water (with increased pH). The theoretical yield of nanocellulose (as determined by Equation 3) was 37.6% (w/w) which was more than twice the yield obtained from unwashed printed recycle PS (17%, Section 4.1.1). This should result in higher cellulose nanoparticle yields during enzymatic hydrolysis.

Table 4.2: Chemical composition of untreated versus washed printed recycled PS with optimised washing conditions. Averages were determined from single measurements of triplicate samples. All standard deviations for the compositions were determined as $< 0.48\%$ (w/w).

Printed Recycle Sludge	Ash % (w/w)	Extractives % (w/w)	Lignin % (w/w)	Glucan % (w/w)	Xylan % (w/w)
Untreated Sludge	62.46	4.61	8.97	17.09	4.23
Washed Sludge	27.71	5.18	9.05	41.37	7.06

4.1.3. Water holding capacity of paper sludge feedstock

WHC is of importance because water adds to the bulk of the material, increasing landfilling disposal costs and water losses to the environment. For bioprocesses, it gives indication to slurry viscosities, which might lead to improper agitation and mass transfer during hydrolysis (Fan & Lynd, 2007).

Figure 4.1 indicates the WHC of printed recycled PS being low (5.08 L/kg PS) compared to that of virgin pulp PS (7.53 L/kg PS). This correlates well with the WHC of 4.5 L/kg PS for printed recycle PS reported by Williams (2017) and the WHC of virgin pulp PS of 8.61 L/kg PS by Boshoff et al. (2016).
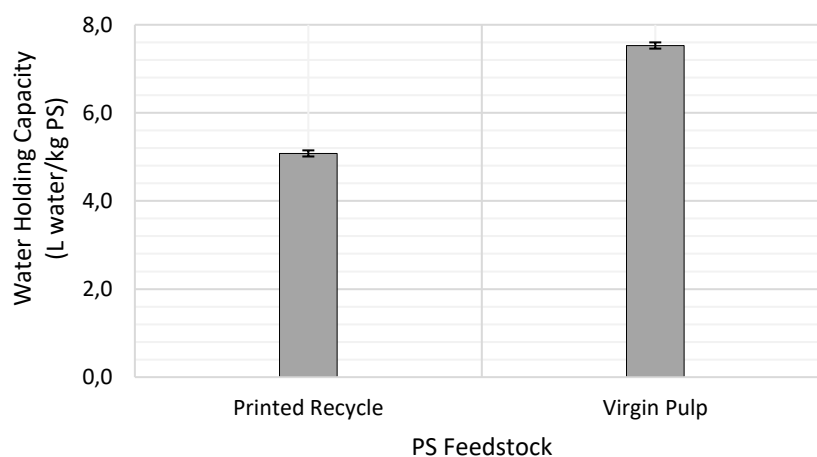
Figure 4.1: Water holding capacity of washed printed recycled PS and virgin pulp PS feedstock. Error bars indicate the standard deviation of single measurements of triplicate samples.

The morphology of the two PS fibre types could explain the smaller WHC values for PS from printed recycle operations when compared to virgin pulping operations. In chemical pulping, particularly with Kraft pulping as in the case of the virgin pulp PS, the lignin and hemicelluloses are dissolved, with intact cellulose chains remaining (Migneault, et al., 2011). Through mechanical pulping, fibres are torn and become brittle during the defibrillation phases of refining, resulting in shorter fibres in comparison to that found in PS from chemical pulping (U.S. Congress, 1989). This was confirmed by particle sizing of both feedstock through SEM imaging (Figure 4.2). Printed recycle PS fibres had lengths of 100 – 300 µm, while that of the virgin pulp PS was in the range of 500 – 1000 µm, as estimated with Image J imaging software (Figure 4.2). Printed recycled PS, which have undergone multiple processing cycles through various processes such as mechanical or/and chemical pulping, will retain less water than that of the longer fibres from virgin pulping operations (Miyamoto, et al., 2009).
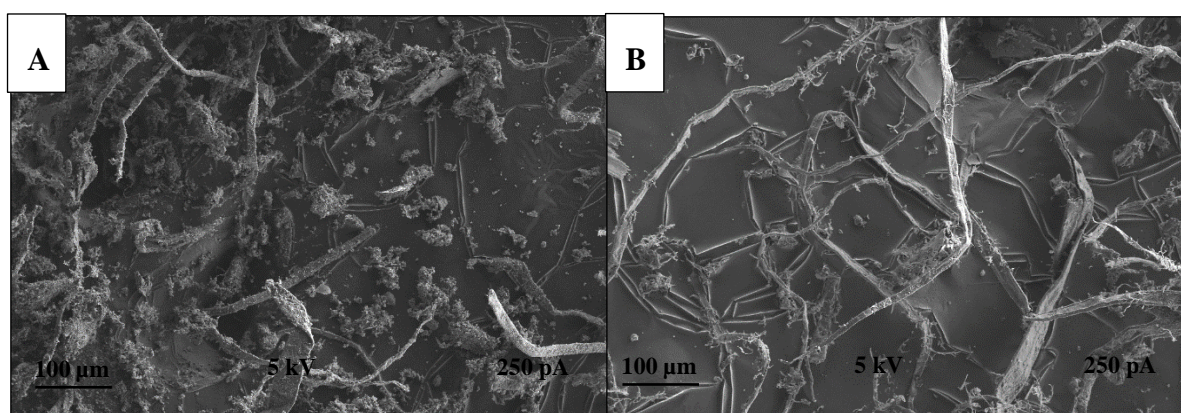
Figure 4.2: SEM images of untreated PS fibres from A) Kimberly-Clark Springs Mill (printed recycle PS) with shorter fibres and B) Sappi Ngodwana Mill (virgin pulp PS) having comparatively longer fibres. The size averages of 100 measurements were determined for 3 - 5 images per sample.

4.1.4. Effect of steam explosion of low-ash content paper sludge on fibre accessibility

Virgin pulp PS with longer fibres and high WHC was tested for pre-treatment with steam explosion to improve the accessibility of the material to cellulase. Steam explosion may increase the surface area of PS and enhance the hydrolysis efficiency and digestibility, by increasing the accessibility of cellulose to enzymes (Pielhop, et al., 2016).

Table 4.3 indicates the chemical composition of untreated and steam exploded PS. The moisture content of the pre-soaked PS was determined to be 73.1%, while the moisture content of the dry PS was 15.4% (Table 3.1) as determined by NREL methods (Hames, et al., 2008). Approximately 45 - 53% of the xylan was removed with the steam explosion pre-treatment. However, for all the steam exploded conditions, the glucan component was decreased with 26 - 32%, which was undesirable for the subsequent isolation of cellulose nanoparticles from the cellulosic component. This could be due to cellulose

solubilisation at the high temperatures, which may be associated with conversion of glucan to by-products (Hendriks & Zeeman, 2009; Cara, et al., 2008).

Table 4.3: Chemical composition of untreated versus steam exploded virgin pulp PS. Averages were determined from single measurements of triplicate samples. All standard deviations of the compositions were determined as < 0.31% (w/w).

T °C	t min	Soaked	Ash % (w/w)	Extractives % (w/w)	Lignin % (w/w)	Glucan % (w/w)	Xylan % (w/w)
	Untreated		8.26	7.09	15.33	61.20	14.06
200	10	Yes	8.56	9.41	20.09	45.16	7.68
200	5	No	9.18	10.35	20.77	42.43	7.37
200	10	No	8.64	11.72	21.50	44.94	7.54
210	5	No	8.89	9.85	20.90	43.30	7.20
210	10	No	9.22	12.14	21.82	41.52	6.64

Enzymatic hydrolysis of the steam pre-treated PS versus untreated PS was conducted with Cellic® CTec2 as active enzyme (15 FPU/gdPS). The glucose concentrations of the enzymatic hydrolysis of the steam exploded PS (Figure 4.3) are only higher for the pre-soaked PS in comparison with the untreated PS, indicating that only the pre-soaked steam-exploded PS had increased digestibility. All the unsoaked PS runs resulted in lower concentrations of glucose in comparison with the untreated PS, indicating that no significant increase in digestibility occurred due to steam explosion. Steam explosion could at best provide a 6.1% increase in digestibility, due to the fibres that were already extensively disrupted by the pulping processes as well as due to the loss of cellulose into glucose hydrolysis products, and therefore was deemed as an ineffective treatment to increase the PS accessibility for hydrolysis. No differences were observed in the cellulose particle size produced by enzymatic hydrolysis of steam-exploded and untreated PS (data not shown).
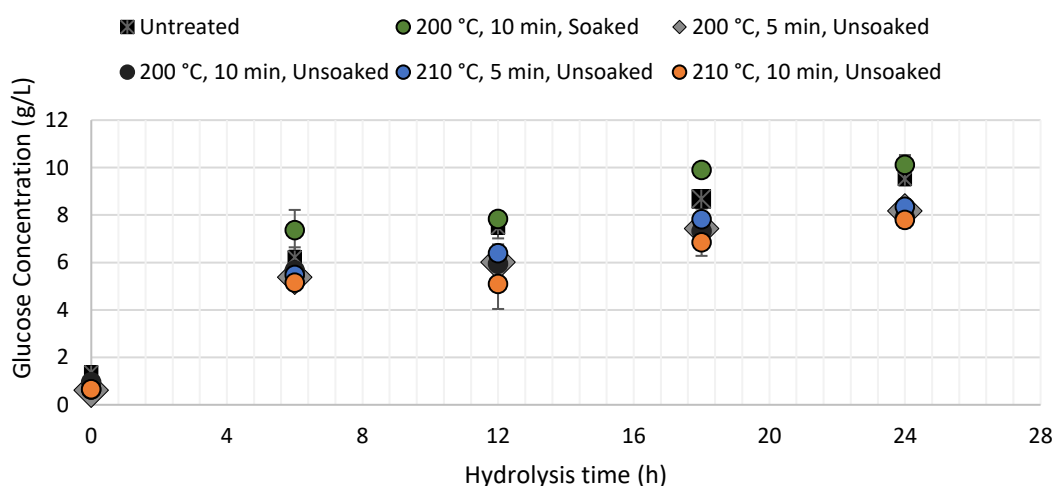
Figure 4.3: Glucose concentrations obtained by enzymatic hydrolysis of steam exploded PS under variant time and temperature conditions. Enzymatic hydrolysis conducted at 50 °C and 150 rpm with a Cellic® CTec2 cellulase dosage of 15 FPU/gdPS. Error bars indicate the standard deviation of single measurements of triplicate samples.

4.2. Screening for enzymatic hydrolysis process conditions for cellulose nanoparticle production

Boshoff et al. (2016) and Robus (2013) showed that commercial cellulases could be used for hydrolysis of glucans and hemicelluloses in South African PS, for bio-ethanol production. Screening experiments were conducted to investigate whether similar commercial cellulases could be used through incomplete/partial hydrolysis of the same types of PS, and thus to stop the hydrolysis process earlier, at a point of cellulose nanoparticles production. Cellulose nanoparticle production at very low solids loadings (0.5 – 1.5% (w/w)), as reported previously (Filson, et al., 2009; Fattahi Meyabadi & Dadashian, 2012), is undesired from an industrial point of view. Enzymatic hydrolysis of PS was therefore completed at higher solids loadings (3 – 9% (w/w)) with dynamic light scattering (DLS), used to determine the mean particle size. Glucose production was assessed by HPLC analysis, as well as the effect of shorter hydrolysis time (t < 32 hrs) on cellulose nanoparticle production. Finally, three enzymes were screened (at 25 FPU/gdPS for the two cellulase cocktails and 100 ECU/gdPS for the monocomponent endoglucanase as selected from literature, Section 2.2.4.2) for their effect on mean particle size, which, together with glucose release, should be minimized. Furthermore, XRD and FTIR analyses were used to determine crystallinity of the cellulose in the PS.

For hydrolysis with Cellic® CTec2, the mean particle sizes of the nanocellulose ranged between 250 and 350 nm at lower (3% w/w) and higher (9% w/w) solids loadings for both PS feedstocks (Table 4.4). The mean particle sizes were marginally larger for the Viscamyl^{TM} Flo, falling in the range of 350 to 450 nm for both feedstocks within 24 to 32 hrs of hydrolysis and for both solids loadings (Table 4.4). For hydrolysis of both feedstocks with FiberCare® R, HPLC analysis conveyed zero glucose yields (Table 4.5) and low cellobiose concentrations of ≤ 0.4 g/L (data not shown), for up to 32 h hydrolysis at both solids loadings. This was expected as oligomer-hydrolysing exoglucanase or glucose-releasing β-glucosidase activities were ot present in the selected enzymes. Therefore, hydrolysis with FiberCare® R produced minimal by-product formation, while mean particle sizes of 200 – 400 nm were produced after 32 hrs (Table 4.4), falling in the same size range as that achieved with Cellic® CTec2.

With regards to the effect of hydrolysis time on mean particle size (Table 4.4), contrdictory trends are apparent with both feedstock, which could partly be due to particle agglomeration, as has also been found by other cellulose nanoparticle researchers (dos Santos, et al., 2013). However, within a hydrolysis time of 32 h, the mean particle size of all the samples decreased to < 500 nm for all three enzymes used, for both feedstock (Table 4.4). This indicated that cellulose particles with nano-sized lengths in the accepted ISO standards range for CNC could be achieved through short-period hydrolysis with the tested commercial cellulase cocktails.

Table 4.4: Effect of PS solids loading on mean particle size during enzymatic hydrolysis to produce cellulose nanoparticles, at a constant cellulase cocktail dosage of 25 FPU/gdPS, or FiberCare® R dosage of 100 ECU/gdPS. Averages were determined from multiple measurements of multiple samples (n = 2 to 4). The standard deviation for all the mean size values were < 80 nm.

Feedstock	Cellulase Type	Solid loading % (w/w)	Mean size at 0 h nm	Mean size at 8 h nm	Mean size at 24 h nm	Mean size at 32 h nm
Printed recycle PS	Cellic® CTec2	3	693	181	322	275
		9	325	346	260	286
	Viscamyl™ Flo	3	619	655	410	454
		9	921	187	424	373
	FiberCare® R	3	451	297	460	307
		9	1157	635	477	388
Virgin pulp PS	Cellic® CTec2	3	1346	211	270	263
		9	1099	282	264	266
	Viscamyl™ Flo	3	603	357	384	414
		9	704	605	361	418
	FiberCare® R	3	1086	292	359	253
		9	678	340	352	240

The glucose yields as a factor of PS solids loading is shown in Table 4.5, with the yield determined as a fraction (%) of the amount of glucan fed. It must be noted that for 0 hour timepoints, the values do not present that of pure 0 hrs due to short delays before sampling, hence sugar release was detected due to instant action of enzymes on solids. At 9% (w/w) solids loading of printed recycle PS, a higher glucose yield of 21.6% was achieved with Cellic® CTec after 32 hrs in comparison to 6.25% at 3% (w/w) solids loading (Table 4.5). With or Viscamyl™ Flo a higher glucose yield of 28.4% was achieved at 9% (w/w) than 26.3% at 3% (w/w) solids loadings at 32 hrs (Table 4.5). Therefore for printed recycle PS, the glucose yields increased with increase in solids loading up to 9% (w/w). This was contrary to the expected decrease in glucose yields at higher solids loadings, as is typically observed due to associated mass transfer limitations and their impact on enzymatic hydrolysis (Boshoff, et al., 2016).

For the virgin pulp PS, a dissimilar trend with solids loading was noticed. At 3% (w/w) solids loading of the virgin pulp PS hydrolysed with Cellic® CTec2, the glucose yield reached 41.6% after 32 hrs (Table 4.4). For a higher 9% (w/w) solids loading of the virgin pulp PS dosed with Cellic® CTec2, a much lower glucose yield of 29.9% for the same time period. For virgin pulp PS hydrolysed with Viscamyl™ Flo, the same trends were observed, with a glucose yield of 42.6% after 32 hrs at 3% (w/w) and a lower 36.4% at 9% (w/w) solids loading. The decrease in glucose yields from enzymatic hydrolysis at higher solids loadings was in agreement with the mass transfer limitations associated with higher solids loadings, which could be exasperated by the increased viscosity of virgin pulp PS, compared to printed recycled PS (Boshoff, et al., 2016).

Hydrolysis with either of the commercial cellulase blends, the resulting glucose yields ($Y_{glucose/glucan}$) were higher from virgin pulp PS (30 – 43%) than from printed recycle PS (6 – 28%), within 32 hrs (Table 4.5). Therefore, the cellulose of the virgin pulp PS was found to be more readily digestible than that of the printed recycle PS, by either Cellic® CTec2 or Viscamyl™ Flo, similar to what was reported previously (Boshoff, et al., 2016).

Table 4.5: Effect of PS solids loading on glucose concentrations during enzymatic hydrolysis to produce cellulose nanoparticles, at a constant cellulase cocktail dosage of 25 FPU/gdPS, or monocomponent endoglucanase dosage of 100 ECU/gdPS. Averages were determined from single measurements of triplicate samples. The standard deviation for all the yield (glucose/glucan) values were < 0.12 g/L.

Feedstock	Cellulase Type	Solid loading % (w/w)	$Y_{glucose/glucan}$ at 0 h % (w/w)	$Y_{glucose/glucan}$ at 8 h % (w/w)	$Y_{glucose/glucan}$ at 24 h % (w/w)	$Y_{glucose/glucan}$ at 32 h % (w/w)
Printed recycle PS	Cellic® CTec2	3	1.09	2.96	5.57	6.25
		9	0.03	7.11	13.6	21.6
	Viscamyl™ Flo	3	0.15	4.25	20.9	26.3
		9	0.29	11.9	18.4	28.4
	FiberCare® R	3	0.0	0.0	0.0	0.0
		9	0.0	0.0	0.0	0.0
Virgin pulp PS	Cellic® CTec2	3	0.00	39.6	41.3	41.6
		9	3.49	27.6	32.5	29.9
	Viscamyl™ Flo	3	4.44	38.6	41.8	42.6
		9	0.31	25.5	33.5	36.4
	FiberCare® R	3	0.0	0.0	0.0	0.0
		9	0.0	0.0	0.0	0.0

The cellulose crystallinity was investigated through XRD (Figure 4.4). A lower cellulose crystallinity of 35.1% was found for the virgin pulp PS in comparison to the 49.4% of the printed recycle PS. FTIR analysis of the two PS feedstock supported the XRD crystallinity findings, as the infrared spectra indicated that the band at 1424 - 1423 cm^{-1}, designated as the cellulose crystalline absorption band (Poletto, et al., 2013), had a higher band intensity for the printed recycle PS (Figure 4.5A) in comparison to the virgin pulp PS (Figure 4.5B). This indicated a higher degree of crystallinity in the cellulose of the printed recycle PS, compared to virgin pulp PS, which agreed with the lower digestibility observed in the enzymatic hydrolysis.

The virgin pulp PS from the chemical (Kraft) pulping process will have undergone alkaline treatments which swell and partially de-crystallize the cellulose (Wang, 2011; Fernandez & Young, 1996), thereby rendering it more amendable to enzymatic hydrolysis. Recycled PS, consisting mostly of fibres obtained through mechanical pulping will have been exposed to less severe chemical modifications of the cellulose structure (Marsden & Gray, 1986), resulting in the observed lower digestibility.
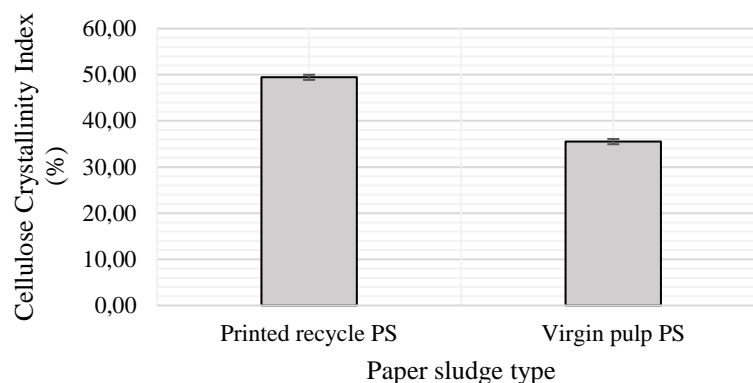
Figure 4.4: Crystallinity indices of untreated PS types (milled to particle sizes of less than 6 mm), calculated with XRD, Segal Peak Height method. Error bars indicate the standard deviation of duplicate measurements of duplicate samples.
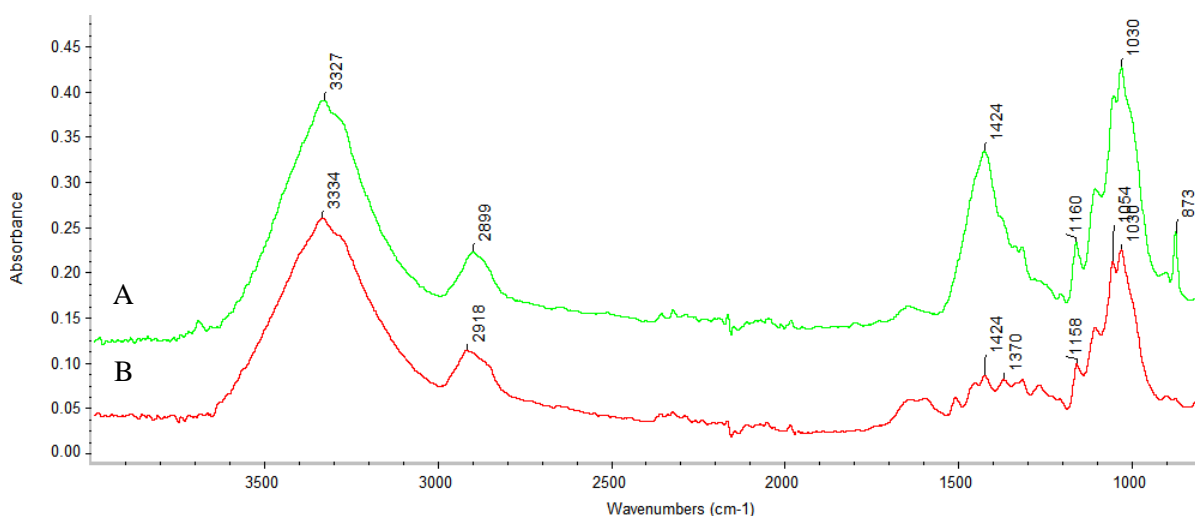
Figure 4.5: FTIR Spectra of A) untreated printed recycle PS and B) untreated virgin pulp PS. Duplicate samples were measured with at least two measurements each.

For virgin pulp PS, more than a quarter of the cellulose raw material was digested to glucose with either of the cellulase enzyme cocktails within 8 hrs, at lower and higher solids loadings (Table 4.5). In order to limit the glucose formation as well as producing a mean particle size range under 500 nm, the hydrolysis time was limited to 24 hrs.

Higher glucose yields were achieved with Viscamyl™ Flo in comparison to Cellic® CTec2, at both low and high solids loadings (Table 4.5). Cellic® CTec2 was selected as the better-suited enzyme cocktail as between the two cocktails, it produced smaller mean particle sizes (Table 4.4) and less by-product formation (Table 4.5). Endoglucanase is well-known for its ability to hydrolyse the amorphous sections in cellulose fibres, by attacking the β-1,4-glycosydic bonds (Ul Haq & Akram, 2017). To obtain a high endoglucanase to exoglucanase ratio, the Cellic® CTec2 (further on referred to as CTec2) was supplemented with the FiberCare® R (further on referred to as FiberCare) to form an endoglucanase-enriched cellulase cocktail. This endoglucanase-enriched cellulase cocktail would target the easy-to-react

48

amorphous regions of cellulose chains and attack the recalcitrant crystalline regions to produce cellulose nanoparticles, and secondly to investigate minimization of by-product (glucose) formation.

4.3. Optimisation of cellulose nanoparticles production from paper sludge

An optimisation of the controlled hydrolysis of PS was conducted through Response Surface Methodology (RSM) to limit the mean particle sizes of the produced cellulose nanoparticles in the range of 1 – 500 nm, while also minimising glucose formation. Statistical design of experiments through use of a CCD was used to complete experimental runs and develop statistical models using the resulting data. The CCD was set up with four variable factors; FiberCare dosage (X_1, 0 – 100 ECU/gdPS), CTec2 dosage (X_2, 0 – 40 FPU/gdPS), solids loading (X_3, 3 – 9% w/w) and hydrolysis time (X_4, 6 – 24 hrs) with their ranges based on the screening results (Section 4.2) and literature findings (Section 2.2.4), with range values specified in Table 4.6. The endoglucanase-enriched cellulase cocktail (CTec2 supplemented with FiberCare), identified from the screening section (Section 4.2) was used for the optimisation. The validity of these models were determined by analysis of variance and validation experiments.

It must be noted that the design included star values (extreme values) with one increment lower than the low level (x_i = -2) (incorporating a control sample for each variable factor) and one increment higher than the high value (x_i = 2), as also shown in Table 4.7 and Table 4.8.

Table 4.6: Factors with levels for CCD design.

Factor	Unit	Star Value $x_i = -2$	Low level $x_i = -1$	Midrange level $x_i = 0$	High level $x_i = 1$	Star Value $x_i = 2$
X_1, FiberCare dosage	ECU/gdPS	0	25	50	75	100
X_2, CTec2 dosage	FPU/gdPS	0	10	20	30	40
X_3, Solids loading	% w/w	0	3	6	9	12
X_4, Hydrolysis Time	hrs	0	6	12	18	24

The responses (mean particle size, Y_1, and glucose concentration, Y_2) from the different runs after enzymatic hydrolysis, centrifugation and glass-membrane filtration are provided in Table 4.7 and Table 4.8) for the printed recycle PS and the virgin pulp PS, respectively. From these responses, statistical models, represented by polynomial equations (Equation 6 in Appendix D), could be plotted in the form of a three-dimensional response surface (Figure 4.7) to show the relationship between selected response and independent variables. Desirability plots were programmed and plotted from the response data in Table 4.7 and Table 4.8 on Statistica software with the smallest mean particle size and the lowest glucose concentration to be the most desirable (desirability ≤ 1).

Table 4.7: Experimental setup with analytical results of printed recycle PS according to CCD, indicating response variables of mean particle size and glucose concentrations. Particle size means were determined from single measurements of triplicate samples. Glucose concentration averages were determined from single measurements of triplicate samples.

Sample no.	X_1 FiberCare Dosage ECU/gdPS	X_2 CTec2 Dosage FPU/gdPS	X_3 Solids Loading % (w/w)	X_4 Hydrolysis Time h	Y_1 Mean Particle Size nm	Y_2 Glucose Concentration g/L	Not included in models Glucose Yield %
1	25	10	9	6	203	10.08	24.60
2	50	40	6	12	198	12.13	44.43
3	25	30	9	18	268	7.09	17.32
4	50	20	6	12	157	2.54	25.82
5	25	10	3	6	202	0.00	0.00
6	25	10	3	18	238	2.21	16.19
7	50	20	6	12	590	7.20	26.37
8	**0**	**20**	**6**	**12**	**263**	**3.04**	**11.15**
9	50	20	0	12	427	0.00	0.00
10	50	20	6	0	318	6.36	23.30
11	75	30	3	6	672	4.47	32.76
12	50	20	12	12	1211	10.22	18.71
13	25	30	3	18	220	3.89	28.48
14	25	30	9	6	683	3.75	9.15
15	25	30	3	6	116	4.28	31.38
16	75	10	9	18	308	7.09	17.32
17	50	20	6	24	422	7.56	27.70
18	75	10	3	18	425	3.34	24.49
19	50	20	6	12	312	7.94	29.09
20	**100**	**20**	**6**	**12**	**441**	**3.16**	**11.58**
21	50	20	6	12	137	4.73	17.32
22	75	30	9	6	145	4.29	10.48
23	75	30	3	18	310	2.89	21.15
24	50	20	6	12	242	7.084	25.81
25	50	20	6	12	398	9.98	36.54
26	75	30	9	18	1029	14.08	34.39
27	25	10	9	18	549	7.25	17.69
28	75	10	9	6	518	3.09	7.54
29	75	10	3	6	139	3.71	27.17
30	**50**	**0**	**6**	**12**	**412**	**0.00**	**0.00**

Table 4.8: Experimental setup with analytical results of virgin pulp PS according to CCD, indicating response variables of mean particle size and glucose concentrations. Particle size means were determined from single measurements of triplicate samples. Glucose concentration averages were determined from single measurements of triplicate samples.

Sample no.	X_1 FiberCare Dosage ECU/gdPS	X_2 CTec2 Dosage FPU/gdPS	X_3 Solids Loading % (w/w)	X_4 Hydrolysis Time h	Y_1 Mean Particle Size nm	Y_2 Glucose Concen-tration g/L	Not included in models Glucose Yield %
31	25	10	9	6	209	15.37	25.37
32	50	40	6	12	296	22.79	56.41
33	25	30	9	18	256	30.51	50.35
34	50	20	6	12	293	18.01	44.59
35	25	10	3	6	369	5.34	26.42
36	25	10	3	18	137	8.70	43.07
37	50	20	6	12	315	19.18	47.50
38	0	20	6	12	305	11.71	28.99
39	50	20	0	12	467	0.00	0.00
40	50	20	6	0	234	13.44	33.26
41	75	30	3	6	244	8.49	42.04
42	50	20	12	12	239	24.59	30.44
43	25	30	3	18	329	10.71	53.01
44	25	30	9	6	255	23.64	39.01
45	25	30	3	6	208	7.99	39.58
46	75	10	9	18	203	35.48	58.56
47	50	20	6	24	258	21.29	52.70
48	75	10	3	18	368	8.67	42.95
49	50	20	6	12	255	18.85	46.66
50	100	20	6	12	283	18.72	46.34
51	50	20	6	12	338	18.05	44.69
52	75	30	9	6	266	24.31	40.12
53	75	30	3	18	333	11.93	59.09
54	50	20	6	12	263	18.34	45.40
55	50	20	6	12	264	18.77	46.47
56	75	30	9	18	237	27.43	45.27
57	25	10	9	18	250	24.87	41.05
58	75	10	9	6	212	16.76	27.67
59	75	10	3	6	186	6.09	30.17
60	50	0	6	12	202	0.00	0.00

Table 4.9: Particle size distribution of enzymatically hydrolysed samples. The standard deviation for all the PdI values were < 0.11. Averages were determined from multiple measurements of triplicate samples

	Printed Recycle			Virgin Pulp	
Sample ID	Mean Size d.nm	PdI	Sample ID	Mean Size d.nm	PdI
1	204	0.56	31	210	0.51
2	125	0.90	32	297	0.31
3	268	0.85	33	256	0.52
4	158	0.37	34	293	0.29
5	202	0.57	35	369	0.58
6	239	0.30	36	138	0.59
7	591	0.77	37	315	0.33
8	264	0.79	38	305	0.30
9	427	0.67	39	467	0.70
10	318	0.41	40	234	0.60
11	672	0.60	41	245	0.27
12	1211	0.87	42	239	0.51
13	221	1.00	43	329	0.37
14	683	0.70	44	256	0.31
15	116	0.50	45	209	0.54
16	309	1.00	46	203	0.51
17	422	0.79	47	259	0.25
18	426	0.62	48	368	0.34
19	313	0.16	49	255	0.40
20	442	0.85	50	283	0.29
21	138	0.59	51	339	0.30
22	146	0.20	52	266	0.41
23	310	0.47	53	333	0.38
24	243	0.26	54	263	0.42
25	398	0.69	55	265	0.28
26	1029	0.50	56	238	0.33
27	550	0.39	57	250	0.26
28	518	0.56	58	212	0.51
29	139	0.74	59	186	0.43
30	413	0.13	60	202	0.65

Smaller mean particle sizes (< 400 nm from Table 4.8) were achieved across the complete tested range of CTec2 dosages and FiberCare dosages for the virgin pulp PS, compared to the printed recycle PS (120 – 1200 nm, Table 4.7). The higher digestibility of the virgin pulp PS (Table 4.5) correlated to the lower particle sizes (Table 4.7) in comparison to printed recycle PS, as observed during the screening experiments (Figure 4.4, Section 4.2).

Higher glucose yields of up to 58.6% (Table 4.8) were achieved for the hydrolysis of virgin pulp PS, than for printed recycle PS (34.4%; Table 4.7). The glucan fraction of virgin pulp PS was not two times higher

(61.20% for virgin pulp PS in Table 4.3 versus 41.37% for washed printed recycle PS in Table 4.2), once again indicating the effect of enzyme-accessible fibre structure due to the extent of chemical pulping processes as 'pre-treatment'. This trend in glucose release further showed a higher extent of hydrolysis of the virgin pulp PS in comparison to that of the printed recycle PS.

The particle size distribution demonstrated by the polydispersity (PdI) of the enzymatic hydrolysed samples (Table 4.9) indicated irregular PdI values with no correlation to the mean particle size, either from printed recycle PS or from virgin pulp PS. The reason may be a result of particles with a wide range of sizes present in the PS samples, and secondly due to the random action of the different cellulase enzymes which fragmented and defibrillated (Arantes, et al., 2014) the fibres and exposed fibrils. This indicated that post-hydrolysis treatment processes were required to increase the quality in terms of particle size distribution.

The model for glucose concentration prediction of virgin pulp PS had a R^2 value of 0.895, which indicated high suitability of the model to describe and predict the data. Furthermore, validity of the glucose concentrations model for virgin pulp PS was confirmed through ANOVA (no lack of fit from F-value and P-value of 3.43 and 0.093, respectively from Table 7.5 in Appendix D). An increase in CTec2 dosage linearly increased the glucose concentrations (Figure 4.7A), due to the synergism between endoglucanase, exoglucanase and β-glucosidase present in CTec2 (Janardhnan, 2012). Similarly, an increase in FiberCare dosage increased the glucose concentrations, which was not expected, as no exoglucanases are present in FiberCare. This could be explained by a synergistic effect between the CTec2 and FiberCare, which enhances the performance of cellulases in the blend other than just the endoglucanses in the CTec2 (Nechyporchuk, 2015). However, simultaneous increase in CTec2 dosage and FiberCare dosage increased the glucose concentrations up to a threshold at 25 FPU/gdPS and 60 ECU/gdPS. This indicated that an increased endo-to-exo ratio allowed for less glucose monomers production (secondary hydrolysis; Figure 4.7) and therefore suggesting higher activity of primary hydrolysis to release cellulose nanoparticles. This was supported by another study which found that the optimum endo-to-exo ratio for total hydrolysis of cellulose to glucose should be low (Kostylev & Wilson, 2012).

Simultaneous increase in solids loading and hydrolysis time led to a linear increase in glucose concentration (Figure 4.7B). At instances where the enzyme dosages and hydrolysis time were constant, lower glucose yields were found at higher solids loadings ($\geq$ 6%), indicating that high solids loadings negatively affected the enzymatic hydrolysis (Table 4.8), as previously seen due to mass transfer limitations (Screening Section 4.2). Another contributing factor could be cellulase inhibition by the cellobiose and glucose by-products (Philippidis, et al., 1993), due to accumulation of these products at higher concentrations as a result of higher solids loadings (Table 4.8). In order to reduce the undesired

cellulose mass loss to monomers (glucose yield less than 40%) from virgin pulp PS, the hydrolysis time and the CTec2 dosage were to be limited to 6 hrs and 10 FPU/gdPS.

A poor fit between the mean particle size model of the virgin pulp PS and the data was indicated by a low R^2-value of 0.481 (Figure 4.7D). Efforts in specifying categories based on size ranges (according to cellulose nanoparticle types from ISO standards) for the mean particle size model instead of specifying the mean size values resulted in increased poorness of fit of the data (data not shown). Previous studies on the acid hydrolysis production of cellulose nanoparticles reported lack of fit of models for the prediction of the mean particle size, even after removal of outlier samples (Bondeson, et al., 2006). This indicated that wide variations in particle sizes for cellulose nanoparticles were typical, resulting in inherent difficulties with fitting statistical models to such data. Nevertheless, the current mean particle size model was deemed statistically meaningful through ANOVA with an insignificant lack of fit (lack of fit F-value of 2.71 and P-value of 0.14 from Table 7.4 in Appendix D). Additionally, as the overall mean particle size range was found to be < 400 nm (Table 4.8), the model was still used for optimisation. The strong synergistic nature of the endoglucanases and exoglucanases present in CTec2 (Chen, 2014), enhanced by the endoglucanase in the FiberCare, released majority of particles with dimensions in nano-ranges. Therefore, the model provides a useful approximation of the mean particle size while minimising the glucose concentration. This, in effect, increase the probability of higher cellulose nanoparticle yields as the by-product formation were minimised, which is the best result that could be achieved with the typically large variations in cellulose nanoparticle size samples (Bondeson, et al., 2006).
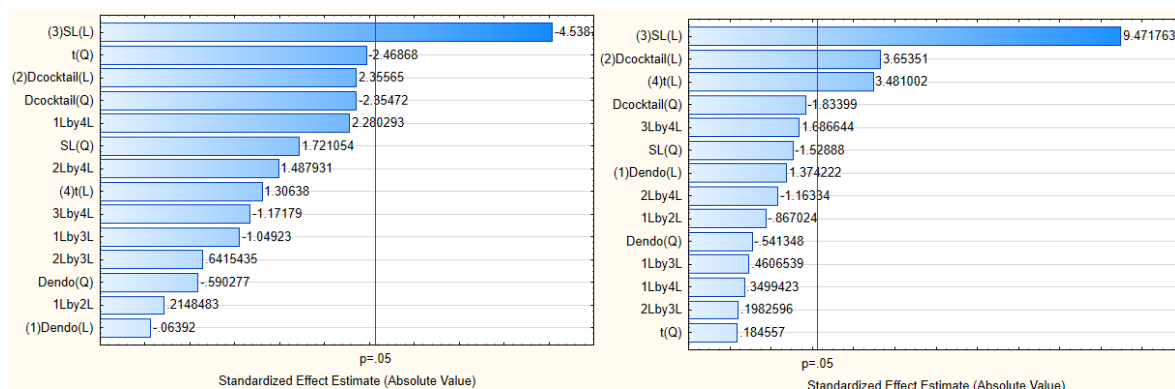
Figure 4.6: Pareto charts of standardized effects for virgin pulp PS feedstock with glucose concentration (left) and mean particle size (right) as variable. The keys L and Q denotes the main effects and the quadratic effects, respectively. The keys SL denotes solids loading (% w/w), t denotes hydrolysis time (hours), $D_{cocktail}$ denotes CTec2 (FPU/gdPS) and D_{endo} denotes FiberCare (ECU/gdPS) for representation purposes. The 1Lby2L, 2Lby3L, etc. denotes the interaction effects of the model.

It was clear from the surface plots (Figure 4.7C and Figure 4.7D) and the regression coefficients from Equation 7 and Table 7.2 in Appendix D that none of the factors (X_1, X_2, X_3 or X_4) independently influenced the mean particle size, but they interacted with each other, causing both positive and negative interaction influences. As indicated from the Pareto charts (Figure 4.6) of standardised effects for virgin pulp PS it is evident that the solids loading was the most significant contributor (p < 0.05) to the mean

particle size, however for the glucose concentration model, the solid loading, CTec2 dosage and hydrolysis time were the strongest contributors to the mean particle size. From the graph in Figure 4.7C and with a P-value of 0.952 (Table 7.2 in Appendix D), it was apparent that the FiberCare dosage had no significant effect on the mean particle size. In order to capture the true benefit of the FiberCare addition, which was speculated to have a more significant effect on the particle diameter in comparison to the measured length, the morphological shape of the cellulose nanoparticles were to be investigated (Section 4.4.2.1).
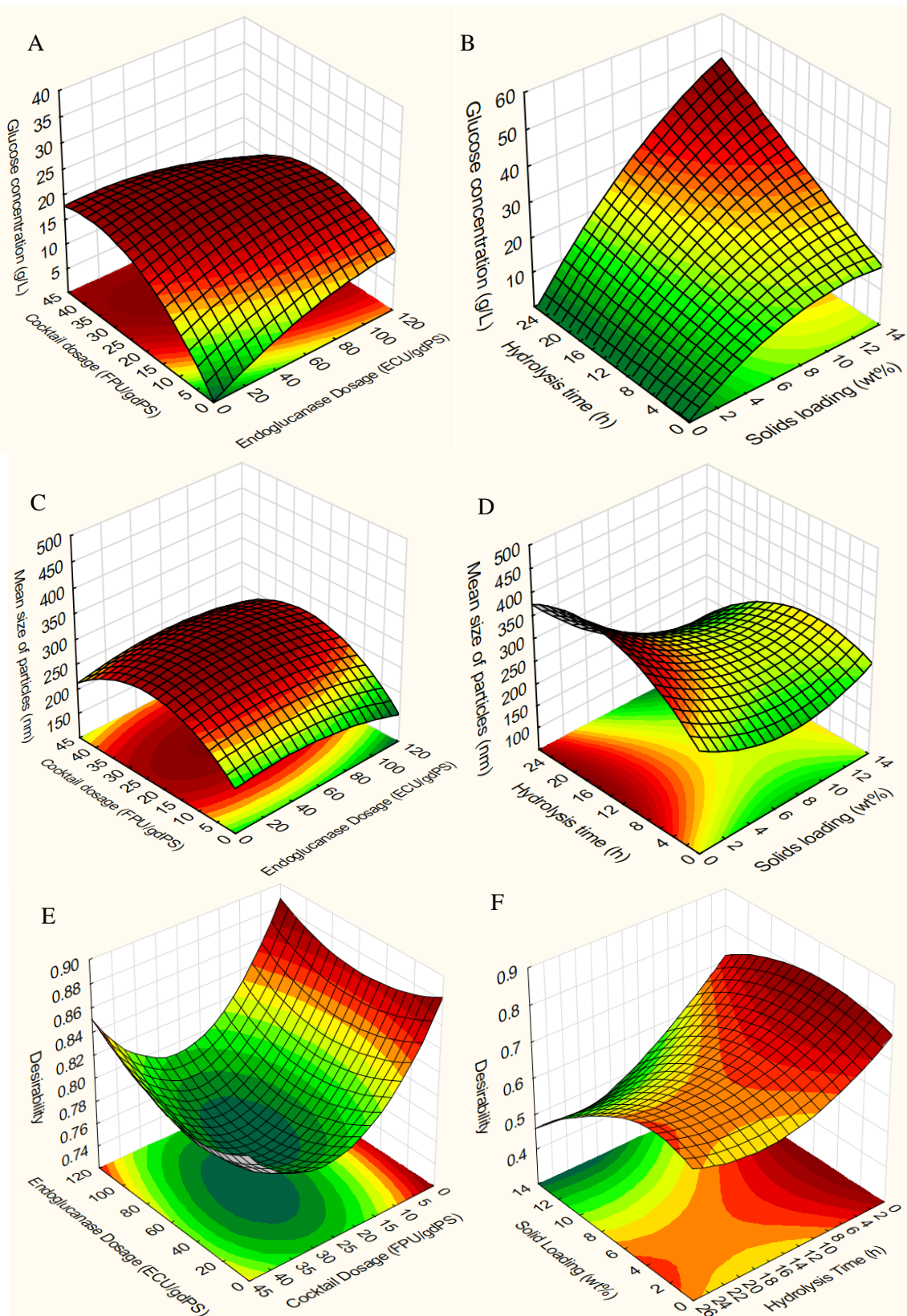
Figure 4.7: Surface plots of the virgin pulp PS predicting the **A)** mean particle size with CTec2 dosage (FPU/gdPS) and FiberCare dosage (ECU/gdPS) as independent variables, **B)** mean particle size with hydrolysis time (h) and solids loading (% w/w) as independent variables, **C)** glucose concentrations with CTec2 dosage (FPU/gdPS) and FiberCare dosage (ECU/gdPS) as independent variables, **D)** glucose concentration with hydrolysis time (h) and solids loading (% w/w) as independent variables, **E)** desirability with CTec2 dosage (FPU/gdPS) and FiberCare dosage (ECU/gdPS) as independent variables, and **F)** desirability with mean particle size with hydrolysis time (h) and solids loading (% w/w) as independent variables

The desirability plots of enzymatic hydrolysis with virgin pulp PS are presented in Figure 4.7E and Figure 4.7F, which combined the two dependent variables, mean particle size and glucose concentration. Due to the inverse parabolic shape of the desirability plot in Figure 4.7E, difficulty with optimisation within the enzyme dosages were experienced. In order to identify the model-predicted optimum ranges, the surface plots were studied individually, in combination with relating contour plots and the numerical solution of the polynomial equations (Equation 7 and Equation 8 in Appendix D). Optimised hydrolysis conditions based on the mean particle size and the glucose concentration models indicated that a high FiberCare dosage (75 ECU/gdPS), a low CTec2 dosage (10 FPU/gdPS), an intermediate hydrolysis time (9 hrs) and a low solids loading (3% w/w), were required for virgin pulp PS. Under these conditions the models predicted the mean particle size and the glucose concentrations to be 288 nm and 5.78 g/L, respectively (Table 4.10). Validation experiments conducted under the optimal conditions indicated that the models used are suitable for predicting the output variables, as the predicted values ($\hat{Y}_i$) of mean particle size and glucose concentration differed no more than 19% and 6%, respectively (Table 4.10) with the experimentally measured response variables (Y_i).

Table 4.10: Optimised treatment conditions proposed by statistical analysis on Statistica in comparison to experimental values of validation experiments. Standard deviations of the mean particle size (determined from single measurements of triplicate samples) for both feedstock are < 33 nm. Standard deviations of glucose concentrations (determined from single measurements of triplicate samples) for both feedstock are < 0.07 g/L.

Feedstock	FiberCare dosage ECU/gdPS	CTec2 Dosage FPU/gdPS	Solids Loading % (w/w)	Hydrolysis Time h	Y_{size} nm	$\hat{Y}_{size}$ nm	$Y_{glucose}$ g/L	$\hat{Y}_{glucose}$ g/L
Virgin Pulp	80	10	3	9	232	288	5.44	5.78

No desirability profiling was applied to the statistical models for the printed recycle PS, due to inaccurate fit of the mean particle size (R^2-value of 0.510) and glucose concentration models (R^2-value of 0.680). The Pareto charts of standardised effects for printed recycle PS (Figure 4.8) indicated the majority of the factors and factor-interactions to have little to insignificant contributions to the glucose concentration and mean particle size. Statistically, there was a lack of fit of the mean particle size model (lack of fit F-value and P-value of 5.34 and 0.039, respectively; Table 7.4 in Appendix D) as well as a lack of fit for the glucose concentration model (lack of fit F-value and P-value of 99.75 and 0.00004, respectively; Table 7.5 in Appendix D). The nature of recycled fibres, relating to polysaccharide hardening and possible changes in the microstructure of the recycled fibres (leading to variable surface free area and in turn, an influenced nature of water interactions into and on the fibre) (Wistara & Young, 1999) could be a reason for inconsistent, decreased cellulase activity on the recycled fibres. This resulted in large standard deviations in the particle sizes and therefore, created statistically insignificant models. Efforts in removing insignificant factors and/or interactions resulted in even higher percentage errors between the predicted values and the experimental values (Table 7.6 in Appendix D).
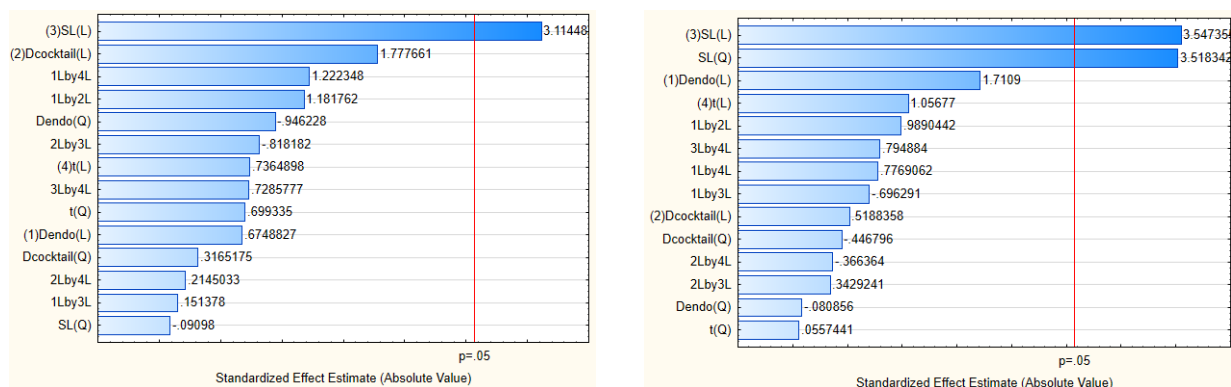
Figure 4.8: Pareto charts of standardized effects for printed recycle PS feedstock with glucose concentration (left) and mean particle size (right) as variable. The keys L and Q denotes the main effects and the quadratic effects, respectively. SL denotes solids loading (% w/w), t denotes hydrolysis time (hours), $D_{cocktail}$ denotes CTec2 (FPU/gdPS) and D_{endo} denotes FiberCare (ECU/gdPS) for representation purposes. The 1Lby2L, 2Lby3L, etc. denotes the interaction effects of the model.

Therefore, it was not possible to use CCD for optimisation of the production of cellulose nanoparticles with printed recycle PS as feedstock. Instead, from careful inspection of the collected data in Table 4.7, a preferential datapoint identification was conducted for the printed recycle PS by minimizing the mean particle size to < 500 nm and simultaneously minimizing the glucose yield. With this approach, three sets of conditions were identified, as highlighted in bold in Table 4.7, from which one run was selected for validation experimentation (Table 4.11). With the validation experiment it was evident that a higher glucose concentration was produced ($Y_{glucose,val}$ = 6.38 g/L) than found in the CCD-optimization testing ($Y_{glucose}$ = 3.16 g/L). However, the particles produced were within the mean size range of < 500 nm ($Y_{size,val}$ = 226 nm).

Table 4.11: Selected treatment conditions proposed by statistical analysis on Statistica in comparison to experimental values of validation experiments. Standard deviations of the mean particle size (determined from single measurements of triplicate samples) for both feedstock are < 33 nm. Standard deviations of glucose concentrations (determined from single measurements of triplicate samples) for both feedstock are < 0.07 g/L.

Feedstock	FiberCare dosage ECU/gdPS	CTec2 Dosage FPU/gdPS	Solids Loading % (w/w)	Hydrolysis Time h	Y_{size} nm	$Y_{size,val}$ nm	$Y_{glucose}$ g/L	$Y_{glucose,val}$ g/L
Printed Recycle PS	100	20	6	12	441	226	3.16	6.38

For printed recycle PS, a high FiberCare dosage (100 ECU/gdPS), intermediate CTec2 dosage (20 FPU/gdPS), intermediate hydrolysis time (12 hrs) and intermediate solids loading (6% w/w), were selected from the aforementioned approach. The shorter hydrolysis time required for the virgin pulp PS was in agreement with the screening results (Section 4.2) due to higher digestibility in comparison to the printed recycle PS. As a result, the printed recycle PS required higher cellulase dosages than that of virgin pulp PS. Low solids loadings (0.5 – 1.5% w/w) are typically preferred for production of cellulose nanoparticles, to increase the enzyme efficiency by reducing mass transfer limitations (Filson, et al., 2009; Fattahi Meyabadi & Dadashian, 2012; Anderson, et al., 2014), which explains the low optimal solids loading of the virgin pulp PS.

58

From the optimisation experiments conducted with printed recycle PS, it was clear that for solids loadings higher in the tested range of 9 – 12% (w/w) the mean particle size had a tendency to be > 500 nm (Table 4.7), possibly due to mass transfer limitations that negatively affected enzymatic hydrolysis (Fattahi Meyabadi & Dadashian, 2012). Therefore, for the desired mean particle size is to be smaller than 500 nm, the solids loading for printed recycle PS was limited to 6% w/w and below. CTec2 dosages ≥ 30 FPU/gdPS resulted in the highest glucose yields obtained within the tested ranges (31.38 - 44.43% from Table 4.7). As this would negatively impact the cellulose nanoparticle yield, the CTec2 dosage was limited to 20 FPU/gdPS.

Based on the abovementioned findings, it was suggested that cellulose nanoparticle production by enzymatic hydrolysis of printed recycle PS could be achieved in a wide operating regime of CTec2 (10 – 20 FPU/gdPS) and FiberCare (50 – 100 ECU/gdPS) dosages resulting in mean particle sizes < 500 nm, apparently due to greater heterogeneity in the printed recycle PS and the cellulose nanoparticles derived from it. It would be recommended that further investigation be undertaken in smaller integrals, especially with extensively de-ashed printed recycle PS, on the ranges specified in Table 4.12.

Table 4.12: Enzymatic hydrolysis operating ranges for factors of CTec2 dosage, FiberCare dosage, hydrolysis time and solids loadings for the production of cellulose nanoparticles

Input Parameter	Units	Min	Max
CTec2 dosage	FPU/gdPS	10	20
FiberCare dosage	ECU/gdPS	50	100
Hydrolysis Time	hrs	9	24
Solids Loading	% w/w	3	6

4.4. Characterisation of cellulose nanoparticles produced by enzymatic hydrolysis of PS

For the production of cellulose nanoparticles, the properties of morphology, shape, crystallinity, polydispersity and the agglomeration are to be considered. SEM imaging was conducted for direct multi-dimensional information about the nanoparticle morphology and structural properties, and FTIR spectroscopy analysis was conducted as it provides a method of gaining direct analytical information on chemical changes that occur during different processing steps (Mandal & Chakrabarty, 2011). It is also a good semi-quantitative indicator of the degree of crystallinity, and purity of samples (Mandal & Chakrabarty, 2011).

Since the 1940s, acid hydrolysis remains the major process for producing CNC (Zhu, et al., 2011), and was therefore used as a benchmark for the cellulose nanoparticles produced by enzymatic hydrolysis of PS. The characteristics of cellulose nanoparticles from acid hydrolysis of PS were determined, to which the cellulose nanoparticles produced by enzymatic hydrolysis, could be compared. Selected PS samples were enzymatically hydrolysed, denatured, centrifuged at 4500 rpm for 30 min and successively glass-

filtered with a vacuum-filter (refer to Figure 3.2 for a process flow diagram). It was investigated whether the majority particles were found in the glass-filtered supernatant or captured in the hydrolysed residual solids (that formed part of the cake that could not be filtered through the glass-membrane mesh pores). At the risk of disposing the majority of the cellulose nanoparticles present in the supernatant, especially with the low yield expected with enzymatic hydrolysis, no washing of the sample was originally conducted. The supernatant was freeze-dried for analysis.

4.4.1. Effect of acid hydrolysis of paper sludge as control process for cellulose nanoparticle production

Two different morphologies, and therefore two types of cellulose nanoparticles were produced through acid hydrolysis of PS. SEM images of acid hydrolysed sample from printed recycle PS, indicated long entangled CNF (Figure 4.9A) as well as non-entangled, agglomerated CNC particles (Figure 4.9B) in the same sample. Similarly, for acid hydrolysis of virgin pulp PS, CNF particles (Figure 4.10A) and CNC particles (Figure 4.10B) were present in the same sample. Although most studies indicate that only a singular morphology is produced, some previous acid hydrolysis studies have reported on similar results of multiple cellulose nanoparticle morphologies within the same sample (Lu & Hsieh, 2010; Desmaisons, et al., 2017).

The mean diameter ranges of the CNF obtained by acid hydrolysis from the both PS samples were 20 - 50 nm, and the mean lengths of CNFs stretching over a few micrometres (Table 4.13). The mean length and mean diameter of the CNC from printed recycle PS were 169 ± 59 nm and 20 ± 6 nm, respectively, while shorter CNC particles with mean lengths and mean diameters in the ranges of 126 ± 63 nm and 26 ± 7 nm, respectively, were found for virgin pulp PS with lower crystallinity (35.5% from Figure 4.4). For dimensions of CNC produced through H_2SO_4 acid hydrolysis, typical sizes reported in literature for diameter and length were $3 – 20$ nm and $100 – 600$ nm, respectively (Rebouillat & Pla, 2013) as well as larger diameters between $3 – 35$ nm and lengths of $0.05 – 4$ μm (Nechyporchuk, 2015; Nguyen, et al., 2013). The agglomerated particles could be attributed to the strong hydrogen bonds between the individual cellulose particles (Deepa, et al., 2015).
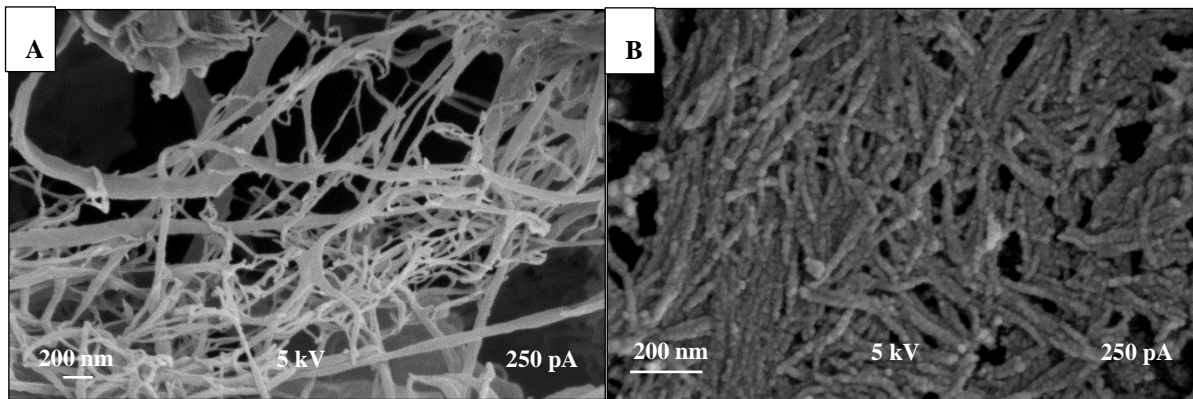
Figure 4.9: SEM images of cellulose nanoparticles obtained from printed recycle paper sludge acid hydrolysed and freeze-dried A) without resuspension at lower magnification B) without resuspension at higher magnification C) re-suspended at 0.1% (w/w) and air-dried overnight at lower magnification D) re-suspended at 0.1% (w/w) and air-dried overnight at higher magnification
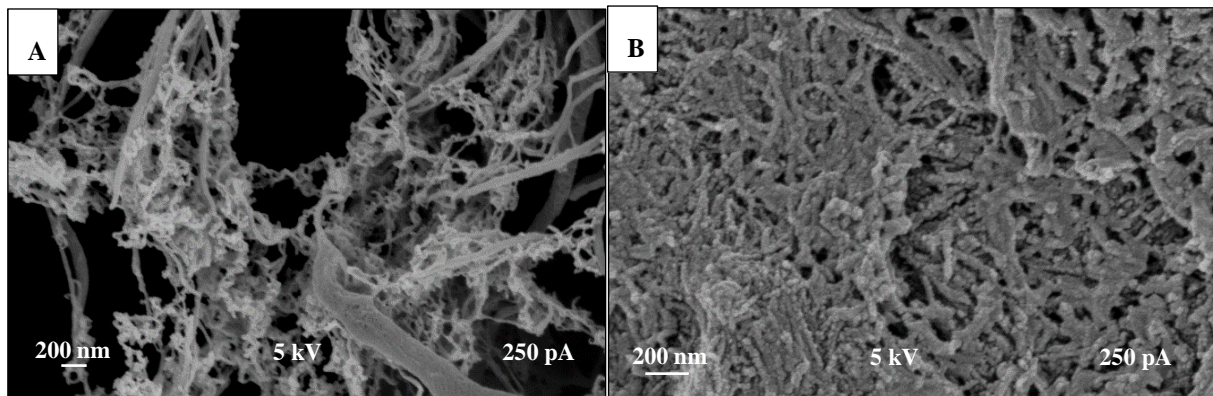
Figure 4.10: SEM images of cellulose nanoparticles obtained from virgin pulp paper sludge acid hydrolysed and freeze-dried A) without resuspension at lower magnification B) without resuspension at higher magnification C) re-suspended at 0.1% (w/w) and air-dried overnight at lower magnification D) re-suspended at 0.1% (w/w) and air-dried overnight at higher magnification

Measurement of the particle sizes of the produced cellulose nanoparticles with DLS provided mean particle sizes of 626 ± 148 nm with a PdI of 0.62 for the printed recycle PS, and 432 ± 104 nm with a PdI of 0.72 for the virgin pulp PS (Table 4.13). The high PdI values confirmed the broad particle size distributions present in both feedstocks, and the DLS size ranges provides a relative midway mean particle length (432 nm for virgin pulp PS and 626 nm for printed recycle PS) from the two sets of dimensions retrieved from the imaging analysis. Furthermore, the aspect ratios of the cellulose nanoparticle sample as a whole were estimated as 16 – 20 for virgin pulp PS and 12 – 31 for printed recycle PS (Table 4.13), both samples falling within the ISO specifications of CNF (International Standards Organization, 2017).

Table 4.13: Characteristics of cellulose nanoparticle samples acid hydrolysed from virgin pulp and printed recycle PS. An average of 100 size measurements were performed for 3 - 5 images per sample. The average of single measurements of triplicate yield samples were determined. The average of duplicate measurements of multiple crystallinity and polydispersity samples were determined (n = 2 – 3).

Feedstock				
Characteristic	Unit	Virgin pulp PS	Printed recycle PS	
CNF length	nm	> 1000	> 1000	
CNF diameter	nm	20 - 50	20 - 50	
CNC length	nm	126 ± 63	169 ± 59	
CNC diameter	nm	26 ± 7	20 ± 6	
Sample mean length (DLS)	nm	432 ± 104	626 ± 148	
Sample aspect ratio	-	16 - 20	12 - 31	
Polydispersity	-	0.72 ± 0.17	0.62 ± 0.10	
Crystallinity	%	64.8 ± 0.81	67.2 ± 1.47	
Yield	%	21.1 ± 2.01	12.3 ± 0.92	

XRD analysis revealed that the crystallinity of the cellulose nanoparticles from virgin pulp PS was 64.8% while that from printed recycle PS was a slightly higher value of 67.2% (Table 4.13). After acid hydrolysis, the crystallinity increased from the raw PS materials (49.4% and 35.5% for printed recycle PS and virgin pulp PS, respectively from Figure 4.4), apparently due to the acid attacking the amorphous regions of the cellulose chains (Paralikar & Bhatawdekar, 1984).
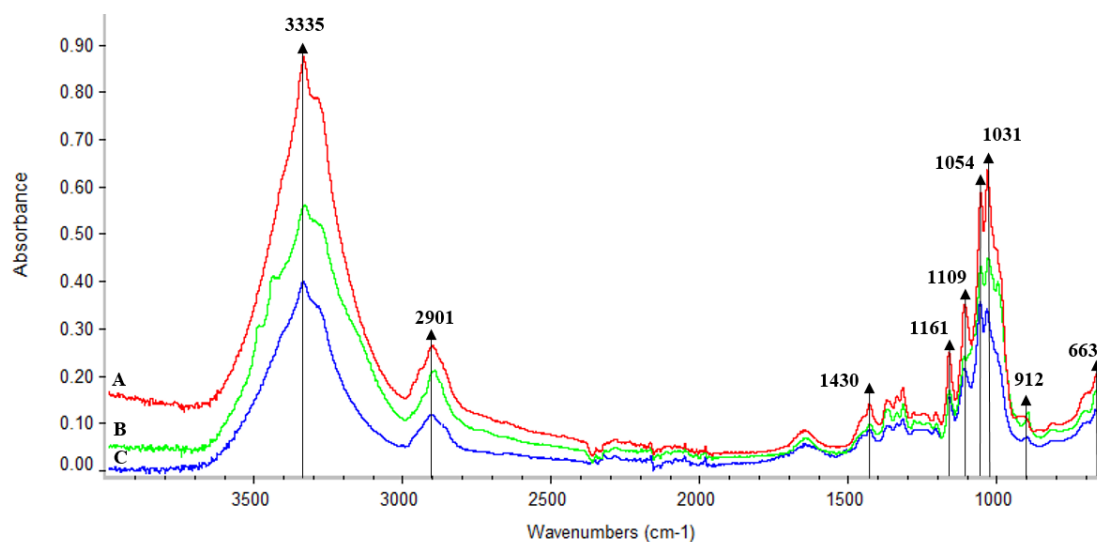
Figure 4.11: FTIR absorption spectra of cellulose nanoparticles A) produced from acid hydrolysis of printed recycle PS, B) commercial CNC control (produced via acid hydrolysis) and C) produced from acid hydrolysis of virgin pulp PS. Duplicate samples were measured with at least duplicate measurements each.

The acid hydrolysed samples (Figure 4.11) from both printed recycle PS (spectrum A) and virgin pulp PS (spectrum C) had dominating peaks in the fingerprint region for cellulosic bonds, correlating extremely well with the bands of the commercially-produced CNC (acid-hydrolysed) control sample (spectrum B). The absorption band at 1430 cm^{-1} indicated the degrees of crystallinity of the samples, which are at the same intensity of that of the commercial CNC control sample. It was clear that the acid hydrolysed samples from waste PS compared very well with the commercial CNC control sample, and

the bands retained their positions after acid hydrolysis, with insignificant amount of impurities; hemicellulose and lignin.

After acid hydrolysis, gravimetric analysis indicated that estimated cellulose nanoparticle yields of 21.1% for virgin pulp PS and 12.3% for printed recycle PS (Table 4.13). These yields were improved from previously reported yields of acid-hydrolysed (and sonicated) CNC from recycled pulp (5 – 10%) (Filson & Dawson-Andoh, 2009) and in the same range as yields of CNC produced through other processes highlighted earlier in this study (Table 2.2).

It was therefore concluded that cellulose nanoparticles with sufficient purity could successfully be produced from acid (H_2SO_4) hydrolysis of virgin pulp and printed recycle PS, with suitable morphology, dimensions and crystallinity according to the ISO standards for CNF (Section 2.2.2).

4.4.2. Effect of individual enzymes and their combination on characteristics of cellulose nanoparticles

As it was established that acid hydrolysis of virgin pulp as well as printed recycle PS produced CNF, both with satisfactory properties according to ISO specifications, the properties (morphology, dimensions and crystallinity) of cellulose nanoparticles produced by enzymatic hydrolysis, were evaluated and compared.

4.4.2.1.   Morphological properties of cellulose nanoparticles produced

Enzymatic hydrolysis of virgin pulp PS at optimised conditions produced cellulose nanoparticles with a spherical shape (Figure 4.12A) and an estimated mean diameter of 137 ± 50 nm (Table 4.14). The non-entangled spherical morphology may have occurred due to the synergistic activity of endoglucanase and exoglucanase present in CTec2, at multiple regions along the cellulose chains, leading to the release of shorter chain fragments (Fattahi Meyabadi, et al., 2014). The endoglucanase and exoglucanase bind to the chain fragments and further hydrolysed at multiple regions along the chain. After repeated hydrolysis along the cellulose chain, the hydrolysed fragments had very low aspect ratio, resembling a spherical morphology (Miyamoto, et al., 2009). It was clear that the cellulose particles were not fully separated and may have been covered with high levels of impurity materials consisting of the residual enzyme, ash, citrate buffer and hemicellulose.
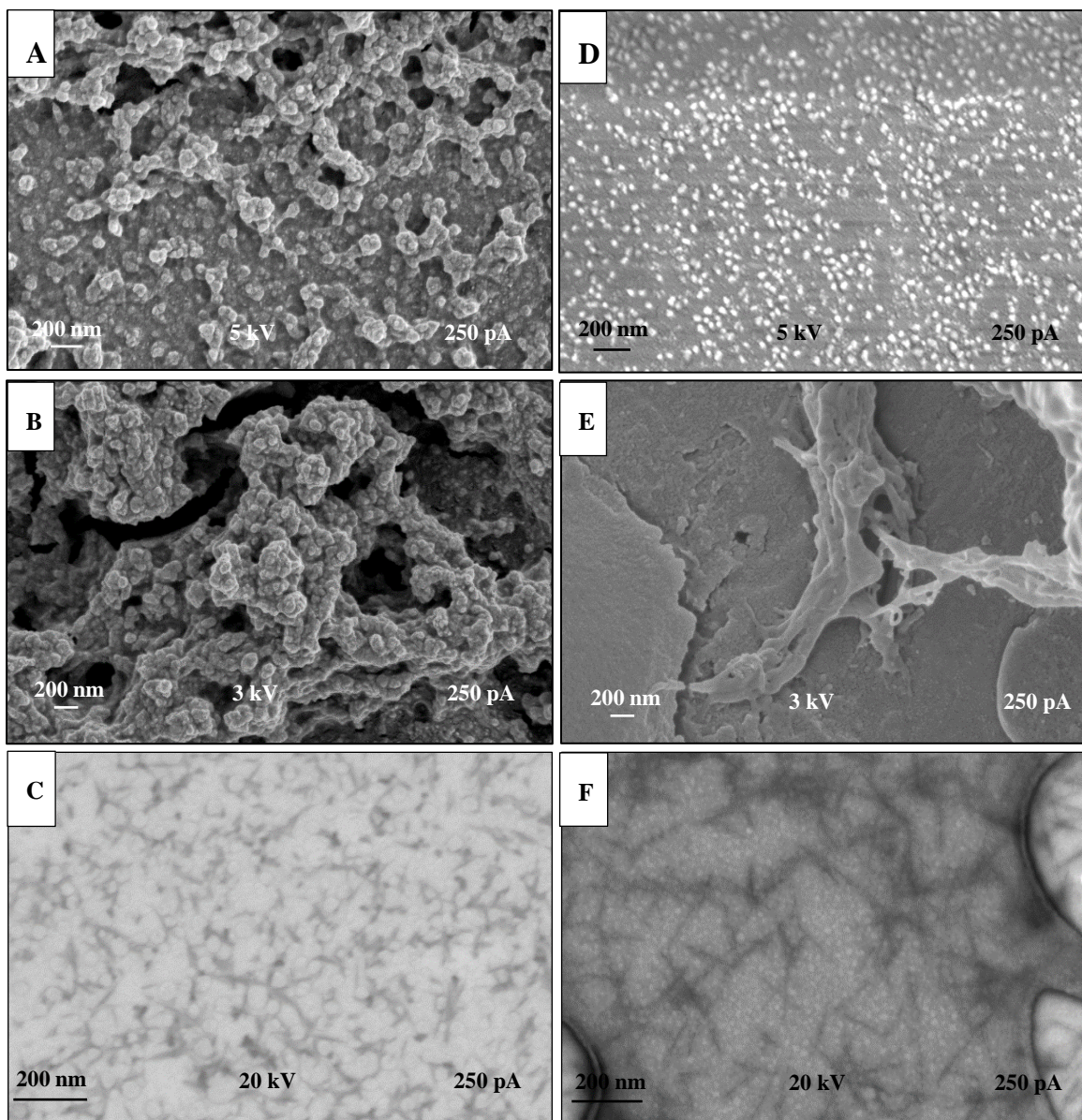
Figure 4.12: SEM images of cellulose nanoparticles obtained from enzyme hydrolysis of **A)** virgin pulp PS, at 3% (w/w) solids loading for 9 hrs of hydrolysis, with FiberCare dosage of 80 ECU/gdPS and CTec2 dosage of 10 FPU/gdPS; **B)** virgin pulp PS, at CTec2 dosage of 20 FPU/gdPS at 6% (w/w) solids loading for a hydrolysis time of 12 hrs **C)** virgin pulp PS, STEM image of virgin pulp PS at a 9% (w/w) solid loading with FiberCare dosage of 100 ECU/gdPS (image processed by convolution with the software Image J for optimised size determination, as presented in Appendix A) **D)** printed recycle PS, at 6% (w/w) solids loading for 12 hrs of hydrolysis, with FiberCare dosage of 100 ECU/gdPS and CTec2 dosage of 20 FPU/gdPS. Sample was treated with drying agent (HMDS) and air-dried overnight. **E)** printed recycle PS, at CTec2 dosage of 20 FPU/gdPS at 6% (w/w) solids loading for a hydrolysis time of 12 hrs **F)** printed recycle PS at a 9% (w/w) solid loading with FiberCare dosage of 100 ECU/gdPS (The white objects was the nature of the carbon lacey microgrid on which the samples were prepared)

It must be noted that the mean diameters (being the only dimension) of the spherical particles did not fall under 100 nm, which would technically not be classified as nanoparticles. However, SCN is very new to the market, with neither ISO nor British standards updated on the required spherical dimensions (International Standards Organization, 2017; British Standards Institution, 2017). Previous articles accepted diameters of up to 570 nm as cellulose nanoparticles (Ioelovich, 2012; Li, et al., 2001; Ioelovich, 2013; Zhang, et al., 2007), and therefore the produced SCN particles in this study should be considered as nanoparticles.

In comparison to virgin pulp PS, smaller SCN particles with diameters of 30 ± 6 nm (Table 4.14) were obtained from the selected conditions (Table 4.11) for printed recycle PS (Figure 4.12D). This sample was treated with HMDS, which provided particles with visual clarity due to less water and adsorbed impurities. This smaller particle size may have been caused by a combination of shorter fibres in the printed recycle PS feedstock, together with more extensive hydrolysis. The mean diameter was very similar to the SCN (referred to as globular nanocrystalline cellulose in the article) obtained with NaOH-pre-treated enzymatic hydrolysis of cotton fibres, which had a size range of $20 - 25$ nm (Chen, et al., 2012). However, the mean diameter size as determined by DLS was 226 ± 33 nm for printed recycle PS and 232 ± 30 nm for virgin pulp PS (Table 4.14), which was larger than the sizes estimated through SEM imaging.

The cellulose nanoparticles produced from CTec2-only hydrolysis (without FiberCare dosage; 20 FPU/gdPS at 6% (w/w) solids loading for a hydrolysis time of 12 hrs) of virgin pulp PS, had a spherical structure with diameters in the range of 80 ± 40 nm (Figure 4.12B). DLS analysis reported mean particle sizes of 305 ± 36 nm for virgin pulp PS (Table 4.14), which was higher than the sizes reported by Image J software, once again indicating particle agglomeration.

For hydrolysis of printed recycle PS under the same CTec2-only conditions (without FiberCare dosage; 20 FPU/gdPS at 6% (w/w) solids loading for a hydrolysis time of 12 hrs), agglomerated particles with an entangled CNF structure (Figure 4.12E) were found. The diameters were determined with Image J software analysis as 125 ± 75 nm (Table 4.14). From DLS sizing, the mean particle size was a larger value of 245 ± 23 nm (Table 4.14). The particle lengths were approximated to a few micrometres while the majority diameters were > 100 nm, classifying it as cellulose microparticles. It is possible that with a decreased endo-to-exo ratio (20 FPU/gdPS CTec2 without endoglucanase enrichment), cellulose microparticles were produced from printed recycle PS. This suggested a beneficial effect of the higher endo-to-exo ratio (due to the FiberCare addition from the selected conditions for printed recycle PS) to printed recycle PS with crystalline to paracrystalline cellulose (Figure 4.4).

STEM imaging indicated that hydrolysis with FiberCare-only (without CTec2 dosage) resulted in non-entangled CNC from virgin pulp PS, with dimensions of 86 ± 32 nm in length and 9 ± 2 nm in diameter (Figure 4.12C). For the case of FiberCare-only hydrolysis of printed recycle PS, non-entangled rod-like CNC were produced, with lengths of 102 ± 38 nm and diameters of 5 ± 2 nm (Figure 4.12F). Due to no presence of exoglucanase, mainly the amorphous regions of the cellulose chains were hydrolysed, resulting in the well-defined, rod-like cellulose crystals (Börjesson & Westman, 2015). These CNC particles exhibited similar dimensions to CNC produced by acid hydrolysis of both PS, falling in the range of 10 - 30 nm in diameter and 60 - 220 nm in length (Table 4.13). Furthermore, the sizes for both dimensions correlated very well with reported CNC obtained through acid hydrolysis of other wood pulps with diameter and length dimensions of $2 - 20$ nm and $100 - 600$ nm, respectively (Kangas, 2014).

Mean particle sizes determined through DLS were approximately two times the size determined by imaging software (260 ± 43 nm for printed recycle PS and 352 ± 81 nm for virgin pulp PS, Table 4.14). This could be due to agglomeration of the cellulose nanoparticles and/or the presence of larger particle sizes present in the samples, as also reported in other studies (Nechyporchuk, 2015; Fattahi Meyabadi, et al., 2014). Therefore, the screening experiments concluded that with the FiberCare, particles having the qualities of CNC particles as classified by ISO standards (Table 2.1), could be obtained by a stand-alone enzymatic hydrolysis process.

Table 4.14: Morphological shape and mean particle sizes (determined with DLS and SEM imaging) of different enzymatic hydrolysis conditions with different ratios of CTec2 to FiberCare dosages. Mean sizes were determined from single measurements of triplicate samples. The size averages of 100 measurements were determined for 3 - 5 SEM images per sample. The average of single measurements of triplicate polydispersity samples were determined.

Feedstock	Solids Loading	Hydrolysis Time	FiberCare Dosage	CTec2 Dosage	Shape	DLS Length	SEM Diameter	PdI
	% w/w	hrs	ECU/gdPS	FPU/gdPS		nm	nm	
Printed Recycle PS	6	12	100	20	spherical	226 ± 33	30 ± 6.0	0.51 ± 0.02
	6	12	0	20	rod-like	263 ± 97	125 ± 75	0.53 ± 0.07
	9	24	100	0	crystals	260 ± 43	5 ± 2.0	0.47 ± 0.05
Virgin Pulp PS	3	9	80	10	spherical	232 ± 30	137 ± 50	0.62 ± 0.04
	6	12	0	20	spherical	305 ± 36	80 ± 40	0.70 ± 0.02
	9	24	100	0	crystals	352 ± 81	9 ± 2.0	0.48 ± 0.11

For hydrolysis with either of the individual commercial enzymes (CTec2 or FiberCare), PdI values in the range of 0.47 – 0.53 and 0.48 – 0.70 were found for printed recycle PS and virgin pulp PS, respectively (Table 4.14). These high PdI values indicated that larger particle sizes and possibly multiple morphologies were present in the samples (Table 4.14), which agreed with the relatively higher mean particle size found by the DLS analysis in comparison to the particle sizes found via SEM imaging (Table 4.14). However, the PdI values of the samples from enzymatic hydrolysis of PS were lower than that of the PdI values recorded for the acid hydrolysis of virgin pulp PS (0.72 ± 0.17) and for the printed recycle PS (0.62 ± 0.10) (Table 4.13).

Through limiting the hydrolysis time and selecting cellulase-specific cocktails, specific types of cellulose nanoparticles could be obtained which is advantageous over the acid hydrolysis process. Enzymatic hydrolysis produced either SCN (Figure 4.12A and D) or CNC (Figure 4.12C and F) as single-morphology products, depending on the ratio of enzyme dosages used, while acid hydrolysis of PS resulted in a mixture of CNC and CNF particles for both feedstock (Figure 4.9 and Figure 4.10). With use of a commercial cellulase blend such as CTec2 (20 FPU/gdPS), SCN could be produced from virgin pulp PS, yet for printed recycle PS, a higher endoglucanase dosage (20 FPU/100 ECU) was required to produce SCN. At a high endo-to-exo ratios for virgin pulp (10 FPU/80 ECU) and a moderate endo-to-exo ratio (20 FPU/100 ECU) for printed recycle PS, SCN was produced. For hydrolysis with a monocomponent endoglucanase (FiberCare), CNC were produced from both PS feedstocks.

Agglomeration of the particles occurred through-out all the enzymatically hydrolysed samples for both feedstock (Figure 4.12). The agglomeration may have been due to destabilized particles, especially at low concentrations due to the strong hydrogen bonds and attractive (van der Waals) interactions, as have been reported in literature (Evans & Wennerstrom, 1999). The cleavage of internal glycosidic bonds by endoglucanase, without chemical alterations of the surface hydroxyl groups may possibly lead to poor aqueous dispersion (Anderson, et al., 2014). Acid hydrolysed nanoparticles often have better dispersion properties due to negatively charged particle surfaces, leading to increased colloidal stabilities (Rebouillat & Pla, 2013). For enzymatic hydrolysis, the instability indicated the requirement of a post-hydrolysis treatment as is often found in literature, such as sonication or homogenisation (Jonoobi, et al., 2015).

Upon drying, the rod-like cellulose particles tend to self-assemble into packed agglomerates (Peng & Chen, 2011). This may occur because of the increase in strong interfibrillar attraction due to hydrogen bonding between the surface hydroxyl groups of cellulose during freeze drying. Similar findings were reported by Anderson, et al., 2014 in a study on enzymatic hydrolysis of wood feedstock for MFC and CNF production. This underlines the necessity of post-hydrolysis purification processes, such as washing or dialysis before isolation of cellulose nanoparticles.

4.4.2.2. Structural properties of cellulose nanoparticles produced

Figure 4.13 shows the FTIR spectra of untreated printed recycle PS, enzymatically hydrolysed printed recycle PS and a CNF control sample. All the samples showed analogous spectra with characteristic peaks of cellulose at 3327, 1424, 1105, 1051 and 1030 cm^{-1} (Table 7.1 in Appendix B indicates the bonds associated with peak wavelengths). Infrared spectra of untreated and hydrolysed virgin pulp PS indicated peaks in the same regions (Figure 4.14). Accordingly, the band at 3800 – 3000 cm^{-1} corresponds to intra- and intermolecular hydrogen bonds of cellulose (Schwanninger, et al., 2004). Any possible change in the number and strength of hydrogen bonds brings about a change in intensity and width of the related bond. A shift and change in width of the related peak seen in Figure 4.13b and Figure 4.14b suggested that the enzymes therefore weakened and split the intramolecular hydrogen bonds in the cellulose from both feedstock, contributing to the destabilizing and agglomeration of the particles. This was not the case in the CNF control sample (Figure 4.13c and Figure 4.14c), where the inter- and intra-molecular hydrogen bonds remained intact after mechanical treatment.

Peaks at the regions of 1574 and 1391 cm^{-1} respectively, were present in both feedstock corresponding to bonds of carboxyl groups (Sritham & Gunaserekaran, 2017; Lakshmanan, 1956). This confirmed the presence of sodium citrate buffer used in the enzymatic hydrolysis reactions. Lower intensities at 1693 and 1275 - 1246 cm^{-1} demonstrated the relatively minor amounts of hemicellulose and lignin present in the sample. Therefore, the FTIR spectra of the enzyme hydrolysed samples from virgin pulp PS as well as the printed recycle PS correlated well with the spectrum of the CNF control sample, yet indicated hemicellulose, lignin and citrate buffer impurities.
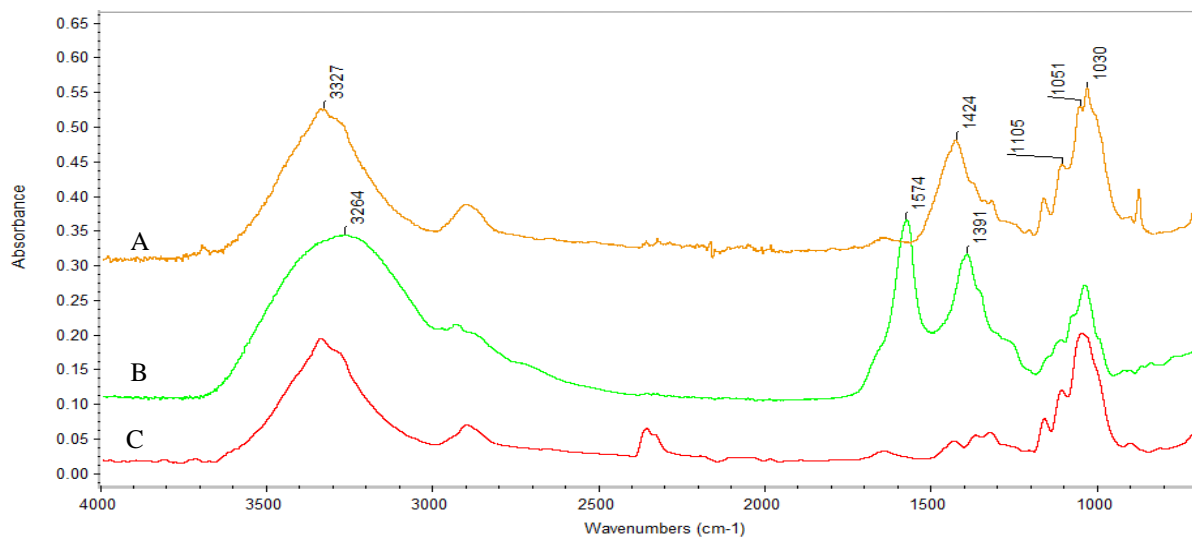
Figure 4.13: Infrared spectra of A) filter-washed printed recycle PS B) enzymatically hydrolysed printed recycle PS and C) CNF control sample. Duplicate samples were measured with at least duplicate measurements each.
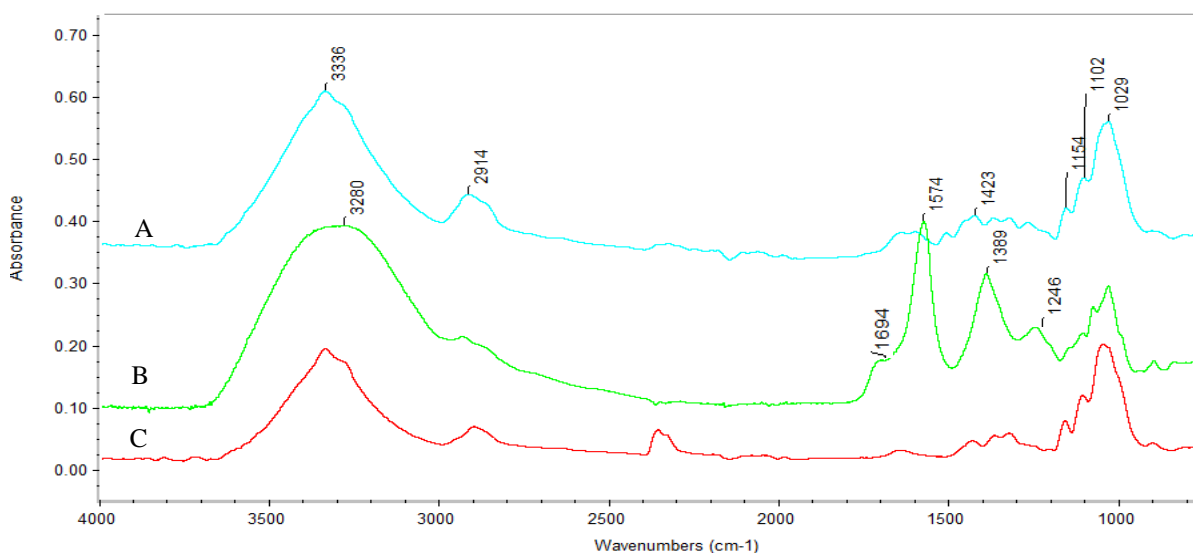
Figure 4.14: Infrared spectra of A) untreated virgin pulp PS B) enzymatically hydrolysed virgin pulp PS and C) CNF control sample. Duplicate samples were measured with at least two measurements each.

4.5. Various downstream processes for quality-improvement of cellulose nanoparticles produced

In comparison to acid hydrolysis, an increased amount of impurities was present in cellulose nanoparticles derived from enzymatic hydrolysis of PS (enzymatic hydrolysis in Figure 4.12 versus acid hydrolysis in Figure 4.9 and Figure 4.10). These impurities may include soluble sugars, salts from the pH-controlling buffer, and non-cellulosic organic material (ash, hemicellulose and lignin). In order to improve the quality of the cellulose nanoparticle product, the particle size distribution (PSD presented by the PdI) and purity were considered. Two processes were considered to increase the quality by reduction of the PdI to achieve a more uniform particle size, namely vacuum microfiltration and high-shear homogenisation. In order to improve the purity, the hydrolysed and glass-filtered supernatant was

68

dialysed, while washing of the residual solids was also investigated in order to extract the entrapped cellulose nanoparticles. Finally, the cellulose nanoparticle yield was determined gravimetrically.

As no CCD-optimised set of conditions could be achieved for the printed recycle PS, an additional range of conditions were selected for investigation of the effect of downstream processing on the purity and the yield of cellulose nanoparticles. These selected conditions indicated with sample numbers in Table 4.15, originate from the hydrolysis conditions according to the CCD design given (and highlighted) in Table 4.7. Conditions in the same ranges from virgin pulp PS were selected for comparison. These conditions were selected according to a mean particle size upper limit of 500 nm according to CNC quality requirements, with further selection based on type of enzyme and the produced glucose concentrations from the CCD runs (Section 4.3), as presented in Table 4.15. CCD-optimised conditions for virgin pulp PS (OVP) and selected conditions for printed recycle PS (SPR) was used as set out in Table 4.10 and Table 4.11, respectively.

Table 4.15: Selection criteria of further investigation of cellulose nanoparticle recovery based on the enzyme used and glucose concentration for each PS feedstock. Selected sample numbers indicate the hydrolysis conditions according to the CCD detailed in Table 4.7 and Table 4.8.

Enzyme	Glucose Level	Printed Recycle PS g/L	Virgin Pulp PS g/L	Selected Printed Recycle Sample No.	Selected Virgin pulp Sample No.
FiberCare	Low	< 3	< 6	30	60
CTec2	Medium	3 - 7	6 - 14	8	38
Combined Cocktail	High	> 7	> 14	19	50

4.5.1. Microfiltration of supernatant for quality-improved cellulose nanoparticle production

Cellulose nanoparticles produced by any process is a complex mixture of nanoscale particles, microscale fibrils and residual fibres in the millimetre scale, hence a size fractionation process was considered with membrane filtration. It was evident that the mean particle sizes of all samples were decreased to ≤ 200 nm after the 0.45 μm membrane microfiltration (Table 4.16). Accordingly, the PdI confirmed narrower distributions after microfiltration, ranging from 0.15 to 0.49 for both feedstock (Table 4.16). The microfiltration resulted in a product that was reasonably uniform in size, independent of the enzyme-type used, and therefore has the potential to produce a high-quality cellulose nanoparticles.

Enzymatic hydrolysis with endoglucanase-enriched cellulase in combination with microfiltration (with a 0.45 μm membrane) provided nanocellulose product with relatively, the highest quality based on mean particle size and polydispersity. After microfiltration, relatively high PdI values (Table 4.16) were confirmed for samples hydrolysed with FiberCare (0.48 for printed recycle PS and 0.49 for virgin pulp PS). In comparison, the PdI values were much lower for the samples hydrolysed with endoglucanase-

enriched cellulase cocktails (0.15 – 0.19 for printed recycle PS and 0.25 – 0.35 for virgin pulp PS) or with CTec2 (0.13 for printed recycle PS and 0.25 for virgin pulp PS). This indicated that for PS hydrolysed with FiberCare, a wide particle size distribution consisted for a maximum size limit of 450 nm, demonstrating the enhanced effect of endoglucanase-enriched cellulase cocktails and its accompanying synergistic effects on the uniformity of the cellulose nanoparticles.

Table 4.16: Mean particle size and PdI of enzymatically hydrolysed samples for both feedstock after glass-membrane - and 0.45 µm-membrane filtration. Samples ID from experimental design conditions sets in Table 4.7 and Table 4.8. Mean sizes were determined from single measurements of triplicate samples. The average of single measurements of triplicate polydispersity samples were determined.

Feedstock	Sample ID	Enzyme	Glass-membrane filtration		0.45 µm-membrane filtration	
			Mean Particle Size nm	PdI	Mean Particle Size nm	PdI
Printed Recycle PS	-	SPR	226 ± 33	0.51 ± 0.02	135 ± 7	0.15 ± 0.09
	8	Combined	264 ± 97	0.79 ± 0.10	125 ± 39	0.13 ± 0.05
	19	CTec2	313 ± 8	0.16 ± 0.08	135 ± 10	0.19 ± 0.02
	30	FiberCare	413 ± 7	1.00 ± 0.00	198 ± 40	0.48 ± 0.17
Virgin Pulp PS	-	OVP	232 ± 30	0.62 ± 0.04	163 ± 15	0.35 ± 0.03
	38	Combined	305 ± 35	0.30 ± 0.04	204 ± 43	0.27 ± 0.01
	50	CTec2	283 ± 18	0.29 ± 0.02	147 ± 9.6	0.25 ± 0.03
	60	FiberCare	202 ± 25	0.65 ± 0.15	158 ± 15	0.49 ± 0.06

Overall from Table 4.16, as observed from the narrower PdI values and smaller mean particle sizes for the printed recycle PS samples confirmed that cellulose nanoparticles with better polydispersity properties were achievable through microfiltration of printed recycle PS in comparison to virgin pulp PS. Microfiltration showed great potential at a lab scale, however, a 0.45 µm membrane may not be feasible at an industrial scale, and therefore high-shear homogenization was considered as an alternative process.

4.5.2. Post-hydrolysis mechanical treatment of supernatant for quality-improved cellulose nanoparticle production

After high-shear homogenization of the selected enzymatically hydrolysed samples (Table 4.17), a lack of substantial trends was observed with regards to the mean particle size and PdI values. It was possible that some level of shearing occurred leading to larger particles to be shortened, yet at the same time agglomeration of the more monodisperse samples occurred, as also found by other researchers (Pääkkö, et al., 2007; Henriksson, et al., 2007).

Table 4.17: Mean particle size and PdI before and after post-hydrolysis homogenisation for 3 x 10 min cycle at 14 000 rpm. Mean sizes were determined from single measurements of triplicate samples. The average of single measurements of triplicate polydispersity samples were determined.

Feedstock	Sample ID	Before homogenization		After homogenization	
		Mean Particle Size d.nm	PdI	Mean Particle Size d.nm	PdI
Printed Recycle PS	SPR	226 ± 33	0.51 ± 0.02	217 ± 35	0.31 ± 0.04
	8	264 ± 97	0.79 ± 0.10	193 ± 10	0.53 ± 0.03
	19	313 ± 8	0.16 ± 0.08	584 ± 144	0.79 ± 0.19
	30	413 ± 7	1.00 ± 0.00	439 ± 18	0.30 ± 0.04
Virgin pulp PS	OVP	232 ± 30	0.62 ± 0.04	331 ± 24	0.33 ± 0.03
	38	305 ± 35	0.30 ± 0.04	292 ± 32	0.37 ± 0.07
	50	283 ± 18	0.29 ± 0.02	401 ± 37	0.52 ± 0.15
	60	202 ± 25	0.65 ± 0.15	366 ± 1	0.54 ± 0.15

In order to investigate the effect of homogenization on larger mean particle sizes, printed recycled PS samples with micrometre mean particle sizes were homogenised under the same conditions (Table 4.10). For the selected samples, the mean particle size and PdI values after homogenization decreased marginally. Therefore, high-shear homogenisation of particles with lower than 1000 nm in mean particle size did not significantly improve the quality of the cellulose nanoparticle product in terms of reducing PdI value and mean particle size. It was therefore suggested that the high-shear homogenisation could be more beneficial as a step before the glass-membrane filtration with accordingly diluted hydrolysed slurries.

Table 4.18: Mean particle size and PdI before and after post-hydrolysis homogenisation for 3 x 10 min cycle at 14 000 rpm. Sample numbers indicate the hydrolysis conditions according to the CCD detailed in Table 4.7. Mean sizes were determined from single measurements of triplicate samples. The average of single measurements of triplicate polydispersity samples were determined.

Sample no.	Before homogenization		After homogenization	
	Mean Particle Size d.nm	PdI	Mean Particle Size d.nm	PdI
26	1029 ± 74	0.496 ± 0.120	954 ± 59	0.443 ± 0.086
12	1211 ± 38	0.872 ± 0.051	802 ± 118	0.786 ± 0.141

4.5.3. Dialysis of enzyme hydrolysed supernatant for purity-improved cellulose nanoparticles

Hydrolysed supernatant containing cellulose nanoparticles were dialysed to remove low molecular weight salts and sugars. After dialysis, the mean particle size for all the samples increased (Table 4.19). This was possibly due to agglomeration caused by the interdiffusion of water with the sample solution where the increase in sample purity causes cellulose nanoparticles to have more frequent encounters that cause their aggregation (Wondraczek, et al., 2013). It must be noted that monomer sugar concentrations (glucose, cellobiose, xylose and arabinose) as analysed for by HPLC analysis for all dialysed samples

were < 0.01 g/L (data not shown). This was good indication that dialysis increased the purity of the samples, yet allowed strong hydrogen bonds of cellulose nanoparticles to cause particle agglomeration.

Table 4.19: Mean particle size and PdI values after dialysis of enzymatically hydrolysed and glass-membrane filtered samples. Mean sizes were determined from single measurements of triplicate samples. The average of single measurements of triplicate polydispersity samples were determined.

Feedstock	Sample no.	Before Dialysis		After Dialysis	
		Mean Particle Size nm	PdI	Mean Particle Size nm	PdI
Printed Recycled PS	ORP	226 ± 33	0.51 ± 0.02	305 ± 27	0.46 ± 0.12
	8	264 ± 97	0.79 ± 0.10	644 ± 142	0.66 ± 0.17
	19	313 ± 8	0.16 ± 0.08	336 ± 92	0.54 ± 0.07
	30	413 ± 7	1.00 ± 0.00	417 ± 90	0.39 ± 0.05
Virgin Pulp PS	OVP	232 ± 30	0.62 ± 0.04	343 ± 141	0.29 ± 0.19
	38	305 ± 35	0.30 ± 0.04	427 ± 59	0.32 ± 0.03
	50	283 ± 18	0.29 ± 0.02	681 ± 36	0.48 ± 0.12
	60	202 ± 25	0.65 ± 0.15	332 ± 43	0.92 ± 0.05

Figure 4.15 indicates the FTIR spectra of selected dialysed samples dosed with A) CTec2 only, B) an endoglucanase-enriched cellulase cocktail and C) FiberCare only, for printed recycle PS. In the same alphabetical sequence, the FTIR spectra of selected dialysed samples from virgin pulp PS was presented by Figure 4.15D, E and F. For all the samples, peaks at 1229, 1073 and 1038 cm^{-1} confirmed the presence of cellulose. It was clear from the peaks at 1636 and 1260 cm^{-1} that non-cellulosic particles are still present after dialysis, including hemicellulose, lignin and sodium citrate. Yet, by the relative intensities of the peaks, it could be noticed that a much lower degree of impurities was present in the cellulose nanoparticles from virgin pulp PS in comparison to that of the printed recycle PS. Therefore, dialysis of enzymatically hydrolysed supernatant increased the purity of the cellulose nanoparticles, by removal of the monomer sugars. However, dialysis of the hydrolysed supernatant was not sufficient to remove the citrate buffer from the cellulose nanoparticle product.
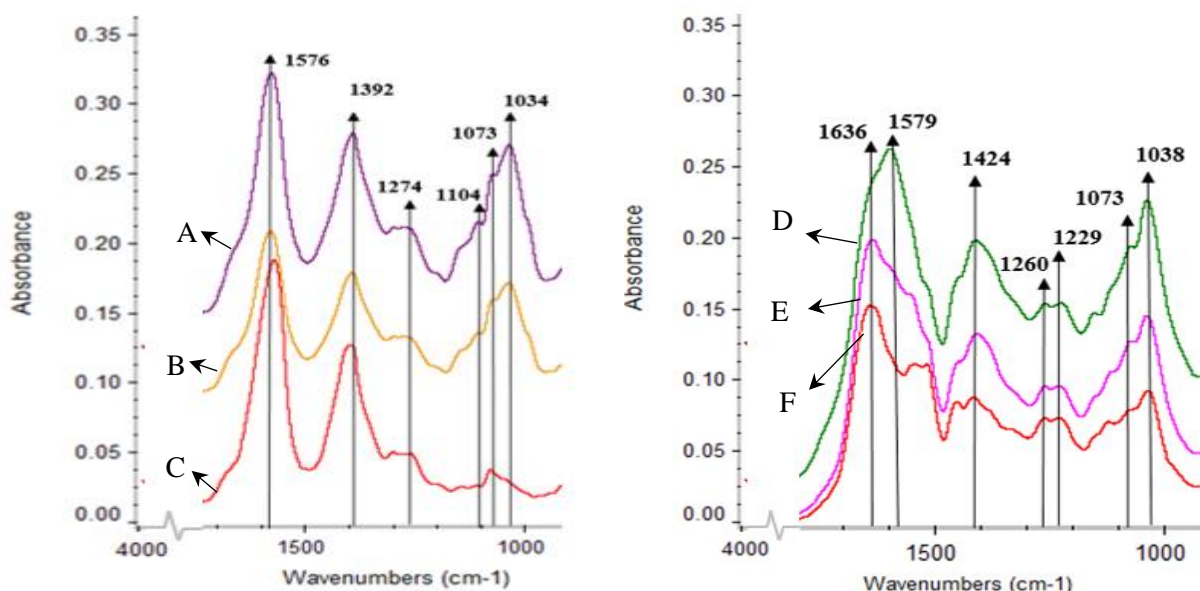
Figure 4.15: FTIR spectra of enzymatically hydrolysed and dialysed A) printed recycle PS with CTec2, B) printed recycle PS with endoglucanase-enriched cellulase cocktail, and C) printed recycle PS with FiberCare only D) virgin pulp PS with CTec2, E) virgin pulp PS with endoglucanase-enriched cellulase cocktail, and F) virgin pulp PS with FiberCare only. Duplicate samples were measured with at least two measurements each.

4.5.4. Washing of enzymatically hydrolysed solids for purity-improved cellulose nanoparticles

Centrifugation washing of enzymatically hydrolysed solid samples were conducted in order to investigate the purity improvement as well as for crystallinity determination through XRD analysis. More than 98% of monomeric sugars (glucose, cellobiose and xylose) were removed from the enzymatically hydrolysed solids samples after three washing steps (Table 4.20). DLS analysis indicated that the mean particle size remained in the same size range (Table 4.20). Three washes in comparison with the required 5 to 7 washes (of the same water volume) after acid hydrolysis indicated how enzymatic hydrolysis could be advantageous over acid hydrolysis by decreased water requirements with a factor of 2 to 4, during cellulose nanoparticle production.

From Table 4.20 it was evident that the PdI values decrease with increase in washing step, for both PS feedstock, while the mean particle size stayed in the same particle size range (200 – 500 nm). This indicated that the particle size distribution changed from a broad one to a narrower distribution, increasing the particle quality. Figure 4.16 shows the FTIR spectra of an enzymatically hydrolysed sample from selected conditions for printed recycle PS after A) one wash step, B) two wash steps and C) three wash steps. It was evident from the decreasing intensity of cellulose-fingerprint peaks at $1106 - 1041$ cm^{-1} that with increase in washing step, the cellulose content was decreased.

73

Table 4.20: Sugar concentrations, mean particle size and PdI of unwashed enzymatically hydrolysed sample (wash step 0) versus washed samples per step. The standard deviation of all the sugar concentrations were determined to be < 0.13 g/L. 0 g/L arabinose concentrations were found for all the samples. The standard deviation of the mean particle size (were determined from single measurements of triplicate samples) for all the samples were < 65 nm and for the PdI (single measurements of triplicate samples) was < 0.1.

Feedstock	Sample	Washing Step	Sugar Concentration (g/L)			Mean Particle Size (nm)	PdI
			Glucose	Cellobiose	Xylose		
Printed Recycle PS	Selected	0	6.38	0.00	1.71	226	0.85
		3	0.10	0.00	0.00	256	0.60
	19	0	7.94	0.00	2.12	313	0.16
		3	0.05	0.00	0.00	240	0.33
	8	0	3.04	0.00	1.82	264	0.79
		3	0.00	0.00	0.00	345	0.48
	30	0	0.00	0.21	0.00	413	1.00
		3	0.00	0.00	0.00	518	0.37
Virgin Pulp PS	Optimised	0	5.44	0.00	1.11	232	0.62
		3	0.00	0.00	0.00	375	0.25
	38	0	11.71	0.00	3.10	305	0.30
		3	0.00	0.00	0.00	452	0.56
	50	0	18.72	0.00	3.85	283	0.29
		3	0.35	0.00	0.05	540	0.15
	60	0	0.00	0.00	0.00	202	0.65
		3	0.00	0.00	0.00	353	0.46
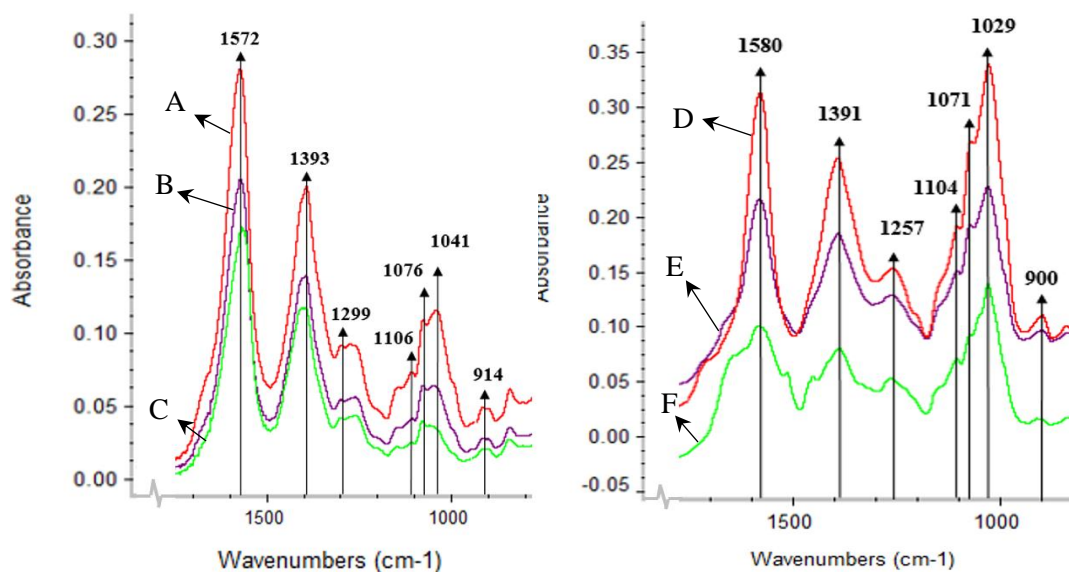
Figure 4.16: FTIR spectra of washed enzymatically hydrolysed samples for A) printed recycle PS after one wash step, B) printed recycle PS after two wash steps and C) printed recycle PS after three wash steps virgin pulp PS washed after D) virgin pulp PS after one wash step, E) virgin pulp PS after two wash steps and F) virgin pulp PS after three wash steps. Duplicate samples were measured with at least two measurements each.

The general trend in spectra was found to be the same for virgin pulp PS (Figure 4.16D – 4.27F). It was evident from the peaks at 1572 and 1393 cm^{-1} that sodium citrate buffer was still present after three washes. For the washing steps of the virgin pulp PS feedstock, the peaks of the carboxyl groups decrease in intensity relative to the cellulose fingerprint peaks (1104 – 1029 cm^{-1}). This indicates that the cellulose

74

nanoparticle product from the virgin pulp PS had increased purity in comparison to the cellulose nanoparticle product from the printed recycle PS.

Elemental analysis through Energy dispersive X-ray spectroscopy was conducted for selected enzymatically hydrolysed and solids-washed samples of printed recycle and virgin pulp PS, as presented in Figure 4.17A and Figure 4.17B, respectively (with raw data in Figure 7.3 and Figure 7.4 in Appendix C). It was clear that some ash component (represented by the Cl and Ca (CaO and $CaCO_3$) in ash) and sodium (Na) from the sodium citrate buffer are still present in the samples after the third washing step, for both feedstock. Yet, the Ca, Na and S are in the minority; for both PS feedstock, less than 8 % (w/w) of the sample was ash and citrate buffer impurity. The lack of nitrogen (N) indicated that insignificant quantities of enzyme were present for samples from both feedstock.
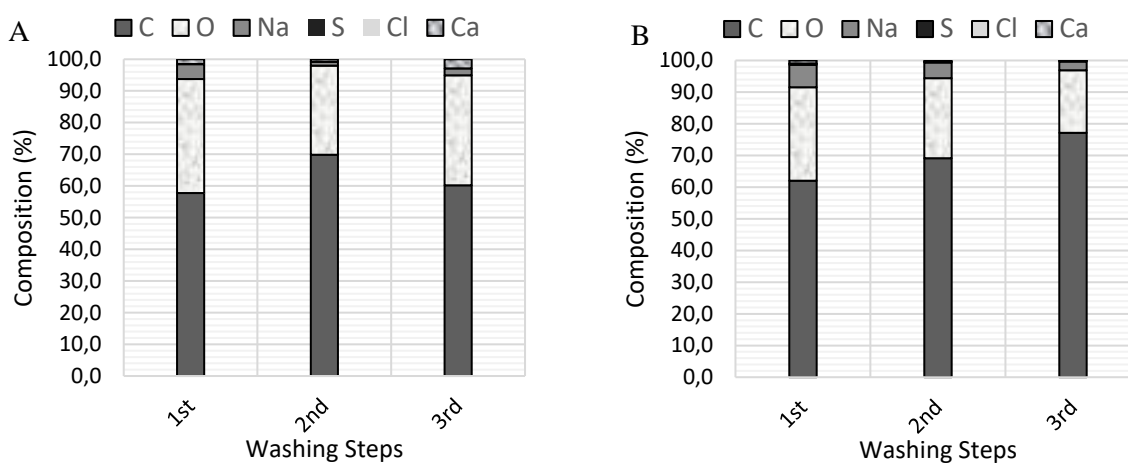
Figure 4.17: Composition of major elements from EDX elemental analysis of samples submitted to centrifugation washing steps of A) printed recycle PS (Standard deviation for all compositions < 3.3%) and B) virgin pulp PS (Standard deviation for all compositions < 0.5%). Appendix D shows representative images which was used to determine the elemental analysis through SEM imaging. Single measurements of duplicate samples were used.

For the virgin pulp, an increasing purity was observed with subsequent washing steps. The same trend was not seen for the printed recycle. Also, the standard deviation in compositions are larger (up to 3.3%) for the printed recycle PS, in comparison to the maximum of 0.5% for the virgin pulp PS. The lack of trend and increased standard deviation might be due to the ash component in the printed recycle PS. In conclusion, the purity of the cellulose nanoparticle products was improved after at least 3 centrifugation washing steps as the impurities were removed to substitute less than 8% (w/w) of the product. This was in good agreement with the FTIR spectra results from the infrared analysis (Figure 4.16).

Table 4.21: Crystallinity of cellulose nanoparticles from enzymatic hydrolysis and raw materials determined by XRD with Peak Height Method.

Feedstock	Crystallinity (%)	
	Untreated PS	Enzymatically hydrolysed
Virgin pulp PS	35.5 ± 0.57	35.8 ± 1.74
Printed recycle PS	49.4 ± 0.55	47.0 ± 0.81

The cellulose crystallinity of the produced cellulose nanoparticles from the optimised conditions for virgin pulp PS and the selected conditions for printed recycle PS were found to be in the same range as that of the raw PS materials (Table 4.21). Although previous literature reported increases in crystallinity after enzymatic treatment of cotton for the production of cellulose nanoparticles (Paralikar & Bhatawdekar, 1984), no significant crystallinity increases were found with the current study. However, as no decrease in crystallinity was observed after enzymatic hydrolysis, it could be explained that the particles retained predominantly paracrystalline and crystalline regions.

4.5.5. Cellulose nanoparticle yield estimation

The cellulose nanoparticle yield is a key characteristic due to its implication for the global cost of the process and was determined from an up-scaled set of enzymatically hydrolysed samples according to the optimum and selected conditions and conditions set out in Table 4.15. From each sample, one part of the hydrolysed supernatant was dialysed, and the other part was washed. The hydrolysed solids mass was also washed.

Yield estimations from washing of the *hydrolysed supernatant* (filtrate) were found to be smaller than 0.001% (data not shown). In comparison, dialysis of the supernatant resulted in yields of < 1.5% for both feedstock (Table 4.22). On the other hand, for yield estimations of the *hydrolysed residual solids* (filter cake) under optimised conditions (Table 4.22), higher yields of 6.0% and 5.9% were achieved for the virgin pulp PS and the printed recycle PS, respectively. It was therefore concluded that firstly, supernatant washing caused product loss compared to dialysis; and secondly, that most of the enzymatically hydrolysed cellulose nanoparticles were entrapped in the hydrolysed solids mass as opposed to the supernatant.

The total cellulose nanoparticle yields were determined from summarising the dialysed supernatant and the washed hydrolysed solids mass (Table 4.22). The highest yield of cellulose nanoparticles for the virgin pulp PS found to be 7.5% at the optimised conditions. For hydrolysis of printed recycle PS, the highest combined yield of 6.9% was obtained at selected conditions of 12 hrs enzymatic hydrolysis of 6% (w/w) solids loading at CTec2 and FiberCare dosages of 20 FPU/gdPS and 100 ECU/gdPS, respectively. This indicated that the selected conditions from the identified possible ranges for printed recycle PS hydrolysis provided acceptable conditions in terms of highest yields in comparison to other tested enzyme dosage ratios.

Table 4.22: Yield estimations of cellulose nanoparticle product of supernatant after hydrolysis, centrifugation, glass-membrane filtration and dialysis (dialysis yield) and yield estimations of product of samples after washing of the residual solids (washing yield). Sample nr identification are according to the CCD design run conditions in Table 4.7 and Table 4.8.

Enzyme	Feedstock	Sample No.	FiberCare Dosage ECU/gdPS	CTec2 Dosage FPU/gdPS	Mean Size nm	Dialysis Yield % (w/w)	Washing Yield % (w/w)	Total Yield % (w/w)
Optimised	VP	-	80	10	232	**1.49**	**5.99**	**7.48**
Selected	PR	20	100	20	226	**0.97**	**5.90**	**6.86**
FiberCare	VP	60	50	0	202	**0.20**	**3.41**	**3.61**
	PR	30	50	0	413	**0.51**	**2.51**	**3.02**
CTec2	VP	38	0	20	305	**0.33**	**1.17**	**1.50**
	PR	8	0	20	264	**0.84**	**5.67**	**6.50**
Endoglucanase-Enriched Cocktail	VP	50	100	20	283	**0.44**	**2.98**	**3.42**
	PR	19	50	20	313	**0.34**	**2.61**	**2.96**

For the printed recycle PS, with the relatively higher crystallinity (Section 4.2) of the two starting material, a cellulose nanoparticle yield of 6.5% (Table 4.22) with a glucose yield of 11.2% (Table 4.7, before washing) was achieved with the CTec2. In comparison, a lower cellulose nanoparticle yield of 3.0% (Table 4.22) with a higher glucose yield of 29.1% (Table 4.7, before washing) was obtained for the endoglucanase-enriched cellulase cocktail. This indicated that a higher endo-to-exo ratio of 20 FPU/100 ECU was required for hydrolysis of printed recycle PS, due to a higher degree of crystalline regions (Figure 4.4) and shorter starting particle sizes (Section 4.1.1), with more available chain ends.

For virgin pulp PS, a cellulose nanoparticle yield of 3.4% (Table 4.22) and glucose yield of 46.3% (Table 4.8 before washing) were achieved for hydrolysis with an endoglucanase-enriched cellulase cocktail with a lower endo-to-exo ratio of 20 FPU/100 ECU. A lower cellulose nanoparticle yield of 1.5% and a 29.0% glucose yield (Table 4.8, before washing) was achieved with CTec2 (Table 4.22), indicating that a low endo-to-exo ratio resulted in higher processive hydrolysis of cellulose to soluble oligomers. From the optimised conditions for virgin pulp PS with a yield of 7.5% and the glucose yield of 26.9%, it was evident that PS with a longer starting particle size (Section 4.1.1) and a low crystallinity (Section 4.2) required a higher endo-to-exo ratio (10 FPU/80 ECU).

Higher yields of $21.1 \pm 2.01\%$ from virgin pulp PS and $12.3 \pm 0.92\%$ from printed recycle PS were achieved through acid hydrolysis (Table 4.12). The low product yields from acid hydrolysis in comparison with literature values which are > 30% (Table 2.2) are a consequence of the lower cellulose content and impurities in the starting material, whereas other studies have started with purer cellulose feedstock (Bondeson, et al., 2006; Satyamurthy, et al., 2011). The generally low yield from enzymatic hydrolysis had been widely reported (Anderson, et al., 2014), even with post-hydrolysis sonication or mechanical treatment (Fattahi Meyabadi & Dadashian, 2012; Marino, et al., 2015). Nevertheless, SCN were produced from enzymatic hydrolysis of PS with mentionable yields and dimensions, morphology and crystallinity (Table 4.23) satisfying the standards according to ISO specifications (Table 2.1).

Comparatively, with acid hydrolysis of the same starting feedstock, a mixture of CNC and CNF was produced, also satisfying the standards according to ISO specifications. The SCN produced through enzymatic hydrolysis of PS could be used for thickening of cosmetic and pharmaceutical products, as well as immobilization of biological active substances and drugs (Zhang, et al., 2007).

Table 4.23: Characteristics of cellulose nanoparticles produced under optimal and selected conditions of enzymatic hydrolysis of PS. Mean sizes were determined from single measurements of triplicate samples. The size averages of 100 measurements were determined for 3 - 5 SEM images per sample. The average of single measurements of triplicate polydispersity samples were determined.

Feedstock Characteristic	Unit	Virgin pulp PS	Printed recycle PS
Morphology		Spherical, non-entangled	Spherical, non-entangled
SCN diameter	nm	137 ± 50	30 ± 6
Sample mean length	nm	226 ± 33	626 ± 148
Polydispersity	-	0.62 ± 0.04	0.51 ± 0.02
Crystallinity	%	35.8 ± 1.74	47.0 ± 0.81
Yield	%	7.5	6.9

Enzymatic hydrolysis of the virgin pulp PS resulted in 9% higher cellulose nanoparticle yield than the printed recycle PS. Between the two feedstock, the maximum yield was obtained for the virgin pulp PS, at 2 times lower CTec2 dosage (10 FPU/gdPS) and 1.25 times lower FiberCare (80 ECU/gdPS). The printed recycle PS gave higher yields at a two times higher solids loading than virgin pulp PS, but this was due to the lower glucan content per gram PS. These results collectively suggest that a stand-alone enzymatic hydrolysis process with virgin pulp PS provides a higher process performance for production of cellulose nanoparticles than printed recycle PS. It was further noted, that even with low R^2-values and lack of fit of the prediction models developed for printed recycle PS, the selected conditions provided yields that was well comparable with that of the optimised conditions of virgin pulp PS. Potential applications with the required attributes per cellulose nanoparticle type are summarised in Table 4.24.

Table 4.24: Possible applications and required physical attributes of different types of cellulose nanoparticles (International Standards Organization, 2017)

Particle Type	Required Morphology	Dimensions	Potential Applications
SCN	• Spherical morphology • High purity • Amorphous, paracrystalline or crystalline	Diameter 40 – 600 nm	• Immobilization of biological active substances and drugs • Cosmetic and pharmaceutical products
CNC	• Rod-like morphology • Moderate to high purity • Paracrystalline or crystalline	Diameter 3 – 50 Length 100 – 4000 nm	• Packaging films • Sensors • Textiles • Personal care products
CNF	• Network-like morphology • Moderate to high purity • Amorphous, paracrystalline and/or crystalline	Diameter 3 – 100 nm Length 100 – 100 000 nm	• Paper processing • Composites • Adhesives

4.6.   Proposed cellulase hydrolysis mechanism

After close inspection of the results from the optimisation experiments and various analyses, it was evident that during cellulase hydrolysis, a range of particle sizes with different morphologies will always be produced as enzymes work synergistically, having different cleaving and hydrogen-splitting actions occurring simultaneously. A possible short-period cellulase hydrolysis mechanism (Figure 4.18) was therefore proposed, to explain the formation of the majority of the nanoparticles. This mechanism was specifically for higher endoglucanase to exoglucanase ratio:

Figure 4.18**a** shows the cellulase enzymes attached to cellulose chains (disrupted chains as shown with SEM imaging in Figure 4.2). Endoglucanase attacked the amorphous areas, swelling the fibrils and releasing insoluble polymer chains. After termination of the endoglucanase at the start of crystalline cellulose regions, new crystalline chain ends were made available for exoglucanase to hydrolyse in a processive (cleaving) custom, releasing soluble oligomers.

Simultaneous hydrolyses at multiple sites decreased the chain diameter and length of the cellulose through scission of the β-D-(1,4)-glycosidic linkages (Figure 4.18**b**). Concurrently, β-glucosidase acted on the soluble oligomers to release glucose monomers (Table 4.7 and Table 4.8). Higher amount of endoglucanase enzymes, in classical endoglucanase-mode, released a higher amount of chain fragments. This limited the exoglucanase action per fragment in effect reducing cellubiose formation. Furthermore, change in the intensity and width of the FTIR band in 3600–3000 cm^{-1} of hydrolyzed PS showed that the cellulase enzyme could weaken and split the hydrogen bonds in the cellulose, creating lose fragments as well as soluble oligomers (Figure 4.11).

Figure 4.18**c** indicates exoglucanases acting on reducing and non-reducing ends of chains created by endoglucanases, shortening the cellulose fragments in length.

Particle size lengths significantly decreased after 9 - 12 h enzymatic hydrolysis (Figure 4.18**d**). Consequently, according to the results of DLS and SEM particle size as well as yield analyses (Table 4.3 and Table 4.22), the enzymatic hydrolysis led to formation of respectable amounts of particles with mostly low aspect ratio, resembling a spherical morphology (Figure 4.12).
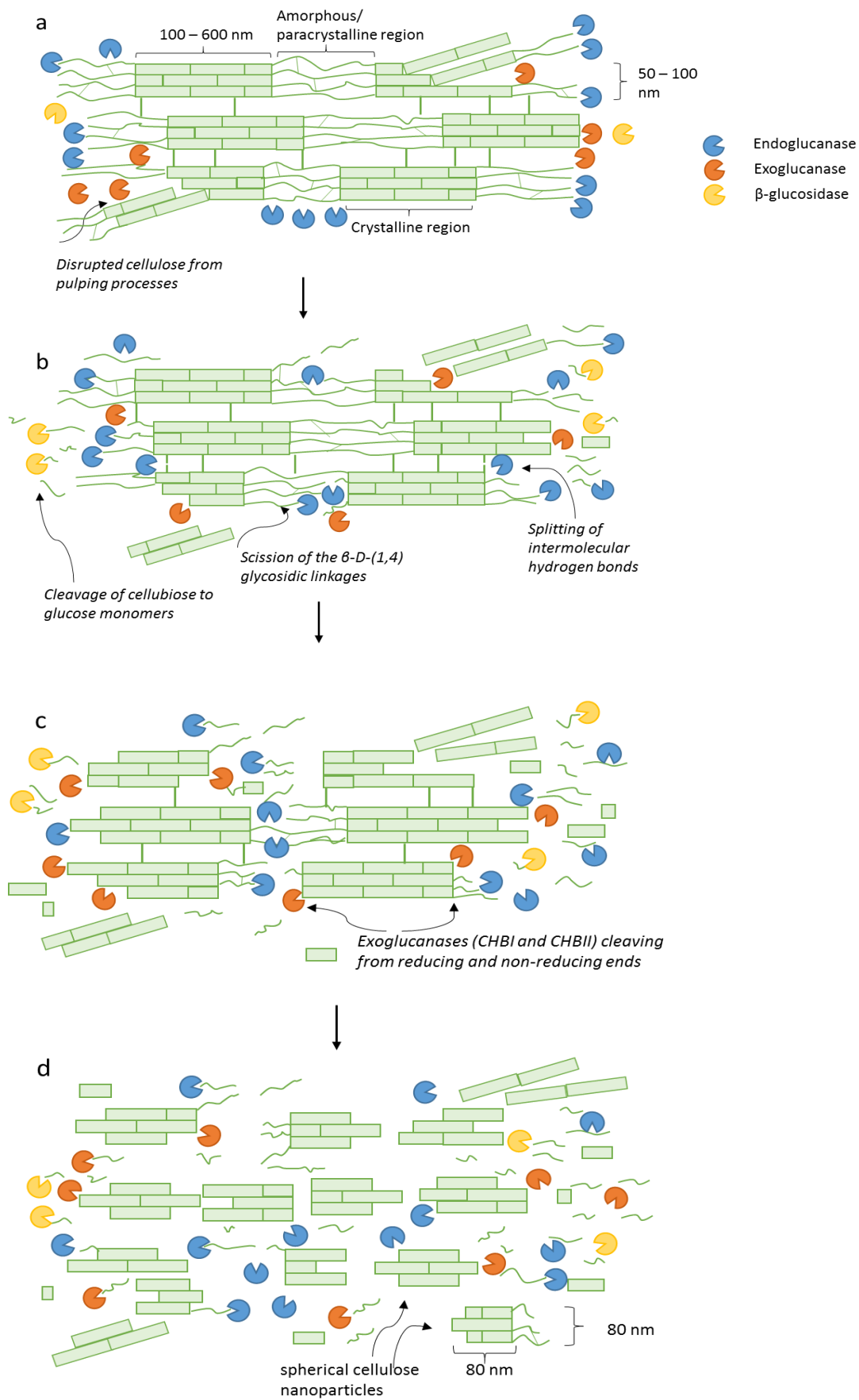
Figure 4.18: Proposed schematic image of nanoparticle production through enzymatic hydrolysis with a fungal cellulase blend. Figure not drawn to scale.

81

4.7. Mass balancing

A mass balance evaluation was conducted for each of the PS feedstocks, with 100 g of dry feedstock assumed as feed basis (Table 4.25). In a closed system, the total amount of glucose into a system (1) should equal the amount of glucose out of a system (2 + 3 + 4). Percentage errors of 11.9% and 10.1% were determined for printed recycle and virgin pulp PS, respectively. These errors could have resulted partly due to the residual solids that could not be captured (mass loss on the filter paper during phase separation or in the reactor flask) as well as partly due to analytical error. Nevertheless, the estimated percentage errors were relatively small and therefore, the mass balance verified the integrity and consistency of the analysis approaches and data.

Table 4.25: Mass balance for the printed recycle PS and virgin pulp PS. 100 g of PS assumed as feed basis

Mass Balance Values	Unit	Printed Recycle	Virgin Pulp
PS Feed Mass Basis	g	100	100
Glucan Fraction in PS[1]	%	42.0	57.2
1. Mass of Glucose in Glucan[2]	g	**37.8**	**51.3**
Yield of Cellulose Nanoparticles Produced[3]	%	6.86	7.48
2. Mass of Glucose in Cellulose Nanoparticles[4]	g	6.18	6.73
3. Mass of Glucose as Hydrolysis Products in Supernatant[5]	g	2.17	2.96
4. Mass of Glucose in Residual Solids[6]	g	24.9	36.4
Mass Summation[7]	g	**33.3**	**46.1**
Percentage Error[8]	%	11.9	10.1

---

[1] Fractions as determined by chemical compositional analysis

[2] Glucan fraction * Anhydro Correction Factor (Equation 3)

[3] Gravimetric Estimation [Total cellulose nanoparticles produced / Mass PS fed *100] (Equation 4)

[4] Glucose amount calculated with Anhydro Correction factor, mass calculated with liquor volume of samples

[5] Analysed with HPLC, mass calculated with liquor volume of samples

[6] Compositional analysis of residual solids, and determined from washing process and dialysis process, mass calculated with liquor volume of samples

[7] Mass summation = [2] + [3] + [4]

[8] Percentage error (%) = ([1] - ∑([2]+[3]+[4]))/[1] * 100

Chapter 5.   General conclusions and recommendations

The aim of this study was to develop and optimize a process for cellulose nanoparticle production from waste PS with enzymatic hydrolysis as the integral process. This was conducted by identifying efficient preparation of two PS feedstock selected from South African paper and pulp mills and screening of commercial enzymes for cellulose nanoparticle production. Based on the screening data, optimisation of virgin pulp PS was done for minimal mean particle size and minimal glucose formation. Due to statistical insignificance of the printed recycle PS optimisation models, a selection procedure was conducted to determine favourable conditions for cellulose nanoparticle production by enzymatic hydrolysis. Downstream processes were studied to improve on purity, quality and yield of the cellulose nanoparticles produced.

5.1. Conclusions

Main conclusions from this study are discussed based on the objectives as specified in Section 2.6.

   i)   Effective PS feedstock preparation for enzymatic hydrolysis

Small-scale disintegration filter-washing significantly reduced the ash content of high ash-content PS which created a high glucan-content feedstock for enzymatic hydrolysis. An achieved ash decrease with as much as 56% lowered the amount of enzyme inhibitors per solid loading and led to increased yield during cellulose nanoparticle production.

Steam explosion of low ash-content PS was found to be an ineffective treatment to increase the PS accessibility for hydrolysis. Insignificant digestibility increases were found for subsequent enzymatic hydrolysis of the steam exploded PS with Cellic® CTec2, as indicated by analysis of glucose concentrations.

   ii)   Selection of enzymes for PS hydrolysis to cellulose nanoparticles

Cellic® CTec2, in comparison with Viscamyl^{TM} Flo, was found to be the better-suited available commercial cellulase cocktail for cellulase blending to create an enzyme cocktail in terms of nanoparticle and minimal by-product formation for both virgin pulp and printed recycle PS. The monocomponent endoglucanase, FiberCare® R produced particles in mean particle size ranges similar to that of the cellulase cocktail Cellic® CTec2, with less by-product formation.

   iii)   Statistical optimisation of enzymatic hydrolysis of PS

Short-time cellulase hydrolysis of virgin pulp as well as printed recycle PS with commercial cocktail, Cellic® CTec2 enriched with the commercial monocomponent endoglucanase, FiberCare® R, resulted in the production of spherical cellulose nanoparticles (SCN). Statistical modelling of the mean particle size from the mechanically-pulped printed recycle PS presented difficulties due to the possible changes

in the microstructure of the recycled fibres, caused inconsistent, decreased cellulase activity on the cellulose chains of the recycled fibres, which resulted in inevitably wide particle size distributions. For virgin pulp PS, the collected data proved to be sufficient for optimisation of the production of cellulose nanoparticles. Optimised conditions for virgin pulp PS were found to be a hydrolysis time of 9 hrs, 3% (w/w) solids loading, low dosages of CTec2 (10 FPU/gdPS) and a FiberCare dosage of 80 ECU/gdPS. Through these optimised hydrolysis conditions for virgin pulp PS, SCN with mean particle size and glucose concentrations of 232 nm and 5.44 g/L were produced. Selected conditions for hydrolysis with printed recycle PS were 12 hrs, 6% (w/w) solids loading, low dosages of CTec2 (20 FPU/gdPS) and a FiberCare dosage of 100 ECU/gdPS. These hydrolysis conditions for printed recycle PS resulted in SCN particles with a mean particle size and glucose concentrations of 226 nm and 6.38 g/L.

By short-time, stand-alone enzymatic hydrolysis conditions, cellulose losses to glucose could be minimised and a selected cellulose nanoparticle type, including CNC and SCN within ISO standard specifications could be produced. This is beneficial over the stand-alone acid hydrolysis process, which produced a mixture of CNC and CNF. For printed recycle PS, cellulase dosages with high endoglucanase to exoglucanase ratio (20 FPU/100 ECU) was required to produce SCN while for virgin pulp PS, lower dosages with an even higher endoglucanase to exoglucanase ratio (10 FPU/80 ECU) was necessary.

iv) Characterisation of cellulose nanoparticles produced through enzymatic hydrolysis compared to acid hydrolysis

Acid hydrolysis produced higher yields of cellulose nanoparticles (10 – 20%) in comparison with the yields through enzymatic hydrolysis (< 10%). However, enzymatic hydrolysis produced either SCN or CNC as single-morphology products, depending on the ratio of enzyme dosages used, which is advantageous over acid hydrolysis of PS that resulted in a mixture of CNC and CNF particles for both feedstock. With a commercial cellulase blend such as CTec2 (20 FPU/gdPS), SCN could be produced from virgin pulp PS. However, for printed recycle PS, a higher endoglucanase dosage (20 FPU/100 ECU) was required to produce SCN. Furthermore, hydrolysis with a monocomponent endoglucanase (FiberCare) resulted in CNC production from both PS feedstocks.

v) Post-hydrolysis processes on quality of cellulose nanoparticles produced from enzymatic hydrolysis

Post-hydrolysis microfiltration increases the quality of SCN produced, due to narrowed particle size distributions. However, microfiltration would not be recommended for industrial applications due to the operating impracticality of 0.45 µm membranes. Results from high-shear homogenization of hydrolysed supernatant suggested that the quality of micrometre mean-sized printed recycle PS samples could be increased, especially before glass-membrane filtration for accordingly diluted hydrolysed slurries. High-shear homogenization for sample with nanometer mean-sized particles, however, were not affected.

vi)   Recovery processes on purity and yield of cellulose nanoparticles from enzymatic hydrolysis

Dialysis and solids-washing recovery processes were found to be essential for product purification and yield estimation. Dialysis of the hydrolysed suspensions improved the purity of the cellulose nanoparticles, as all sugar impurities were removed. Washing of the hydrolysed solids resulted in sugar concentrations of < 0.1 g/L for both virgin pulp and printed recycle PS feedstock. FTIR and elemental analysis confirmed that after washing of the cellulose nanoparticle product, minority fraction was non-cellulosic materials. Higher yields for both PS feedstock were achieved with washing of the residual solids part of the hydrolysed sample in comparison to dialysis of the supernatant part of the sample. After purification, final and maximised cellulose SCN yields of 6.9% for were achieved with enzymatic hydrolysis of printed recycle PS under selected, endoglucanase-enriched conditions and 7.5% for virgin pulp PS under optimised conditions.

Summary

This study provides a potential green method for the production of cellulose nanoparticles from waste PS, containing a low or high ash component, using different ratios of monocomponent endoglucanase and cellulase cocktails. Enzymatic hydrolysis of virgin pulp PS provides a higher process performance for the production of cellulose nanoparticles than printed recycle PS, based on the use of lower enzyme dosages, lower by-product formation and higher final yields achieved. However, printed recycle PS has an advantage of the possibility of higher solids loading compared to virgin pulp PS.

5.2. Recommendations and future work

Post-hydrolysis recovery and purification steps

Investigation of the effects of decreasing the starting material particle size to < 200 μm as well as using effluent water instead of a pH-controlling buffer for enzymatic hydrolysis, could lead to increased product purity and quality, saving costs on downstream processes. Enzymatic hydrolysis of pulp and paper effluent has been used for biohydrogen production (Lakshmidevi & Muthukumar, 2010), and could therefore hold potential for use in production of cellulose nanoparticles.

It is possible that a dilution of the enzymatically hydrolysed slurry before glass-membrane filtration would benefit more from the high-shear homogenisation treatment, which would also increase the yield. The use of high-pressure homogenisers are more common in literature due to its increased efficiency of producing cellulose nanoparticles, and could therefore also be recommended (Besbes, et al., 2011; Qing, et al., 2013).

Improved cellulose nanoparticle analyses

The use of spray-drying of hydrolysed suspensions instead of freeze-drying could prevent particle agglomeration, easing solids analyses and yield estimations (Peng & Chen, 2011). STEM imaging was a more effective microscopy analysis, as gold-coating was required for SEM analysis for enhanced conductivity which could interfere with particle morphology determinations.

Co-production of bioethanol and cellulose nanoparticles

For maximized use of PS as a feedstock and minimizing the hydrolysis residue, an integrated system for production of cellulose nanoparticles must be considered (Zhu, et al., 2011). Integrating a cellulose nanoparticles process with a sugar or bioethanol production process could offer promising results and add economic value. Duran et al. (2011) reports on an exhaustive economic analysis for producing CNW as a co-product in an ethanol bio-refinery with use of ASPEN Plus-based process models. The data suggested that production of CNW would be an enhancement to the economic feasibility of a wheat straw to ethanol production.

Reference List

Abraham, E. et al., 2011. Extraction of nanocellulose fibrils from lignocellulosic fibres: A novel approach. *Carbohydrate Polymers,* Volume 86, p. 1468– 1475.

Adina, C., Florinela, F., Abdelmounen, T. & Carmen, S., 2010. Application Of FTIR Spectroscopy For A Rapid Determination Of Some Hydrolytic Enzymes Activity On Sea Buckthorn Substrate. *Romanian Biotechnological Letters,* 15(6), pp. 5738 - 5744.

Africa Green Media, 2013. *Paper consumption to reach 500m tons.* [Online] Available at: http://africagreenmedia.co.za/paper-consumption-to-reach-500m-tons/ [Accessed 2016 April 16].

Alemdar, A. & Sain, M., 2008. Isolation and characterization of nanofibers from agricultural residues - Wheat straw and soy hulls. *Bioresource Technology,* Volume 99, pp. 1664 - 1671.

Aliyu, M. & Hepher, M. J., 2000. Effects of ultrasound energy on degradation of cellulose material. *Ultrasonics Sonochemistry,* Volume 7, pp. 265-268.

Anderson, S. R. et al., 2014. Enzymatic preparation of nanocrystalline and microcrystalline cellulose. *Tappi Journal,* 13(5), pp. 35 - 42.

Ankerfors, M., 2015. *Microfibrillated cellulose: Energy-efficient preparation techniques and applications in paper,* Stockholm: KTH Royal Institute of Technology .

Ankerfors, M., Lindström, T. & Henriksson, G., 2007. *Method for Manufacturing of Microfibrillated Cellulose.* Stockholm, Sweden, Patent No. WO 2007/091942 A1.

Ankerfors, M., Lindström, T. & Henriksson, G., 2009. *Method for Manufacturing of Microfibrillated Cellulose.* Stockholm, Sweden, Patent No. WO 2007/091942 A1.

Arantes, V., Gourlay, . K. & Saddler, J., 2014. The enzymatic hydrolysis of pretreated pulp fibers predominantly involves "peeling/erosion" modes of action. *Biotechnology for Biofuels,* 7(87), pp. 1-10.

Asaraf, M. & Finkiel, M., 2015. *Tuttnauer - Autoclave Sterilization Process Guide.* [Online] Available at: https://tuttnauer.com/autoclave [Accessed 13 May 2016].

Balat, M., Balat, H. & Oz, C., 2008. Progress in bioethanol processing. *Progress in energy and combustion science,* Volume 34, pp. 551-573.

Beck-Candanedo, S., Roman, M. & Gray, D., 2005. Effect of Reaction Conditions on the Properties and Behavior of Wood Cellulose Nanocrystal Suspensions. *Biomacromolecules,* Volume 6, pp. 1048-1054.

Beltramino, F. et al., 2016. Optimization of sulfuric acid hydrolysis conditions for preparation of nanocrystalline cellulose from enzymatically pretreated fibers. *Cellulose.*

Besbes, I., Vilar, M. R. & Boufi, S., 2011. Nanofibrillated cellulose from Alfa, Eucalyptus and Pine fibres: Preparation characteristics and reinforcing potential. *Carbohydrate Polymers,* Volume 86, pp. 1198-1206.

Bhatnagar, A. & Sain, M., 2005. Processing of Cellulose Nanofiber-reinforced Composites. *Journal of Reinforced Plastics and Composites,* Volume 24, pp. 1259 - 1268.

Bilodeau, M. & Paradis, M. A., 2013. *Energy Efficient Process for Preparing Nanocellulose Fibres.* Bangor, ME, Patent No. WO 2013/188657 A1.

Blanchette, R. A., 1991. Delignification by Wood-Decay Fungi. *Annual Review of Phytopathology,* Volume 29, pp. 381-98.

Bondeson, D., Mathew, A. & Oksman, K., 2006. Optimiszation of the isolation of nanocrystals from microcrystalline cellulose by acid hydrolysis. *Cellulose,* Volume 13, pp. 171-180.

Börjesson, M. & Westman, G., 2015. Crystalline Nanocellulose — Preparation, Modification,and Properties. In: *Cellulose - Fundamental Aspects and Current Trends.* Gothenburg: Intech, pp. 159 - 192.

Boshoff, S., 2015. *Characterisation and fermentation of waste paper sludge for bioethanol production,* Stellenbosch: Faculty of Engineering at Stellenbosch University.

Boshoff, S., 2016a. *Personal Communication.* Stellenbosch University: MPact.

Boshoff, S., Gottumukkala, L. D., van Rensburg, E. & Görgens, J., 2016. Paper sludge (PS) to bioethanol: Evaluation of virgin and recycle mill to sludge for low enzyme, high-solids fermentation. *Bioresource Technology,* Volume 203, pp. 103-111.

Boshoff, S., Gottumukkala, L. D., van Rensburg, E. & Görgens, J. F., 2016. Paper sludge (PS) to bioethanol: Evaluation of virgin and recycle mill sludge for low enzyme, high-solids fermentation. *Bioresource Technology,* Volume 203, pp. 103-111.

Braun, B., Dorgan, J. R. & Chandler, J. P., 2008. Cellulosic Nanowhiskers. Theory and Application of Light Scattering from Polydisperse Spheroids in the Rayleigh-Gans-Debye Regime. *Biomacromolecules,* Volume 9, pp. 1255-1263.

Brinchi, L., Cotana, F., Fortunati, E. & Kenny, J. M., 2013. Production of nanocrystalline cellulose from lignocellulosic biomass: Technology and applications. *Carbohydrate Polymers,* Volume 94, pp. 154-169.

British Standards Institution, 2017. *Nanotechnology British Standards.* [Online] Available at: https://shop.bsigroup.com/Browse-By-Subject/Nanotechnology/ [Accessed 5 Aug 2017].

Bujanovic, B. et al., 2010. Polyoxometalates in Oxidative Delignification of Chemical Pulps: Effect on Lignin. *Materials,* Volume 3, pp. 1888-1903.

Camberato, J. J. et al., 2006. Pulp and paper mill by-products as soil amendments and plant nutrient sources. *Canadian Journal of Soil Science,* pp. 641-653.

Cara, C. et al., 2008. Production of fuel ethanol from steam-explosion pretreated olive tree pruning. *Fuel,* Volume 87, pp. 692-700.

Chen, H., 2014. *Process Development and Fundamental Study on Enzymatic Hydrolysis of Cellulosic Biomass to Fermentable Sugars for Ethanol Production.,* Raleigh, North Carolina: Graduate Faculty of North Carolina State University.

Chen, W. et al., 2011. Individualization of cellulose nanofibers from wood using high-intensity ultrasonication combined with chemical pretreatments. *Carbohydrate Polymers,* Volume 83, pp. 1804-1811.

Chen, X., Deng, X., Shen, W. & Jiang, L., 2012. Controlled enzymolysis preparation of nanocrystalline cellulose from pretreated cotton fibers. *Bioresources,* 7(3), pp. 4237-4248.

Cherizol, R., Sain, M. & Tjong, J., 2015. Evaluation of the influence of fibre aspect ratio and fibre content on the rheological characteristics of high yield pulp fibre reinforced polyamide 11 "HYP/PA11" green composite. *Polymer Chemistry,* Volume 5, pp. 1-8.

Chirayil, C. J., Mathew, L. & Thomas, S., 2014. Review of recent research in nano cellulose preparation from different lignocellulosic fibers. *Review on Advanced Materials Science,* Volume 37, pp. 20-28.

Chiyanzy, I. et al., 2015. Spent coffee ground mass solubilisation by steam explosion and enzymatic hydrolysis. *Journal of Chemical Technology and Biotechnology,* 90(3), pp. 449-458.

Ciolacu, D., Ciolacu, F. & Popa, V. I., 2010. Amorphous Cellulose - Structure and Characterization. *Cellulose Chemistry and Technology,* Volume 45, pp. 13 - 21.

Cohen, R., Suzuki, M. R. & Hammel, K. E., 2005. Processive Endoglucanase Active in Crystalline Cellulose Hydrolysis by the Brown Rot Basidiomycete Gloeophyllum trabeum. *Applied and Environmental Microbiology,* 71(5), pp. 2412-2417.

Conley, K., Godbout, L., Whitehead, M. A. (. & van de Ven, T. G., 2016. Origin of the twist of cellulosic materials. *Carbohydrate Polymers,* Volume 135, pp. 285-290.

Cowie, J., Bilek, T. M., Wegner, T. H. & Shatkin, J. A., 2014. Market of projections of cellulose nanomaterials-enables products - Part 2: Volume Estimates. *Nanocellulose Markets Tappi Journal,* 13(6), pp. 57-69.

Crespo, C., Badshah, M., Alvarez, M. & Mattiasson, B., 2012. Ethanol production by continuous fermentation of D-(+)-cellobiose, D-(+)-xylose and sugarcane bagasse hydrolysate using the thermoanaerobe Caloramator boliviensis. *Bioresource Technology,* Volume 103, pp. 186-191.

Cui, L. et al., 2012. Influence of Steam Explosion Pretreatment on the Composition and Structure of Wheat Straw. *BioResources,* 7(3), pp. 4202-4213.

Deepa, B. et al., 2015. Utilization of various lignocellulosic biomass for the production of nanocellulose: a comparative study. *Cellulose,* pp. 1-16.

Desmaisons, J. et al., 2017. A new quality index for benchmarking of different cellulose nanofibrils. *Carbohydrate Polymers,* Volume 174, pp. 318-328.

Destexhe, A., 2007. *Novozymes - Advancing cellulosic ethanol.* [Online] Available at: http://www.ieabioenergy.com/wp-content/uploads/2013/10/P03-Advancing-cellulosic-ethanol-A.-Destexhe.pdf
[Accessed 3 May 2017].

Dufresne, A., 2013. *Biosourced nanoparticles: an emerging family of nanofillers,* Mons, Belgium: The International School of Paper, Print Media and Biomaterials (Pagora).

Dufresne, A., Cavaille, J.-Y. & Vignon, M. R., 1997. Mechanical behavior of sheets prepared from sugar beet cellulose microfibrils. *Journal of Applied Polymer Science,* Volume 64, pp. 1185-1194.

Duran, N. et al., 2011. A minireview of cellulose nanocrystals and its potential integration as co-product in bioethanol production. *Journal of the Chilean Chemical Society,* 56(2), pp. 672 - 677.

Dwiarti, L., Boonchird, C., Harashima, S. & Park, E. Y., 2012. Simultaneous saccharification and fermentation of paper sludge without pretreatment using cellulase from Acremonium cellulolyticus and thermotolerant Saccharomyces cerevisiae. *Biomass and Bioenergy,* Volume 42, pp. 114-122.

Enzyme Solutions Pty. Ltd., 2016. *Enzyme Solutions - Grain Processing.* [Online] Available at: http://www.enzymesolutions.com.au/catalogue/4453/grain-processing.html
[Accessed 4 August 2016].

Evans, F. & Wennerstrom, H., 1999. *The Colloidal Domain: Where Physics, Chemistry, Biology and Technology Meet.* 2nd ed. New York: John Wiley & Sons Inc.

Fairman, E., 2014. *Avoiding Aggregation During Drying and Rehydration of Nanocellulose,* Maine: Honors College, University of Maine.

Fang, H., Zhao, C. & Song, X.-Y., 2010. Optimization of enzymatic hydrolysis of steam-exploded corn stover by two approaches: Response surface methodology or using cellulase from mixed cultures of Trichoderma reesei RUT-C30 and Aspergillus niger NL02. *Bioresource Technology,* Volume 101, pp. 4111-4119.

Fan, Z. & Lynd, L. R., 2007. Conversion of paper sludge to ethanol. I: Impact of feeding frequency and mixing energy characterization. *Bioprocess and Biosystem Engineering,* Volume 30, pp. 27-34.

Fattahi Meyabadi, T. & Dadashian, F., 2012. Optimization of Enzymatic Hydrolysis of Waste Cotton Fibers for Nanoparticles Production Using Response Surface Methodology. *Fibers and Polymers,* 13(3), pp. 313-321.

Fattahi Meyabadi, T. F., Dadashian, F., Sadeghi, G. M. M. & Asl, H. E. Z., 2014. Spherical cellulose nanoparticles preparation from waste cotton using a green method. *Powder Technology,* Volume 261, pp. 232-240.

Fengel, D. & Wegener, G., 2003. *Wood: Chemistry, Ultrastructure, Reactions.* München: Kessel Verlag.

Fernandez, E. O. & Young, R. A., 1996. Properties of cellulose pulp from acid and basic processes. *Cellulose,* Volume 3, pp. 21-44.

Ferreira, L. C., Souza, T. S. O., Fdz-Polanco, F. & Pérez-Elvira, S. I., 2014. Thermal steam explosion pretreatment to enhance anaerobic biodegradability of the solid fraction of pig manure. *Bioresource Technology,* Volume 152, pp. 393-398.

Filson, P. B. & Dawson-Andoh, B. E., 2009. Sono-chemical preparation of cellulose nanocrystals from lignocellulose derived materials. *Bioresource Technology,* Volume 100, pp. 2259-2264.

Filson, P. B., Dawson-Andoh, B. E. & Schwegler-Berry, D., 2009. Enzymatic-mediated production of cellulose nanocrystals from recycled pulp. *The Royal Society of Chemistry,* Volume 11, pp. 1808-1814.

FisherSolve, 2017. *Fisher International - Mill Support.* [Online] Available at: https://www.fisheri.com/mill-support/ [Accessed 18 Sept 2017].

FP&M SETA, 2014. *A profile of the paper and pulp sub-sector,* s.l.: IQbusiness.

Frone, A. N., Panaitescu, D. M. & Donescu, D., 2011. Some aspects concerning the isolation of cellulose micro- and nano-fibers. *UPB Scientific Bulletin, Series B: Chemistry and Materials,* 73(2), pp. 134-152.

Fytili, D. & Zabaniotou, A., 2008. Utilization of sewage sludge in EU application of old and new methods—A review. *Renewable and Sustainable Energy Reviews,* Volume 12, pp. 116-140.

Garcia, A., Labidi, J., Belgacem, M. N. & Bras, J., 2016. The nanocellulose biorefinery: woody versus herbaceous agricultural wastes for NCC production. *Cellulose,* Volume 24, pp. 1-12.

Goršek, A. & Pečar, D., 2015. The Influence of Cellulose Type on Enzymatic Hydrolysis Efficiency. *Chemical Engineering Transactions,* Volume 43, pp. 421 - 426.

Gottumukkala, L. D. & Gorgens, J. F., 2016. Biobutanol production from lignocellulosics. In: A. P. E. G. Ram Sarup Singh, ed. *Biofuels: Production and Future Perspectives.* s.l.:CRC Press, Taylor and Francis Group.

Grunert, M. & Winter, W. T., 2002. Nanocomposites of Cellulose Acetate Butyrate Reinforced with Cellulose Nanocrystals. *Journal of Polymers and the Environment,* 20(112), pp. 27-30.

Habibi, Y. et al., 2008. Bionanocomposites based on poly(epsilon-caprolactone)-grafted cellulose nanocrystals by ring-opening polymerization. *Journal of Materials Chemistry,* Volume 18, pp. 5002-5010.

Hall, M. et al., 2010. Cellulose crystallinity – a key predictor of the enzymatic hydrolysis rate. *FEBS Journal,* Volume 277, pp. 1571-1582.

Hames, B. et al., 2008. *Preparation of Samples for Compositional Analysis,* Colorado: National Renewable Energy Laboratory.

Hanley, S. J., Revol, J.-F., Godbout, L. & Gray, D. G., 1997. Atomic force microscopy and transmission electron microscopy of cellulose from Micrasterias denticulata; evidence for a chiral helical microfibril twist. *Cellulose,* Volume 4, pp. 209-220.

Hendriks, A. & Zeeman, G., 2009. Pretreatments to enhance the digestibility of lignocellulosic biomass. *Bioresource Technology,* Volume 100, pp. 10-18.

Henriksson, M., Henriksson, G., Berglund, L. A. & Lindström, T., 2007. An environmentally friendly method for enzyme-assisted preparation of microfibrillated cellulose (MFC) nanofibres. *ScienceDirect,* Volume 43, pp. 3434-3441.

Herpoël-Gimbert, I. et al., 2008. Comparative secretome analyses of two Trichoderma reesei RUT-C30 and CL847 hypersecretory strains. *Biotechnology for Biofuels,* 1(18), pp. 1-12.

Hsu, J. C. & Hu, S.-H., 2002. *Recovery of fibers from a fiver processing waste sludge.* United States, Patent No. US 6,372,085 B1.

Ibarra, D., Kopcke, V. & Ek, M., 2010. Behavior of different monocomponent endoglucanases on the accessibility and reactivity of dissolving-grade pulps for viscose process. *Enzyme and Microbial Technology,* Volume 47, pp. 355-362.

International Standards Organization, 2008. *ISO 22412:2008(en) - Particle size analysis — Dynamic light scattering (DLS).* [Online] Available at: https://www.iso.org/obp/ui/#iso:std:iso:22412:ed-1:v1:en [Accessed 20 May 2016].

International Standards Organization, 2017. *ISO/TS 20477:2017(en) Nanotechnologies — Standard terms and their definition for cellulose nanomaterial.* [Online] Available at: https://www.iso.org/obp/ui/#iso:std:iso:ts:20477:ed-1:v1:en [Accessed 29 August 2017].

Ioelovich, M., 2008. Cellulose as a nanostructured polymer: A short review. *Bioresources,* 3(4), pp. 1403-1418.

Ioelovich, M., 2012. Optimal Conditions for Isolation of Nanocrystalline Cellulose Particles. *Nanoscience and Nanotechnology,* 2(2), pp. 9-13.

Ioelovich, M., 2013. Nanoparticles of amorphous cellulose and their properties. *American Journal of Nanoscience and Nanotechnology,* 1(1), pp. 41-45.

Ioelovich, M., 2014. Peculiarities of Cellulose Nanoparticles. *Tappi Journal,* 13(5), pp. 45-52.

Ioelovic, M. & Morag, E., 2012. Study of Enzymatic Hydrolysis of Pretreated Biomass at Increased Solids Loading. *BioResources,* 7(4), pp. 4672-4682.

Janardhnan, S., 2012. *Isolation of Cellulose Nanofibres: Elucidation of a Novel Approach Utilizing Fungal Pretreatment,* Toronto: University of Toronto.

Jonoobi, M., Mathew, A. P. & Oksman, K., 2012. Producing low-cost cellulose nanofiber from sludge as new source of raw materials. *Industrial Crops and Products,* Volume 40, pp. 232-238.

Jonoobi, M. et al., 2015. Different preparation methods and properties of nanostructured cellulose from various natural resources and residues: a review. *Cellulose,* Volume 22, pp. 935-969.

Josefsson, P., Hendriksson, G. & Wagberg, L., 2008. The physical action of cellulases revealed by a quartz crystal microbalance study using ultrathin cellulose films and pure cellulases. *Biomacromolecules,* Volume 9, pp. 249-254.

Kádár, Z., Szengyel, Z. & Réczey, K., 2004. Simultaneous saccharification and fermentation (SSF) of industrial wastes for the production of ethanol. *Industrial Crops and Products,* Volume 20, pp. 103-110.

Kalia, S. et al., 2011. Cellulose-Based Bio- and Nanocomposites: A Review. *International Journal of Polymer Science,* pp. 1-35.

Kangas, H., 2014. *Guide to cellulose nanomaterials - English summary,* Finland: VTT.

Kang, L., Wang, W., Pallapolu, V. R. & Lee, Y. Y., 2011. Enhanced ethanol production from de-ashed paper sludge by simultaneous saccharification and fermentation and simultaneous saccharification and co-fermentation. *BioResources,* 6(4), pp. 3791-3808.

Karlsson, J., Siika-aho, M., Tenkanen, M. & Tjerneld, F., 2002. Enzymatic properties of the low molecular mass endoglucanases Cel12A (EG III) and Cel45A (EG V) of Trichoderma reesei. *Journal of Biotechnology,* Volume 99, pp. 63-78.

Kazimierczak, J. et al., 2016. *Method of Preparing Cellulose Nano-Fibers From Stalks of Annual Plants.* s.l. Patent No. WO 2016/013946 A1.

Kimberly-Clark Springs, 2017. *Personal Communication* [Interview] (6 June 2017).

Klemm, D. et al., 2011. Nanocelluloses: A New Family of Nature-Based Materials. *Angewandte Chemie,* Volume 50, pp. 5438-5466.

Ko, J. K., Ximenes, E., Kim, Y. & Ladisch, M. R., 2015. Adsorption of enzyme onto lignins of liquid hot water pretreated hardwoods. *Biotechnology and Bioengineering,* Volume 112, pp. 447 - 456.

Kostylev, M. & Wilson, D., 2012. Synergistic interactions in cellulose hydrolysis. *Biofuels,* Volume 31, pp. 61-70.

Kumar, P., Barrett, D. M., Delwiche, M. J. & Stroeve, P., 2009. Methods for Pretreatment of Lignocellulosic Biomass for Efficient Hydrolysis and Biofuel Production. *Industrial & Engineering Chemistry Research.*

Kumar, R., Singh, S. & Singh, O. V., 2008. Bioconversion of lignocellulosic biomass:. *biochemical and molecular perspectives,* Volume 35, pp. 377-391.

Kumar, R. & Wyman, C. E., 2014. Strong Cellulase Inhibition by Mannan Polysaccharides in Cellulose Conversion to Sugars. *Biotechnology and Bioengineering,* pp. 1-13.

Lai, X. L., 2010. *Bioproducts from sulfite pulping: Bioconversion of sugar streams from pulp, sludge, and spent sulfite liquor,* Washington: School of Forest Resources, University of Washington.

Lakshmanan, B. R., 1956. *Infrared absorption spectrum of sodium citrate,* Bangalore: Indian Institute of Science.

Lakshmidevi, R. & Muthukumar, K., 2010. Enzymatic saccharification and fermentation of paper and pulp industry effluent for biohydrogen production. *International Journal for Hydrogen Energy,* Volume 35, pp. 3389-3400.

Lam, P. S., 2011. *Steam Explosion of Biomass to Produce Durable Wood Pellets,* Hong Kong : Hong Kong University of Science and Technology.

Lavoine, N., Desloges, I., Dufresne, A. & Bras, J., 2012. Microfibrillated cellulose – Its barrier properties and applications in cellulosic materials: A review. *Carbohydrate Polymers,* Volume 90, pp. 735-764.

Leung, A. C. W. et al., 2011. Characteristics and properties of carboxylated cellulose nanocrystals prepared from a novel one-step procedure. *Small,* Volume 7, pp. 302-305.

Li, C. et al., 2013. Scale-up and evaluation of high solid ionic liquid pretreatment and enzymatic hydrolysis of switchgrass. *Biotechnology for Biofuels,* 6(153), pp. 1-13.

Lindman, B. et al., 2017. The relevance of cellulose structural features and interactions on dissolution, regeneration, gelation and plasticization phenomena. *Physical Chemistry Chemical Physics,* p. DOI:10.1039/C7CP02409F.

Lindström, T., Ankerfors, M. & Henriksson, G., 2007. *Method for Manufacturing of Microfibrillated Cellulose.* Stockholm, Sweden, Patent No. WO 2007/091942 A1.

Lin, Y., Wang, D., Liang, J. & Li, G., 2012. Mesophilic anaerobic co-digestion of pulp and paper sludge and food waste for methane production in a fed-batch basis. *Environmental Technology,* 33(23), pp. 2627-2633.

Li, Q. et al., 2013. Nanocellulose Life Cycle Assessment. *American Chemical Society Sustainable Chemical Engineering,* Volume 1, pp. 919-928.

Lisperguer, J., Perez, P. & Urizar, S., 2009. Structure and thermal properties of lignins: Characterization by Infrared Spectroscopy and Differerntial Scanning Calorimetry. *Journal of the Chilean Chemical Society,* 54(4), pp. 460-463.

Liu, H., Fu, S., Li, H. & Zhan, H., 2009. Visualization of enzymatic hydrolysis of cellulose using AFM phase imaging. *Enzyme and Microbial Technology,* Volume 45, pp. 274-281.

Li, X.-F., Ding, E.-y. & Li, G.-k., 2001. A method of preparing spherical nano-crystal cellulose with mixed crystalline forms of cellulose I and II. *Chinese Journal of Polymer Science,* Volume 3, pp. 291-296.

Li, Y. & Ragauskas, A. J., 2011. Cellulose nano whiskers as a reinforcing filler in polyurethanes. In: D. B. Reddy, ed. *Advances in Diverse Industrial Applications of Nanocomposites.* Rijeka: InTec, pp. 17-36.

Lu, P. & Hsieh, Y.-L., 2010. Preparation and properties of cellulose nanocrystals: Rods, spheres and network. *Carbohydrate Polymers,* Volume 82, pp. 329-336.

Macdonald, C. J., 2004. *Water Usage in the South African Pulp and Paper Industry,* Durban: School of Chemical Engineering University of KwaZulu-Natal.

Mahmood, T. & Elliott, A., 2006. A review of secondary sludge reduction technologies for the pulp and paper industry. *Water Research,* Volume 40, pp. 2093-2112.

Malvern Instruments Ltd, 2004. *Zetasizer Nano Series User Manual.* 1 ed. Worcestershire: Malvern Instruments.

Mandal, A. & Chakrabarty, D., 2011. Isolation of nanocellulose from waste sugarcane bagasse (SCB) and its characterization. *Carbohydrate Polymers,* Volume 86, pp. 1292-1299.

Mangalam, A. P., Simonsen, J. & Benigh, A. S., 2009. Cellulose/DNA Hybrid Nanomaterials. *Biomacromolecules,* Volume 10, p. 497–504.

Marino, M., da Silva, L. L., Duran, N. & Tasic, L., 2015. Enhanced Materials from Nature: Nanocellulose from Citrus Waste. *Molecules,* Volume 20, pp. 5908-5923.

Marques, S., Alves, L., Roseiro, J. C. & Girio, F. M., 2008. Conversion of recycled paper sludge to ethanol by SHF and SSF using Pichia stipitis. *Biomass and bioenergy,* Volume 32, pp. 400-406.

Marsden, W. L. & Gray, P. P., 1986. Enzymatic Hydrolysis of Cellulose in Lignocellulosic Materials. *CRC Critical Reviews in Biotechnology,* 3(3), pp. 235-276.

Medronho, B. et al., 2015. Probing cellulose amphiphilicity. *Nordic Pulp & Paper Research Journal,* 30(1), pp. 58-66.

Migneault, S. et al., 2011. Binderless fiberboard made from primary and and secondary pulp and paper sludge. *Wood and Fiber Science,* 43(2), pp. 181 - 193.

Milford, H., Gerald, B. & Vesselin, M., 2001. *Produciton of microcrystalline cellulose by reactive extrusion.* Lincoln, Patent No. US 6228 213 B1.

Min, B. C., Bhayani, B. V., Jampana, V. S. & Ramarao, B. V., 2015. Enhancement of the enzymatic hydrolysis of fines from recycled paper mill waste rejects. *Bioresources and Bioprocessing,* 40(2), pp. 1-10.

Missoum, K., Belgacem, M. N. & Bras, J., 2013. Nanofibrillated Cellulose Surface Modification: A Review. *Materials,* Volume 6, pp. 1745-1766.

Miyamoto, H. et al., 2009. Structural reorganization of molecular sheets derived from cellulose II by molecular dynamics simulations. *Carbohydrate Research,* Volume 344, pp. 1085-1094.

Mohan, D., Pittman, C. U. & Steele, P. H., 2006. Pyrolysis of Wood/Biomass for Bio-oil: A Critical Review. *Energy and Fuels,* Volume 20, pp. 848-889.

Monte, M. C., Fuente, E., Blanco, A. & Negro, C., 2009. *Waste Management from Pulp and Paper Production in the European Union,* Madrid: Chemical Engineering Department, Complutense University of Madrid.

Montgomery, L. & Bochmann, G., 2014. *Pretreatment of feedstock for enhanced biogas production,* Vienna: IEA Bioenergy.

Moon, R. J. et al., 2011. Cellulose nanomaterial review: Structure, properties and nanocomposites. *The Royal Society of Chemistry,* Volume 40, pp. 3941-3994.

Moon, R. J., Schueneman, G. T. & Simonsen, J., 2016. Overview of Cellulose Nanomaterials, Their Capabilities and Applications. *The Minerals, Metals & Materials Society,* 68(9), pp. 2383-2394.

Morandi, G., Heath, L. & Thielemans, W., 2009. Cellulose Nanocrystals Grafted with Polystyrene Chains through Surface-Initiated Atom Transfer Radical Polymerization (SI-ATRP). *Langmuir,* 25(14), p. 8280–8286.

Mörseburg , K. & Chinga-Carrasco, G., 2009. Assessing the combined benefits of clay and nanofibrillated cellulose in layered TMP-based sheets. *Springer,* Volume 16, p. 795–806.

Moser, C., Lindstrom, M. E. & Henriksson, G., 2015. Toward Industrially feasible methods for following the process of manufacturing cellulose nanofibres. *Bioresources,* 10(2), pp. 2360-2375.

Mtibe, A. et al., 2015. A comparative study on properties of micro and nanopapers produced from cellulose and cellulose nanofibres. *Carbohydrate Polymers,* Volume 118, pp. 1-8.

Mtibe, A. & Muniyasamy, S., 2016. Development of Sustainable Biobased Polymer and Bio-composite Materials from Agricultural Biomass. In: Port Elizabeth: s.n.

Nadanathangam, V. & Satyamurthy, P., 2011. Prepapration of Spherical Na nocellulose by Anaerobic Microbial Consortium. *International Proceedings of Chemical, Biological and Environmental Engineering,* Volume 7, pp. 181-183.

Nam, S., French, A. D., Condon, B. D. & Concho, M., 2016. Segal crystallinity index revisited by the simulation of X-ray diffraction patterns of cotton cellulose I-beta and cellulose II. *Carbohydrate Polymers,* Volume 135, pp. 1-9.

Nechyporchuk, O., 2015. *Cellulose nanofibers for the production of biocomposites,* Grenoble : Chemical and Process Engineering.

Nechyporchuk, O., 2015. *Cellulose nanofibers for the production of bionanocomposites,* Lisbon: Chemical and Process Engineering. University of Grenoble Alpes.

Nguyen, H. D. et al., 2013. A novel method for preparing microfibrillated cellulose from bamboo fibers. *Advances in Natural Sciences: Nanoscience and Nanotechnology,* Volume 4, pp. 1-9.

Novozymes Bioenergy, 2012. *Cellulosic ethanol - Novozymes Cellic CTec and HTec2 - Enzymes for the hydroysis of lignocellulosic,* Kobenhavn: Novozymes.

Novozymes, 2016. *FiberCare R Safety Data Sheet,* Kobenhavn: Novozymes.

Ochoa de Alda, J. A., 2008. Feasibility of recycling pulp and paper mill sludge in the paper and board industries. *Reources, Conservation and Recycling,* Volume 52, pp. 965-972.

Oksman, K., Etang, J. A., Mathew, A. P. & Jonoobi, M., 2011. Cellulose nanowhiskers separated from a bio-residue from wood bioethanol production. *Biomass and Bioenergy,* Volume 35, pp. 146-152.

Oksman, K., Mathew, A. P., Bondeson, D. & Kvien, I., 2006. Manufacturing process of cellulose whiskers/polylactic acid nanocomposites. *Composites Science and Technology,* Volume 66, pp. 2776-2784.

Oksman, K. et al., 2014. *Handbook of Green Materials - Bionanomaterials: separation processes, characterization and properties.* 5 ed. London: World Scientific.

Pääkkö, M. et al., 2007. Enzymatic Hydrolysis Combined with Mechanical Shearing and High-Pressure Homogenization for Nanoscale Cellulose Fibrils and Strong Gels. *Biomacromolecules,* Issue 8, pp. 1934-1941.

PAMSA, 2012. *The Wood Foundation.* [Online] Available at: http://thewoodfoundation.co.za/members-hub/association-members/pamsa.html [Accessed 2 March 2016].

Pandey, J. K. et al., 2009. Evaluation of morphological architecture of cellulose chains in grass during conversion from macro to nano dimensions. *e-Polymer,* Volume 102, pp. 1-15.

Paralikar, K. M. & Bhatawdekar, S. P., 1984. Hydrolysis of Cotton Fibres by Cellulose Enzyme. *Journal of Applied Polymer Science,* Volume 29, pp. 2573-2580.

Paralikar, S. A., Simonsen, J. & Lombardi, J., 2008. Poly(vinyl alcohol)/cellulose nanocrystal barrier membranes. *Journal of Membrane Science,* Volume 320, pp. 248-258.

Park, S. et al., 2010. Cellulose crystallinity index: measurement techniques and their impact on interpreting cellulase performance. *Biotechnology for Biofuels,* 3(10), pp. 1 - 10.

Paulapuro, H., 2008. *Papermaking Part 1, Stock Preparation and Wet End.* 2nd ed. Helsinki: Finnish Paper Engineers' Association.

Peng, L. & Chen, Y., 2011. Conversion of paper sludge to ethanol by separate hydrolysis and fermentation (SHF) using Saccharomyces cerevisiae. *Biomass & Bioenergy,* Volume 35, pp. 1600-1606.

Peng, Y., Gardner, D. J. & Han, Y., 2012. Drying cellulose nanofibrils: in search of a suitable method. *Cellulose,* 19(1), pp. 91-102.

Petersson, L., Kvien, I. & Oksman, K., 2007. Structure and thermal properties of poly(lactic acid)/cellulose whiskers nanocomposites materials. *Comosites Science and Technology,* Volume 67, pp. 2535-2544.

Philippidis, G. P., Smith, T. K. & Wyman, C. E., 1993. Study of the Enzymatic Hydrolysis of Cellulose for Production of Fuel Ethanol by the Simultaneous Saccharification and Fermentation Process. *Biotechnology and Bioengineering,* Volume 41, pp. 846-853.

Pielhop, T., Amgarten, J., von Rohr, P. R. & Studer, M. H., 2016. Biotechnology for Biofuels. *Steam explosion pretreatment of softwood: the effect of the explosive decompression on enzymatic digestibility,* Volume 9, pp. 1-13.

Poletto, M., Pistor, V. & Zattera, A. J., 2013. Structural Characteristics and Thermal Properties of Native Cellulose. In: *Cellulose - Fundamental Aspects.* s.l.:InTech, pp. 45 - 68.

Prasetyo, J. et al., 2011. Bioconversion of paper sludge to biofuel by simultaneous saccharification and fermentation using a cellulase of paper sludge origin and thermotolerant Saccharomyces cerevisiae TJ14. *Biotechnology for Biofuels,* 4(35), pp. 1-13.

Prasetyo, J. & Park, E. Y., 2013. Waste paper sludge as a potential biomass for bio-ethanol production. *Korean Journal of Chemical Engineering,* 30(2), pp. 253-261.

Qing, Y. et al., 2013. A comparative study of cellulose nanofibrils disintegrated via A comparative study of cellulose nanofibrils disintegrated viamultiple processing approaches. *Carbohydrate Polymers,* Volume 97, pp. 226-234.

Qing, Y. et al., 2013. A comparative study of cellulose nanofibrils disintegrated via multiple processing approaches. *Carbohydrate Polymers,* Volume 97, pp. 226-234.

Qu, C. et al., 2013. Optimization of ultrasonic extraction of polysaccharides from Ziziphus jujuba Mill. by response surface methodology. *Chemistry Central Journal,* 7(160), pp. 1-7.

Rebouillat, S. & Pla, F., 2013. State of the Art Manufacturing and Engineering of Nanocellulose: A Review of Available Data and Industrial Applications. *Journal of Biomaterials and Nanobiotechnology,* Volume 4, pp. 165-188.

Rebouillat, S. & Pla, F., 2013. State of the Art Manufacturing and Engineering of State of the Art Manufacturing and Engineering of Nanocellulose: A Review of Available Data and Industrial Applications. *Journal of Biomaterials and Nanobiotechnology,* Volume 4, pp. 165-188.

Reese, E. R., 1977. Degradation of Polymeric Carbohydrates by Microbial Enzymes. In: F. A. Loewus & V. C. Runeckles, eds. *The Structure, Biosynthesis, and Degradation of Wood.* Natick, Massachusetts: Springer US, pp. 311-367.

Retsch GmbH, 2017. *Retsch - Solutions in milling and sieving.* [Online] Available at: http://www.retsch.com/products/milling/ball-mills/mixer-mill-cryomill/function-features [Accessed 16 May 2017].

Ridout, A., Carrier, M., Collard, F.-X. & Görgens, J., 2016. Energy conversion assessment of vacuum, slow and fast pyrolysis processes for low and high ash paper waste sludge. *Energy Conversion and Management,* Volume 111, pp. 103-114.

RISI, 2011. *Press Release: Innventia builds world's first nanocellulose pilot plant in Stockholm, Sweden.* [Online]
Available at: https://legacy.risiinfo.com/technologyarchives/papermaking/Innventia-builds-worlds-first-nanocellulose-pilot-plant-in-Stockholm-Sweden.html
[Accessed 15 Apr 2017].

Roberts, K. M. et al., 2011. The effects of water interactions in cellulose suspensions on mass transfer and saccharification efficiency at high solids loadings. *Cellulose,* Volume 18, pp. 759-773.

Robus, C. L. L., 2013. *Production of bioethanol from paper sludge using simultaneous saccharification and fermentation,* Stellenbosch: Faculty of Engineering at Stellenbosch University.

Robus, C. L. L., 2013. *Production of Bioethanol from Paper Sludge using Simultaneous Saccharification and Fermentation,* Stellenbosch: Faculty of Chemical Engineering, Stellenbosch University.

Robus, C. L. L., Gottumukkala, L. D., van Rensburg, E. & Gorgens, J. F., 2016. Feasible process development and techno-economic evaluation of paper sludge to bioethanol conversion: South African paper mills scenario. *Renewable Energy,* Volume 92, pp. 333 - 345.

Rojas, O. J., Montero, G. A. & Habibi, Y., 2009. Electronspun nancomposites from polystyrene loaded with cellulose nanowhiskers. *Applied Polymer Science,* Volume 113, pp. 927-935.

Rosa, M. et al., 2010. Cellulose nanowhiskers from coconut husk fibers: Effect of preparation conditions on their thermal and morphological behavior. *Carbohydrate Polymers,* Volume 81, pp. 83-92.

Sabiha-Hanim, S. & Aziatul-Akma, A., 2016. Polymer characterization of cellulose and hemicellulose. In: A. Méndez-Vilas & . A. Solano-Martín, eds. *Polymer science: research advances, practical applications and educational aspects.* Spain: Formatex Research Center, pp. 404 - 411.

Saito, T., Kimura, S., Nishiyama, Y. & Isogai, A., 2007. Cellulose Nanofibers Prepared by TEMPO-Mediated Oxidation of Native Cellulose. *Biomacromolecules,* Volume 8, pp. 2485-2491.

Salajková, M., 2013. *Wood Nanocellulose Materials and Effects from Surface Modification of Nanoparticles,* Stockholm: KTH Royal Institute of Technology, School of Chemical Science and Engineering.

Salehudin, M. H. et al., 2012. *Cellulose Nanofiber Isolation and Its Fabrication into Bio-polymer - A Review.* Johor, International Conference on Agricultural and Food Engineering for Life.

Satyamurthy, P., Jain, P., Balasubramanya, R. H. & Vigneshwaran, N., 2011. Preparation and characterisation of cellulose nanowhiskers from cotton fibres by controlled microbial hydrolysis. *Carbohydrate Polymers,* Volume 83, pp. 122-129.

Satyamurthy, P. & Vigneshwaran, N., 2013. A novel process for synthesis of spherical nanocellulose by controlled hydrolysis of microcrystalline cellulose using anaerobic microbial consortium. *Enzyme and Microbial Technology,* Volume 52, pp. 20-25.

Schwanninger, M., Rodrigues, J. C., Pereira, H. & Hinterstoisser, B., 2004. Effects of short-time vibratory ball milling on the shape of FT-IR spectra of wood and cellulose. *Vibrational Spectroscopy,* Volume 36, pp. 23-40.

Scott, G. M. & Smith, A., 1995. *Sludge Characteristics and Disposal Alternatived for the Pulp and Paper Industry.* Atlanta, International Environmental Conference Proceedings.

Shatkin, J. A., Wegner, T. H., Bilek, T. M. & Cowie, J., 2014. Market projections of cellulose nanomaterial-enabled products - Part 1: Applications. *Nanocellulose Markets Tappi Journal,* 13(5), pp. 9-16.

Silveira, M. H. L., Rau, M., Bon, E. P. d. S. & Andreaus, J., 2012. A simple and fast method for the determination of endo- and exo-cellulase activity in cellulase preparations using filter paper. *Enzyme and microbial technology,* Volume 51, pp. 280-285.

Siqueira, G., Bras, J. & Dufresne, A., 2010. Cellulosic Bionanocomposites: A Review of Preparation, Properties and Applications. *Polymers,* Volume 2, pp. 728-765.

Siroky, J. et al., 2010. Attenuated total reflectance Fourier-transform Infrared spectroscopy analysis of crystallinity changes in lyocell following continuous treatment with sodium hydroxide. *Cellulose,* Volume 17, pp. 103-115.

Sluiter, A. et al., 2008. *Determination of Total Solids in Biomass and Total Dissolved Solids in Liquid Process Samples,* Golden, Colorado: National Renewable Energy Laboratory.

Sluiter, A. et al., 2005a. *Determination of Ash in Biomass,* Golden, Colorado: National Renewable Energy Laboratory.

Sluiter, A. et al., 2011. *Determination of Structural Carbohydrates and Lignin in Biomass,* Golen, Colorado: National Renewable Energy Laboratory.

Sluiter, A. et al., 2005b. *Determination of Extractives in Biomass,* Golden, Colorado: National Renewable Energy Laboratory.

Sluiter, J. & Sluiter, A., 2011. *Summative Mass Closure - Laboratory Analytical Procedure (LAP) Review and Integration: Pretreated Slurries,* Colorado: National Renewable Energy Laboratory.

Song, Q., Winter, W. T., Bujanovic, B. M. & Amidon, T. E., 2014. Nanofibrillated Cellulose (NFC): A High-Value Co-Product that Improves the Economics of Cellulosic Ethanol Production. *Energies,* Volume 7, pp. 607-618.

Sritham, E. & Gunaserekaran, S., 2017. FTIR spectroscopic evaluation of sucrose-maltodextrin-sodium citrate bioglass. *Food Hydrolcolloids,* pp. 1-12.

Stelte, W., 2012. *Steam explosion for biomass pre-treatment,* Taastrup: Danish Technological Institute.

Teeri, T. T. et al., 1995. Modes of action of two Trichoderma reesei cellobiohydrolases. *Carbohydrate Bioengineering,* pp. 211-224.

Thybo, P. & Hovgaard, L., 2008. Droplet Size Measurements for Spray Dryer Scale-Up. *Pharmaceutical Development and Technology,* Volume 13, pp. 93-104.

Tokoh, C., Takabe, K., Fujita, M. & Saiki, H., 1998. Cellulose synthesized by Acetobacter xylinum in the presence of acetyl glucomannan. *Cellulose,* Volume 5, pp. 249-261.

Tonoli, G. H. et al., 2012. Cellulose micro/nanofibres from Eucalyptus kraft pulp: Preparation and properties. *Carbohydrate Polymers,* Volume 89, pp. 80 - 88 .

Transparency Market Research Analysis, 2015. *Nanocellulose Market for Composites, Paper Processing, Food & Beverages, Paints & Coatings, Oil & Gas, Personal Care, and Other End-users - Global Industry Analysis, Size, Share, Growth, Trends and Forecast, 2015 - 2023,* New York: Transparency Market Research.

U.S. Congress, 1989. The pulp and paper making processes. In: J. H. Gibbons, ed. *Technologies for Reducing Dioxin in the Manufacture of Bleached Wood Pulp.* Washington DC: Washington DC: U.S. Government Printing Office, pp. 17-26.

Uetani, K. & Yano, H., 2011. Nanofibrillation of Wood Pulp Using a High-Speed Blender. *Biomacromolecules,* Volume 12, pp. 348-353.

Ul Haq, I. & Akram, F., 2017. Enhanced Production of a Recombinant Multidomain Thermostable GH9 Processive Endo-1,4-β-Glucanase (CenC) from Ruminiclostridium thermocellum in a Mesophilic Host Through Various Cultivation and Induction Strategies. *Applied Biochemistry and Biotechnology,* pp. 1-18.

University of Maine, 2016. *University of Maine - The Process Development Center.* [Online] Available at: http://umaine.edu/pdc/facilities-available-for-use/nanocellulose-facility/nanocellulose-spec-sheets-and-safety-data-sheets/
[Accessed 4 October 2016].

Vassilev, S. V., Baxter, D. & Vassileva, C. G., 2013. An overview of the behaviour of biomass during combustion: Part I. Phase-mineral transformations of organic and inorganic matter. *Fuel,* Volume 112, pp. 391-449.

Vena, P. F., 2005. *Thermomechanical Pulping (TMP), Chemithermomechanical Pulping (CTMP) and Biothermomechanical Pulping (BTMP) of Bugweed (Solanum Mauritianum) and Pinus Patula,* Stellenbosch: Department of Wood Science, University of Stellenbosch.

Vigneshwaran, N., Satyamurthy,, P. & Prateek, J., 2014. Biological production of nanocellulose and potential application in agricultural and forest product industry. In: D. Rickerby, ed. *Nanotechnology for Sustainable Manufacturing.* s.l.:CRC Press, pp. 79-91.

Visser, E. M., Leal, T. F., de Almeida , M. N. & Guimarães, V. M., 2015. Increased enzymatic hydrolysis of sugarcane bagasse from enzyme recycling. *Biotechnology for Biofuels,* 8(5), pp. 2-9.

Walker, L. P. & Wilson, D. B., 1991. Enzymatic Hydrolysis of Cellulose: An Overview. *Bioresource Technology,* Volume 36, pp. 3-14.

Wang, B. & Sain, M., 2007. Dispersion of soybean stock-based nanofiber in a plastic matrix. *Polymer International,* Volume 56, pp. 538-546.

Wang, H. H. (., 2011. Cellulose and pulp. In: *Forest and forest plants.* Pingtung: Encyclopedia of Life Support Systems, pp. 1-7.

Wang, N., Ding, E. & Cheng, R., 2007. Thermal degradation behaviours of spherical cellulose nanocrystals with sulfate groups. *Polymer,* Volume 48, pp. 3486-3493.

Wang, W., Kang, L. & Lee, Y. Y., 2010. Production of Cellulase from Kraft Paper Mill Sludge by Trichoderma Reesei Rut C-30. *Applied Biochem Biotechnol,* Volume 161, pp. 382-394.

Watson, B. J. et al., 2009. Processive Endoglucanases Mediate Degradation of Cellulose by Saccharophagus degradans. *Journal of Bacteriology,* 191(18), pp. 5697-5705.

Williams, Unpublished Data, A., 2017. *The production of bioethanol and biogas from paper sludge,* Stellenbosch: Chemical Engineering, Stellenbosch University.

Williams, A., 2017. *Co-production of ethanol and biogas from paper sludge waste, with process scale-up,* Stellenbosch: Stellenbosch University.

Williams, A., 2017. *The production of bioethanol ans biogas from paper sludge,* Stellenbosch: Stellenbosch University.

Wistara, N. & Young, R. A., 1999. Properties and treatments of pulps from recycled paper. Part I. Physical and chemical properties of pulps. *Cellulose,* Volume 6, pp. 291-324.

Wondraczek, H., Petzold-Welcke, K., Fardim, P. & Heinze, T., 2013. Nanoparticles from conventional cellulose esters: evaluation of preparation methods. *Cellulose,* Volume 20, pp. 751-760.

Yamane, C. et al., 2006. Two Different Surface Properties of Regenerated Cellulose due to Structural Anisotropy. *Polymer Journal,* 38(8), pp. 819-826.

Yue, Y., 2011. *A comparative study of cellulose I and II fibers and nanocrystals,* Louisiana: B.S., Heilongjiang Institute of Science and Technology.

Yu, J. et al., 2009. Combinations of mild physical or chemical pretreatment with biological pretreatment for enzymatic hydrolysis of rice hull. *Bioresource Technology,* Volume 100, p. 903–908.

Zhang, J., Elder, T. J., Pu, Y. & Ragauskas, A. J., 2007. Facile synthesis of spherical cellulose nanoparticles. *Carbohydrate Polymers,* Volume 69, pp. 607-611.

Zhang, X.-Z. & Zhang, Y.-H. P., 2013. Cellulases: Charactereistics, sources, production and applications. In: H. A. E. a. N. T. Shang-Tian Yang, ed. *Bioprocessing Technologies in Biorefi nery for Sustainable Production of Fuels, Chemicals, and Polymers.* s.l.:John Wiley & Sons, Inc, pp. 131 - 146.

Zhao, J. et al., 2014. Mechanically robust, flame-retardant and anti-bacterial nanocomposite films comprised of cellulose nanofibrils and magnesium hydroxide nanoplatelets in a regenerated cellulose matrix. *Cellulose,* Volume 21, p. 1859–1872.

Zhu, J. Y., Sabo, R. & Luo, X., 2011. Integrated production of nano-fibrillated cellulose and cellulosic biofuel (ethanol) by enzymatic fractionation of wood fibers. *Green Chemistry,* Volume 13, pp. 1339-1344.

Zhu, M., Xu, W. & Li, X., 2012. Bioconversion of Different Paper Sludge to Ethanol by Yeast Using Separate Hydrolysis and Fermentation. *Proceedings of 2012 International Conference on Biobase Material Science and Engineering (BMSE),* Volume 3, pp. 141-145.

Zimmerman, T., 2007. *Cellulose Fibrils in Wood Cell Walls and Their Potential for technical applications,* Zurich: Department of Biology, University of Hamburg.

Appendices

Appendix A: Image Processing

The image was converted to 8-bit, Gaussian blurred, convoluted and with the use of the 'Find edges' plug-in in Image J software, processed for optimised mean particle size estimation.
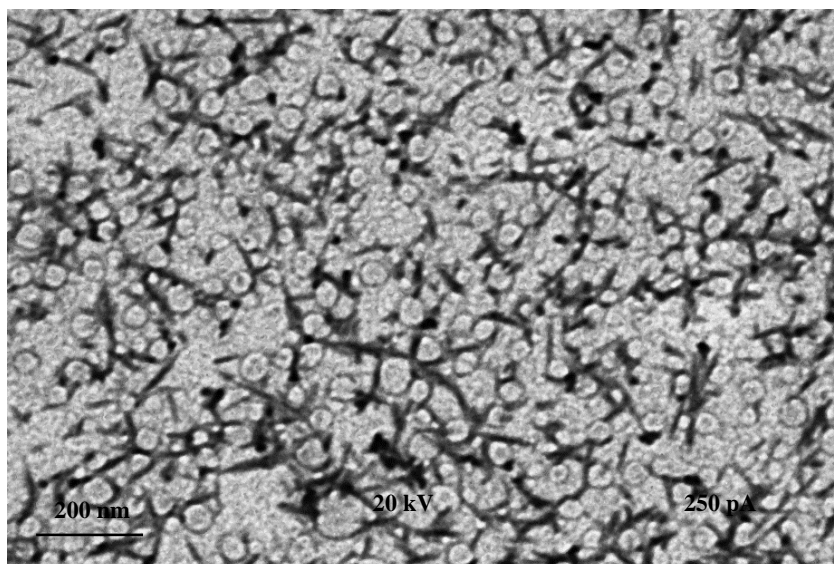

Figure 7.1: STEM image of cellulose nanocrystals from enzymatically hydrolysed virgin pulp PS
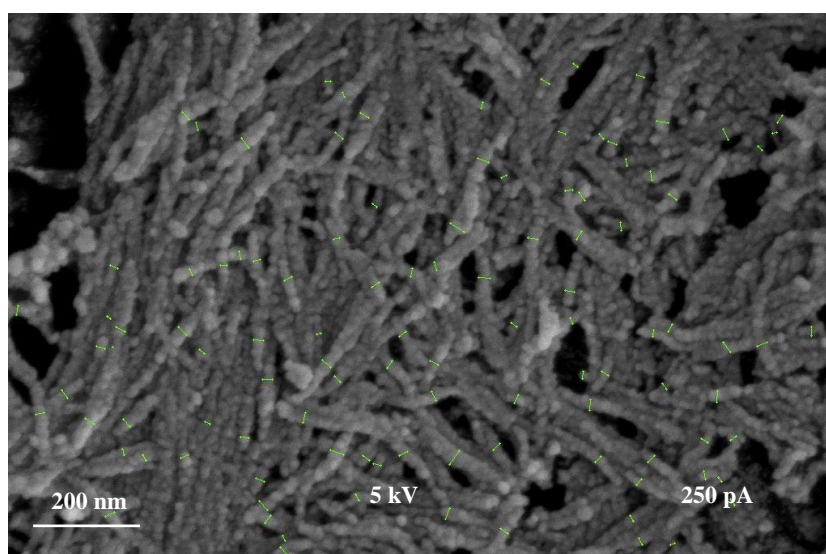

Figure 7.2: SEM image processing to determine lengths of cellulose nanoparticles obtained by acid hydrolysis of printed recycle PS as representative of image processing to estimate dimensions with Image J and SEM_Img_Studio imaging programs.

Appendix B: Infrared spectra bond classification

Table 7.1: Peak wavelength of infrared absorption bands, the corresponding interpretation according to literature

Wavenumber (cm⁻¹)	Interpretation/Assignment	Component Identification	Reference
3488 - 3340	Intramolecular hydrogen bond stretching	Cellulose	Schwanninger, et al., 2004; Siroky, et al., 2010
2910 - 2890	CH stretching (cellulose II)	Cellulose	Schwanninger, et al., 2004; Siroky, et al., 2010
1740 - 1693	C=O stretch, aromatics	Hemicellulose, lignin	Schwanninger, et al., 2004; Sabiha-Hanim & Aziatul-Akma, 2016; Lisperguer, et al., 2009)
1646	O-H bending, absorbed water	Cellulose	Poletto, et al., 2013
1579 - 1565	Symmetric oscillations of carboxylate ion COO⁻	Citrate	Lakshmanan, 1956; Sritham & Gunaserekaran, 2017
1517	C=O stretching, aromatic skeletal vibrations	Hemicellulose, lignin	Schwanninger, et al., 2004; Lisperguer, et al., 2009
1442 - 1420	CH, CH2 and OCH in-plane bending vibrations	Cellulose (crystalline)	Poletto, et al., 2013; Ciolacu, et al., 2010
1392	Asymmetric oscillations of carboxylate ion COO⁻	Citrate	Sritham & Gunaserekaran, 2017; Lakshmanan, 1956
1373	CH deformation vibration	Cellulose	Siroky, et al., 2010
1275	C-H deformation, C=O stretch	Hemicellulose, lignin	Schwanninger, et al., 2004
1248 - 1245	O–H in-plain deformation at C6, also C=O stretching	Cellulose. hemicellulose	Schwanninger, et al., 2004
1122 - 1100	Asymmetric in-phase ring, C-C and C-O stretching	Cellulose	Schwanninger, et al., 2004; Siroky, et al., 2010
1078 - 1052	C-O valence vibrating from C3-O3H	Cellulose	Poletto, et al., 2013; Ciolacu, et al., 2010
1029 - 988	C-O valence vibration C6	Cellulose	Poletto, et al., 2013; Ciolacu, et al., 2010; Adina, et al., 2010
912	C-H out-of-plane, aromatic	Cellulose, lignin	Schwanninger, et al., 2004
898 - 832	COC, CCO, CCH deformation of C5 and C6 atoms	Cellulose (amorphous)	Poletto, et al., 2013; Nguyen, et al., 2013: Ciolacu, et al., 2010

Appendix C: Elemental Analysis
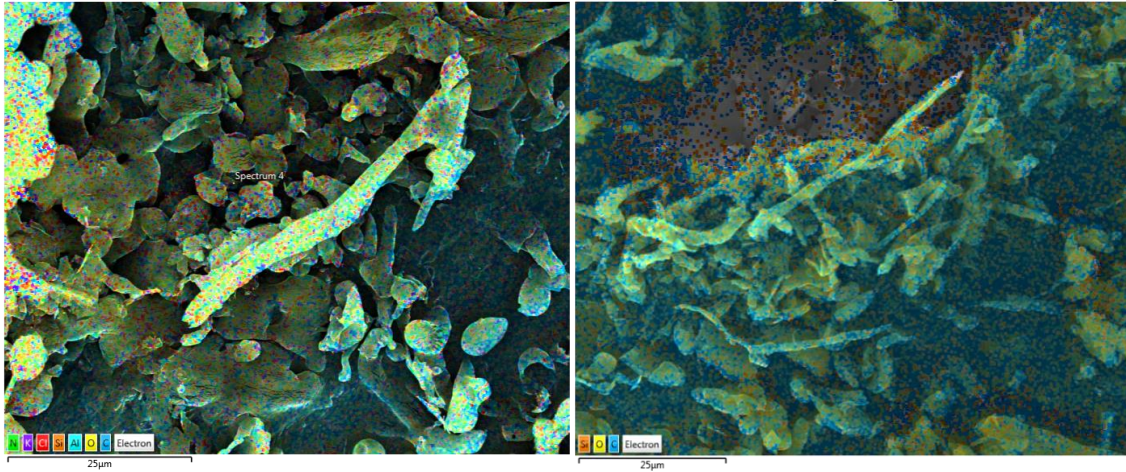
Figure 7.3: Elemental analysis (through electron microscopy imaging) of a printed recycle PS sample, enzymatically hydrolysed, centrifuged, glass-filtered and washed. The gold and aluminium elements, Au and Al, were subtracted during analysis as it was from the stub on which the sample was mounted and the coating for better conductivity.
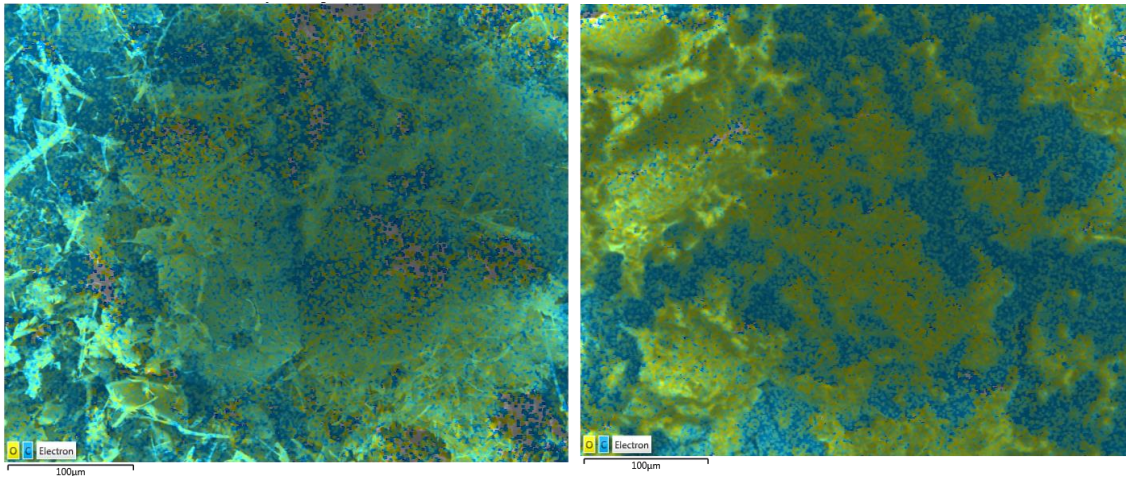
Figure 7.4: Elemental analysis through electron microscopy imaging of a virgin pulp PS sample, enzymatically hydrolysed, centrifuged, glass-filtered and washed. The gold and aluminium elements, Au and Al, were subtracted during analysis as it was from the stub on which the sample was mounted and the coating for better conductivity.

Appendix D: Statistical model development and ANOVA Analysis

The data obtained from the experimental runs in Table 4.7 and Table 4.8 were used to develop models for the prediction of the mean particle size and the glucose concentrations for the virgin pulp and printed recycle PS feedstock. Mathematical relationships between the independent variables (FiberCare dosage X_1, cellulase cocktail dosage X_2, solids loading X_3 and hydrolysis time X_4) and the responses of these variables (the mean particle size Y_1 and glucose concentration Y_2) aid in identifying trends within the hydrolysis process and are presented by a quadratic polynomial equation:

Equation 6 $\quad Y_i = b_0 + b_1X_1 + b_2X_2 + b_3X_3 + b_4X_4 + b_{11}X_1^2 + b_{22}X_2^2 + b_{33}X_3^2 + b_{44}X_4^2 +$
$b_{12}X_1X_2 + b_{13}X_1X_3 + b_{14}X_1X_4 + b_{23}X_2X_3 + b_{24}X_2X_4 + b_{34}X_3X_4$

where b_0 is intercept, b_1, b_2, b_3 and b_4 are linear coefficients, b_{11}, b_{22}, b_{33} and b_{44} are squared coefficients, and b_{12}, b_{13}, b_{14}, b_{23}, b_{24} and b_{34} are the interaction coefficients. The empirical relationships relating the mean particle size ($Y_{S,size}$) and the glucose ($Y_{S,glucose}$) concentration from virgin pulp PS to the four independent variables are presented as second-order polynomial correlations in Equation 7 and Equation 8, respectively.

Equation 7
$$Y_{S,size} = 287 - 0.38X_1 + 3.69X_2 - 16.1X_3 + 4.74X_4 - 0.38X_1^2 - 0.15X_2^2 + 1.22X_3^2 - 0.44X_4^2 + 0.01X_1X_2 - 0.12X_1X_3 + 0.13X_1X_4 + 0.18X_2X_3 + 0.21X_2X_4 - 0.54X_3X_4$$

Equation 8
$$Y_{S,glucose} = -18.3 + 0.11X_1 + 1.19X_2 + 2.49X_3 + 0.08X_4 - 0.001X_1^2 - 0.01X_2^2 - 0.13X_3^2 - 0.004X_4^2 - 0.003X_1X_2 + 0.01X_1X_3 + 0.002X_1X_4 + 0.01X_2X_3 - 0.02X_2X_4 + 0.09X_3X_4$$

Table 7.2: Analysis of variance for the fitted quadratic polynomial model for virgin pulp PS feedstock with mean particle size as response value

Factor	DF	SS	MS	F-value	p-value	95% CI low	95% CI high
X_1: Endoglucanase Dosage	1	4.54	4.54	0.004	0.952	-17.92	17.04
X_1^2	1	386.8	386.8	0.348	0.581	-20.11	12.59
X_2: Cellulase cocktail Dosage	1	6160	6160	5.549	0.065	-1.461	33.50
X_2^2	1	6155	6155	5.544	0.065	-31.33	1.373
X_3: Solids Loading	1	22868	22868	20.60	0.006	-48.35	-13.38
X_3^2	1	3288	3288	2.962	0.145	-5.404	27.30
X_4: Hydrolysis Time	1	1894	1894	1.706	0.248	-8.597	26.36
X_4^2	1	6765	6765	6.094	0.056	-32.05	0.64
X_1^2	1	51.24	51.24	0.046	0.838	-19.62	23.20
X_1X_3	1	1222	1222	1.101	0.342	-30.15	12.67
X_1X_4	1	5772	5772	5.199	0.071	-2.418	40.41
X_2X_3	1	456.9	456.8	0.412	0.549	-16.06	26.76
X_2X_4	1	2457	2457	2.213	0.196	-9.018	33.81
X_3X_4	1	1524	1524	1.373	0.294	-31.17	11.65
Residual error	15	924251	61616				
Lack of fit	10	780339	78034	2.712	0.141		
Pure error	5	143912	28782				
Cor Total	29	1887032					

Table 7.3: Analysis of variance for the fitted quadratic polynomial model for virgin pulp PS feedstock with glucose concentration as response value

Factor	DF	SS	MS	F-value	p-value	95% CI low	95% CI high
X_1: Endoglucanase Dosage	1	28.29	28.29	1.888	0.189	-0.598	2.770
X_1^2	1	4.391	4.391	0.293	0.596	-1.975	1.175
X_2: Cellulase cocktail Dosage	1	200.0	200.0	13.34	0.002	1.202	4.571
X_2^2	1	50.40	50.40	3.363	0.086	-2.931	0.219
X_3: Solids Loading	1	1344	1344	89.71	0.000	5.800	9.168
X_3^2	1	35.02	35.02	2.337	0.147	-2.705	0.445
X_4: Hydrolysis Time	1	181.5	181.5	12.12	0.003	1.066	4.434
X_4^2	1	0.510	0.510	0.034	0.856	-1.439	1.712
X_1^2	1	11.26	11.26	0.752	0.399	-2.902	1.224
X_1X_3	1	3.180	3.180	0.212	0.651	-1.616	2.508
X_1X_4	1	1.835	1.835	0.122	0.731	-1.724	2.401
X_2X_3	1	0.589	0.589	0.039	0.845	-1.871	2.254
X_2X_4	1	20.28	20.28	1.353	0.262	-3.188	0.936
X_3X_4	1	42.62	42.62	2.844	0.112	-0.430	3.694
Residual error	15	112.4	7.496				
Lack of fit	10	98.14	9.814	3.428	0.093		
Pure error	5	14.31	2.862				
Cor Total	29	351.2					

Table 7.4: Analysis of variance for the fitted quadratic polynomial model for printed recycle PS feedstock with mean particle size as response value

Factor	DF	SS	MS	F-value	p-value	95% CI low	95% CI high
X_1: Endoglucanase Dosage	1	84251	84251	1.367	0.260	-29.7	148.2
X_1^2	1	188.2	188.2	0.003	0.956	-85.8	80.65
X_2: Cellulase cocktail Dosage	1	7748	7748	0.125	0.727	-71.0	106.9
X_2^2	1	5746	5746	0.093	0.764	-97.7	68.79
X_3: Solids Loading	1	362190	362189	5.878	0.028	33.8	211.8
X_3^2	1	356289	356289	5.782	0.029	30.7	197.2
X_4: Hydrolysis Time	1	32143	32143	0.521	0.481	-52.4	125.61
X_4^2	1	89.4	89.4	0.001	0.970	-81.4	85.07
X_1^2	1	28155	28155	0.456	0.509	-67.0	150.9
X_1X_3	1	13954	13954	0.226	0.641	-138.5	79.49
X_1X_4	1	17373	17372	0.281	0.603	-76.0	141.9
X_2X_3	1	3385	3385	0.054	0.817	-94.4	123.5
X_2X_4	1	3863	3863	0.062	0.805	-124.5	93.48
X_3X_4	1	18186	18186	0.295	0.594	-75.3	142.7
Residual error	15	64783	4318				
Lack of fit	10	59233	5923	5.336	0.039		
Pure error	5	5550	1110				
Cor Total	29	124790					

Table 7.5: Analysis of variance for the fitted quadratic polynomial model for printed recycle PS feedstock with glucose concentration as response value

Factor	DF	SS	MS	F-value	p-value	95% CI low	95% CI high
X_1: Endoglucanase Dosage	1	0.9037	0.9037	0.120	0.733	-0.997	1.385
X_1^2	1	32.667	32.667	4.357	0.054	-2.205	0.022
X_2: Cellulase cocktail Dosage	1	43.333	43.333	5.780	0.029	0.152	2.534
X_2^2	1	3.3740	3.3740	0.450	0.512	-1.465	0.763
X_3: Solids Loading	1	114.26	114.25	15.24	0.001	0.990	3.373
X_3^2	1	9.5391	9.5391	1.272	0.277	-1.704	0.524
X_4: Hydrolysis Time	1	11.456	11.455	1.528	0.235	-0.500	1.882
X_4^2	1	0.4369	0.4369	0.058	0.812	-1.240	0.988
X_1^2	1	5.0865	5.0865	0.678	0.423	-0.895	2.022
X_1X_3	1	0.8275	0.8275	0.110	0.744	-1.686	1.231
X_1X_4	1	5.6644	5.6644	0.756	0.398	-0.864	2.054
X_2X_3	1	1.2963	1.2963	0.172	0.683	-1.743	1.174
X_2X_4	1	4.1353	4.1353	0.551	0.469	-0.950	1.967
X_3X_4	1	13.051	13.051	1.740	0.206	-0.555	2.362
Residual error	15	224.77	14.985				
Lack of fit	10	223.65	22.365	99.75	0.00004		
Pure error	5	1.121	0.224				
Cor Total	29	2139.9					

The percentage errors of the different models compared to the experimental values were determined (Equation 5) to test which provided the best predictions (Table 7.6). The model with only significant 'pure error' effects had percentage errors ranging from 4.4 - 26.2%, while the model with only the significant effects based on the 'residual' had high errors ranging from 90 – 174%. In comparison, the complete model had the most accurate predictions with the minimum percentage errors ranging from 2.9 to 17.7 %. The percentage errors were presented specifically for the glucose concentration model of virgin pulp PS, but the same trend was found for the remaining three models, and therefore the complete models were considered for optimisation.

Table 7.6: Percentage errors of glucose concentration models of the virgin pulp PS with and without insignificant terms according to residual statistical analysis and pure error statistical analysis. The data of the first four entries of the CCD design were considered for representation, with the same trend applying to all the entries. Sample numbers provided are identification of experiment conditions as set out in Table 4.8

Sample no.	Experimental Glucose Concentration	Complete predicted model	Percentage error	Model with significant residual effects only	Percentage error	Model with significant pure error effects only	Percentage error
	g/L	g/L	%	g/L	%	g/L	%
31	15.4	12.6	17.7	34.2	122.8	11.9	22.3
32	22.8	18.9	17.1	62.4	173.6	16.8	26.2
33	30.5	28.6	6.3	58.0	90.0	25.6	16.0
34	18.0	18.5	2.9	38.6	114.6	17.2	4.4